Characterization of a novel polyextremotolerant fungus, *Exophiala viscosa,* with insights into its melanin regulation and ecological niche

Erin C. Carr[1]*, Quin Barton[2], Sarah Grambo[3], Mitchell Sullivan[1], Cecile M. Renfro[4], Alan Kuo[5], Jasmyn Pangilinan[5], Anna Lipzen[5], Keykhosrow Keymanesh[5], Emily Savage[5], Kerrie Barry[5], Igor V. Grigoriev[5,6], Wayne R. Riekhof[1], Steven D. Harris[7,8]

1) University of Nebraska-Lincoln, School of Biological Sciences, Lincoln, Nebraska 68588; 2) University of Nebraska-Lincoln, Department of Biochemistry, Lincoln, Nebraska 68588; 3) Iowa State University, Roy J. Carver Department of Biochemistry, Biophysics, and Molecular Biology, Ames, Iowa 50011; 4) University of Nebraska-Lincoln, Department of Agronomy and Horticulture, Lincoln, Nebraska 68588; 5) US Department of Energy Joint Genome Institute, Lawrence Berkeley National Laboratory, Berkeley, California 94720; 6) Department of Plant and Microbial Biology, University of California Berkeley, Berkeley, California 94720; 7) Iowa State University, Department of Plant Pathology and Microbiology, Ames, Iowa 50011; 8) Iowa State University, Department of Entomology Ames, Iowa 50011

*Corresponding Author: Erin C. Carr

E-mail: erin.creasey@huskers.unl.edu
Legacy email: erin.carr1216@gmail.com
Mailing address:
1901 Vine St.
Room E136
Lincoln, NE 68503

Abstract

Black yeasts are polyextremotolerant fungi that contain high amounts of melanin in their cell wall and maintain a primarily yeast form. These fungi grow in xeric, nutrient deplete environments which implies that they require highly flexible metabolisms and have been suggested to contain the ability to form lichen-like mutualisms with nearby algae and bacteria. However, the exact ecological niche and interactions between these fungi and their surrounding community is not well understood. We have isolated two novel black yeasts from the genus *Exophiala* that were recovered from dryland biological soil crusts. Despite notable differences in colony and cellular morphology, both fungi appear to be members of the same species, which has been named *Exophiala viscosa (i.e., E. viscosa* JF 03-3 Goopy *and E. viscosa* JF 03-4F Slimy*)*. A combination of whole genome sequencing, phenotypic experiments, and melanin regulation experiments have been performed on these isolates to fully characterize these fungi and help decipher their fundamental niches within the biological soil crust consortium. Our results reveal that *E. viscosa* is capable of utilizing a wide variety of carbon and nitrogen

sources potentially derived from symbiotic microbes, can withstand many forms of abiotic stresses, and excrete melanin that can potentially provide UV resistance to the biological soil crust community. Besides the identification of a novel species within the genus *Exophiala*, our study also provides new insight into the regulation of melanin production in polyextremotolerant fungi.

Background

The production of melanin is a key functional trait observed in many fungi spanning the fungal kingdom (Bell & Wheeler, 1986; Zanne et al., 2020). The diverse protective functions of melanin (e.g., metal resistance, ROS and RNS tolerance, UV resistance) underscores its broad utility in mitigating the impacts of stress despite the potential cost of its synthesis (Schroeder et al., 2020). Fungi are capable of producing three different types of melanin: pheomelanin, allomelanin, and pyomelanin, all of which have their own independent biosynthetic pathways (Pal et al., 2014; Perez-Cuesta et al., 2020). Allomelanin is formed from the polymerization of 1,8-DHN, which requires the use of polyketide synthase for initial steps in production (Perez-Cuesta et al., 2020; Płonka & Grabacka, 2006) (**Figure 1**). Pyomelanin and pheomelanin share an initial substrate of Tyrosine, but pheomelanin derives from L-DOPA, whereas pyomelanin is created via tyrosine degradation (Perez-Cuesta et al., 2020; Płonka & Grabacka, 2006) (**Figure 1**). Allomelanin and pheomelanin are often referred to as DHN-melanin and DOPA-melanin respectively, given their chemical precursors.

Unfortunately, due to the unique characteristics of melanins and their association with larger biomolecules, we do not know the complete structure of any type of melanin (Cao et al., 2021). However, given that we do know their chemical constituents, it is possible to draw some inferences about the relationship between structure and function of a particular type of melanin. For instance, out of the three types of melanin fungi can produce, only pheomelanin has a chemical precursor, 5-CysDOPA, with both nitrogen and sulfur in its structure (Płonka & Grabacka, 2006). Notably, all three fungal melanins are synthesized via independent pathways, which enables the targeted use of chemical inhibitors to block one pathway without interfering with the others. For example, previous studies have extensively used the chemical melanin blockers kojic acid and phthalide to block pheomelanin and allomelanin respectively (Pal et al., 2014) (**Figure 1**). Use of these chemical blockers allowed previous studies to identify the primary melanin biosynthetic pathway employed by individual fungal species (Pal et al., 2014).

Polyextremotolerant fungi are a polyphyletic group that can be divided morphologically into black yeast and microcolonial/meristematic fungi types (Gostinčar et al., 2012). These two sub-types are distinct in their morphology; black yeast fungi are primarily yeasts but can be dimorphic, whereas microcolonial fungi are typically filamentous, pseudohyphal, or produce other unique morphologies such as spherical cells (Ametrano et al., 2017; De Hoog et al., 2003; Gostinčar et al., 2011). However, all polyextremotolerant fungi share the capacity to produce melanin, which presumably accounts for much of their polyextremotolerance. Most polyextremotolerant fungi are in the subdivision Pezizomycotina, residing mainly within Eurotiomycetes and Dothidiomycetes (Gostinčar et al., 2009).

Melanin is arguably the defining feature of polyextremotolerant fungi given that they form unmistakably black colonies. Because of its structure and association with the cell wall, melanin imbues polyextremotolerant fungi with resistance to multiple forms of stress. Most commonly known is ultraviolet (UV) light resistance, as melanin absorbs light in the UV part of the spectrum (Kobayashi et al., 1993). However, melanin is also capable of quenching reactive oxygen species (ROS) and reactive nitrogen species (RNS), providing tolerance to toxic metals, reducing desiccation, and enabling use of ionizing radiation as an energy source (Cordero & Casadevall, 2017; Dadachova et al., 2007; Gessler et al., 2014; Płonka & Grabacka, 2006; Zanne et al., 2020). Collectively, these functions of melanin are thought to enhance the ability of polyextremotolerant fungi to colonize habitats that are otherwise inhospitable to most forms of life.

Polyextremotolerant fungi tend to occupy extreme niches such as rock surfaces, external brick and marble walls, soil surfaces, and even the inside of dishwashers (Gostinčar et al., 2009; Zupančič et al., 2016). Characteristic features of these environments includes the relative paucity of nutrients and the frequent presence of a community biofilm consisting of photosynthetic organisms and/or bacteria (Gostinčar et al., 2012). Strikingly, these microbes are rarely found alone in their habitats, which suggests that multi-species interactions between fungi, bacteria, and photosynthetic organisms underlie the formation and function of these communities. That is, the ability of polyextremotolerant fungi to successfully adapt to their niche must depend on complex yet poorly understood interactions with other microbes.

We have isolated two polyextremotolerant fungi from a biological soil crust (BSC) in British Columbia, Canada. These novel fungi are of the genus *Exophiala*, which has previously been found in BSCs (Bates et al., 2006). Biological soil crusts are unique dryland biofilms that form on the surface of xeric desert soils where little to no plants are able to grow (Belnap, 2003; Belnap et al., 2001). They are

98 notable for their extensive cyanobacteria population, which seeds the initial formation of all BSCs and
99 creates the main source of nitrogen for the rest of the community (Belnap, 2002). Once the initial crust
100 is established, it is then inundated with a consortium of bacteria, fungi, algae, archaea, lichens, and
101 mosses (Bates et al., 2010; Lan et al., 2012; Maier et al., 2016). This community is a permanent fixture
102 on the land they occupy unless physically disturbed, much like other biofilms (Belnap & Eldridge, 2001;
103 Donlan & Costerton, 2002). As a result of the arid conditions to which BSCs are often exposed, their
104 resident microbes are constantly exposed to extreme abiotic factors that must be countered to enable
105 survival (Bowker et al., 2010). Some of these abiotic extremes are: UV radiation (especially at higher
106 altitudes and latitudes) (Bowker et al., 2002), desiccation and osmotic pressures (Rajeev et al., 2013),
107 and temperature fluctuations both daily and annually (Belnap et al., 2001; Bowker et al., 2002; Pócs,
108 2009). Accordingly, microbes that reside within BSCs must therefore possess adaptations that allow
109 them to withstand these abiotic extremes.

110 An extensive amount of research has been dedicated to certain members of the BSC
111 community, but one such less studied microbe has been the "free-living" fungal taxa. These fungi are
112 non-lichenized (Teixeira et al., 2017) yet are still thriving in an environment where there are no plants to
113 infect or decompose (Belnap & Lange, 2003), and no obvious source of nutrients aside from
114 contributions of the other members of the BSC community (Belnap & Lange, 2003). This would imply
115 that even though these fungi are not lichenized *per se*, they would have to engage in lichen-like
116 interactions with the BSC community to obtain vital nutrients for proliferation. While previous
117 researchers have postulated the idea of transient interactions between non-lichenized fungi and other
118 microbes (Gostinčar et al., 2012; Grube et al., 2015; Hom & Murray, 2014), confirmation of this in BSCs
119 is potentially challenging given their taxonomic complexity.

120 Despite the importance of microbial interactions in enabling the successful formation of BSCs in
121 a niche characterized by poor nutrient and water availability, the fungal components of BSCs and their
122 relative functions within the interaction network remain poorly understood. Here, we combine genome
123 sequencing with computational tools and culture-based phenotyping to describe two strains of a new
124 species of black yeast fungi associated with BSCs. We report on their carbon and nitrogen utilization
125 profiles, stress responses, and lipid accumulation patterns. In addition, we characterize their capacity for
126 melanin production and generate valuable insight into mechanisms that might be involved in regulating
127 the synthesis of these compounds so that melanin production contributes to the BSC community.

128

129 # Methods

130 *Fungal Strains and Media*

131 Two strains of a novel species of fungi are described here: *Exophiala viscosa* JF 03-3F Goopy CBS
132 148801 and *Exophiala viscosa* JF 03-4F Slimy CBS 148802. *E. viscosa* is typically grown in malt extract
133 medium (MEA; see **Table 1** for media recipe) at room temperature in an Erlenmeyer flask at 1/10th the
134 volume of the flask, shaking at 160 rpm. Additional strains used in this study were *Saccharomyces*
135 *cerevisiae* ML440 and BY4741, and *E. dermatitidis* wild type (WT) strain ATCC 34100. *S. cerevisiae* strains
136 are grown in Yeast Peptone Dextrose medium (YPD; **Table 1** for media recipe), and *E. dermatitidis* is
137 grown in MEA.

138 *Fungal Isolation and Identification Methods*

139 Fungi were isolated from a BSC in British Columbia (B.C.), Canada, Latitude: 52.94997°,
140 Longitude: -119.41919°. Soil samples were taken from the top 2 cm of the BSC. A 0.1 g portion of the
141 crust was re-suspended in 1 mL of water, ground with a sterile micropestle, and diluted with a dilution
142 factor (DF) of 10 till they reached 10,000x dilution. Each dilution was then spread out onto two different
143 MEA petri plates containing either no antibiotics or a plate containing: Ampicillin (100 mg/L final
144 concentration), Chloramphenicol (50 mg/L), Gentamycin (10 mg/L), and Cycloheximide (100 mg/L). The
145 plates were then incubated in a Percival light incubator at 23 °C with a 12 hr light/dark cycle and
146 examined daily using a dissection microscope to check for small black colonies. Once a potential black
147 colony was seen, half of it was removed and transferred to a new MEA petri plate with no antibiotics. It
148 was vital to examine the plates daily, because even in the presence of antibiotics many unwanted fast-
149 growing microbes would grow on the plates and cover up the slower growing polyextremotolerant
150 fungal colonies. Once a pure culture of each isolate was grown up (approximately 2 weeks), they were
151 preserved in 30% glycerol and stored in the -80 °C freezer.

152 DNA sequencing of amplified internal transcribed spacer (ITS) sequences was used to initially
153 identify the isolates. DNA was extracted using the Qiagen DNeasy Powersoil DNA extraction kit. Primers
154 used to isolate the ITS region were: ITS1- (5'-TCC GTA GGT GAA CCT GCG G-3') and ITS4- (5'-TCC TCC GCT
155 TAT TGA TAT GC-3') (White et al., 1990). A BioRad MJ Mini Personal Thermal Cycler was used, with the
156 program set as: 1) 95 °C for 5:00 (5 minutes), 2) 94 °C for 0:30 (30 seconds), 3) 55 °C for 0:30, 4) 72 °C for
157 1:30, 5) Return to Step 2 35 times, 6) 72 °C for 5:00. Resulting PCRs were then checked via gel
158 electrophoresis in 1% agar run at 80 V for 1 hr. Isolated ITS regions were sequenced using the Eurofins

159 sequencing facility with their in-house ITS primers as the sequencing primers, and the sequences were
160 subsequently identified using the basic local alignment search tool (BLAST) of the National Center for
161 Biotechnological Information (NCBI) database to look for potential taxa matches.

162 *DNA Extraction and RNA Extraction for Whole Genome Sequencing and Annotation*

163 A cetyltrimethylammonium bromide (CTAB) based DNA extraction method was performed to
164 obtain high molecular weight DNA for whole genome sequencing. The DNA extraction method used was
165 derived from (Cubero et al., 1999). Changes to the original protocol include: 1) switching
166 polyvinylpolypyrrolidone (PVPP) for the same concentration of polyvinylpyrrolidone (PVP), 2) use of
167 bead beating tubes with liquid nitrogen-frozen cells and the extraction buffer instead of a mortar and
168 pestle for breaking open the cells, and 3) heating up the elution buffer to 65 °C before eluting the final
169 DNA. These changes were made to optimize the protocol for liquid-grown fungal cells instead of lichen
170 material. Cells for the DNA extraction were grown up in 25 mL of liquid MEA in 250 mL Erlenmeyer flasks
171 for 5 days at room temperature with 160 rpm shaking. 1 mL of the grown cells was used for the DNA
172 extraction after washing with water twice. Protocol for CTAB extraction method can be found on
173 protocols.io.

174 RNA was obtained using the Qiagen RNeasy Mini Kit (Cat. No. 74104). Cells were grown in 25 mL
175 of three different liquid media types (MEA, YPD, and MNV; see **Table 1**) in 250 mL Erlenmeyer flasks at
176 room temperature for 5 days (as described above), and 1-2 mL of cells were used for the RNA extraction.
177 Cells were washed with DEPC-treated water and flash frozen in liquid nitrogen in 1.5 mL microcentrifuge
178 tubes. RNA extraction was then performed according to the methods by the RNeasy kit.

179 *Genome Assembly and Annotation*

180 Both genomes and transcriptomes were sequenced using Illumina technology. For
181 transcriptomes, a plate-based RNA sample prep was performed on the PerkinElmer Sciclone next
182 generation sequencing (NGS) robotic liquid handling system using Illuminas TruSeq Stranded mRNA high
183 throughput (HT) sample prep kit utilizing poly-A selection of mRNA following the protocol outlined by
184 Illumina in their user guide: https://support.illumina.com/sequencing/sequencing_kits/truseq-stranded-
185 mrna.html, and with the following conditions: total RNA starting material was 1 µg per sample and 8
186 cycles of PCR was used for library amplification. The prepared libraries were quantified using KAPA
187 Biosystems' next-generation sequencing library qPCR kit and run on a Roche LightCycler 480 real-time
188 PCR instrument. The libraries were then multiplexed and prepared for sequencing on the Illumina
189 NovaSeq sequencer using NovaSeq XP v1 reagent kits, S4 flow cell, following a 2x150 indexed run recipe.

190 BBDuk was used for trimming and filtering sequencing reads
191 (https://sourceforge.net/projects/bbmap/). Raw reads were evaluated for artifact sequence by k-mer
192 matching (k-mer=25), allowing 1 mismatch and detected artifacts were trimmed from the 3' end of the
193 reads. RNA spike-in reads, PhiX reads and reads containing any Ns were removed. Quality trimming was
194 performed using the phred trimming method set at Q6. Finally, following trimming, reads under the
195 length threshold were removed (minimum length 25 bases or 1/3 of the original read length –
196 whichever is longer). Filtered reads were assembled into consensus sequences using Trinity ver. 2.3.2
197 (Grabherr et al., 2011). Specific Trinity options that were utilized were: --jaccard_clip, --run_as_paired, --
198 min_per_id_same_path 95, --normalize_reads.

199 For genomes, DNA library preparation for Illumina sequencing was performed on the
200 PerkinElmer Sciclone NGS robotic liquid handling system using Kapa Biosystems library preparation kit.
201 200 ng of sample DNA was sheared to 300 bp using a Covaris LE220 focused-ultrasonicator. The sheared
202 DNA fragments were size selected by double-SPRI and then the selected fragments were end-repaired,
203 A-tailed, and ligated with Illumina compatible sequencing adaptors from IDT containing a unique
204 molecular index barcode for each sample library. The prepared libraries were quantified using KAPA
205 Biosystems' next-generation sequencing library qPCR kit and run on a Roche LightCycler 480 real-time
206 PCR instrument. The quantified libraries were then multiplexed with other libraries, and the pool of
207 libraries was then prepared for sequencing on the Illumina HiSeq sequencing platform utilizing a TruSeq
208 paired-end cluster kit, v4, and Illumina's cBot instrument to generate a clustered flow cell for
209 sequencing. Sequencing of the flow cell was performed on the Illumina HiSeq2500 sequencer using
210 HiSeq TruSeq SBS sequencing kits, v4, following a 2x150 indexed run recipe.

211 An initial assembly of the target genome was generated using VelvetOptimiser version 2.1.7 (3)
212 with Velvet version 1.2.07 (Zerbino & Birney, 2008) using the following parameters; "–s 61 –e 97 –i 4 –t
213 4, --o "-ins_length 250 -min_contig_lgth 500"". The resulting assembly was used to simulate 28X of a
214 2x100 bp 3000 +/- 300bp insert long read mate-pair library with wgsim version 0.3.1-r13
215 (https://github.com/lh3/wgsim) using "-e 0 -1 100 -2 100 -r 0 -R 0 -X 0 -d 3000 -s 30". 25X of the
216 simulated long read mate-pair was then co-assembled together with 125X of the original Illumina
217 filtered fastq with AllPathsLG release version R49403 (Gnerre et al., 2011) to produce the final nuclear
218 assembly. A simulated long read assembly was required because AllpathsLG requires both a long read
219 and short read insert library and having both types of libraries was beyond the cost of this project.
220 Therefore, a subsample of the original Illumina short read inserts and the newly simulated long read

221 insert data was fed into AllpathsLG. This methodology was shown to produce superior assemblies over
222 other assemblers with a single short insert library. The genome was then annotated using JGI
223 Annotation pipeline (Grigoriev et al., 2014). The JGI Annotation Pipeline, 1) detects and masks repeats
224 and transposable elements, 2) predicts genes using a variety of methods, 3) characterizes each
225 conceptually translated protein using a variety of methods, 4) chooses a 'best' gene model at each locus
226 to provide a filtered working set, 5) clusters the filtered sets into draft gene families, and 6) creates a JGI
227 Genome Portal with tools for public access and community-driven curation of the annotation (Grigoriev
228 et al., 2012; Kuo et al., 2014).

229 The assembly scaffolds were masked by RepeatMasker (http://www.repeatmasker.org/) using
230 both the manually curated Repbase library (Jurka, 2000) and a library of de novo repeats discovered by
231 RepeatScout (Price et al., 2005). Transcript-based gene models were derived by assembling Illumina-
232 sequenced RNA reads into contigs which were then modeled on genomic scaffolds using EST MAP
233 (http://www.softberry.com) and COMBEST (Zhou et al., 2015). Protein-based gene models were
234 predicted using GeneWise (Birney & Durbin, 2000) and FGENESH+ (Salamov & Solovyev, 2000) seeded
235 by BLASTx alignments of genomic sequence against sequences from the NCBI non-redundant protein set
236 nr (Altschul et al., 1990). Ab initio gene models were predicted using GeneMark-ES (Ter-Hovhannisyan et
237 al., 2008) and FGENESH, the latter trained on a set of putative full-length transcripts and reliable
238 protein-based models. GeneWise models were completed using scaffold data to find start and stop
239 codons. RNA contig alignments to the genome were used to verify, complete, and extend the gene
240 models.

241 All predicted gene models were functionally annotated by the JGI Annotation Pipeline using
242 InterProScan (Zdobnov & Apweiler, 2001), blastp alignments against nr and highly curated databases
243 such as SwissProt (Bairoch et al., 2005), KEGG (Ogata et al., 1999), and Pfam (Bateman et al., 2004).
244 KEGG hits were used to map EC numbers (Bairoch, 2000); InterPro, KEGG, and SwissProt hits were used
245 to map GO terms (Ashburner et al., 2000). In addition, predicted proteins were annotated according to
246 KOG classification (Koonin et al., 2004). Protein targeting predictions were made with signalP (Nielsen et
247 al., 1999) and TMHMM (Krogh et al., 2001). Because the gene-prediction steps usually generated
248 multiple gene models per locus, the Pipeline selected a single representative gene model for each locus
249 based on protein similarity, RNA coverage, and functional annotation, leading to a filtered set of gene
250 models for downstream analysis. All filtered model proteins in a genome were aligned \ to each other
251 and to those of other related genomes by blastp. The alignment scores were used as a distance metric

252 for clustering by MCL (http://www.micans.org/mcl/) into a first draft of candidate multigene families for
253 each genome.

254 All genomic scaffolds, RNA contigs, gene models and clusters, and functional predictions
255 thereof, may be accessed through MycoCosm Herpotrichiellaceae PhyloGroup Portal
256 (https://mycocosm.jgi.doe.gov/Herpotrichiellaceae/) and the MycCosm Black Yeasts EcoGroup Portal
257 (https://mycocosm.jgi.doe.gov/black_yeasts/). The assemblies and annotations of both genomes are
258 available at the fungal genome portal MycoCosm (Grigoriev et al., 2014); https://mycocosm.jgi.doe.gov)
259 and in the DDBJ/EMBL/GenBank repository under accessions JALDXI000000000 and JALDXH000000000.

260 *Phylogenetic Analyses*

261 Our single-copy homologous protein sequence approximate maximum likelihood phylogenetic
262 tree was constructed from the protein sequences of 24 taxa which represent a sampling of the family
263 Herpotrichielleaceae in which *E. viscosa* JF 03-3F and JF 03-4F reside. We created this tree using the
264 pipeline described in Kuo et al. (2014). To obtain the largest set of data for phylogenetic analysis
265 available, we defined homologous proteins across all 24 genomes using Best Bidirectional Blast (BBB)
266 pairs via blastp across all proteins of all the genomes from their FilteredModels or ExternalModels files
267 available on Mycocosm, with an e-value 1e-05 cutoff for BBBs. Clusters were compiled using in-house
268 JGI scripts. If there are e.g. N genomes, we first compute BBBs individually for each pair of genomes (in
269 total N*(N-1)/2 pairs) and then using BBBs as an input computed for each pair of genomes. Another
270 script finds BBBs which are present in all N genomes, so these are sets of N genes (one from each
271 species or strain) which are BBB to each other in all N genomes. Resulting defined homologous proteins
272 across all 24 genomes were then used as our sequences for the rest of the pipeline. These sequences
273 were aligned with Mafft v7.123b with no alterations (Katoh et al., 2002). That alignment was then
274 trimmed using Gblocks 0.91b with options -b4=5 -b5=h to have a minimum of 5 positions per block and
275 allowing up to half of those to be gaps (Castresana, 2000). The resulting trimmed alignment was then
276 input into FastTree version 2.1.5 SSE3 with options -gamma -wag (Price et al., 2009). The tree file was
277 then input into FigTree for visual optimization, and edited in Adobe Illustrator to highlight the new
278 species.

279 The combined Bayesian and maximum likelihood concatenated gene phylogenetic trees were
280 constructed using 18S rDNA, 28S rDNA, and ITS sequences of *Exophiala, Pheoannellomyces,* and
281 *Endocarpon* species available from NCBI GenBank. Accession numbers and strains of fungi used for
282 phylogenetic analyses are listed in **Table 2**. Specific fungal species and genes were chosen based on

283 relatedness to our new fungus via BLAST alignment, and the availability of all marker genes needed for
284 analyses. The marker gene *RPB1* was also concatenated to the others tested for all species except
285 *Phaeoannellomyces elegans* and *Exophiala crusticola* which did not have an available *RPB1* sequence in
286 NCBI. Alignments of individual gene sets were performed using the program MEGA X (Kumar et al.,
287 2018). Alignment of the sequences was done using MUSCLE aligner (Edgar, 2004). Gap open was set to -
288 400.00, gap extend set to 0.00, max memory was set to 2048 MB, max iterations was 16, cluster method
289 used was UPGMA, and minimal diagonal length was 24. Trimming was done by hand, first by removing
290 any excess ends, then only essential gaps that formed where one or two taxa contained inserted
291 nucleotides were removed. This allowed for the parts of the ITS and *RPB1* regions that remain highly
292 variable even across the same genus to be kept, whereas when trimming was attempted with Gblocks
293 with all least stringent options selected, only the most conserved regions were maintained resulting in
294 improper phylogenies (e.g., *Exophiala eucalyptorum* 121638 did not cluster with other *Exophiala* species
295 but was eventually removed from the tree for clarity). The alignments were then uploaded to Geneious
296 Prime 2023.0.4 (Kearse et al., 2012). Individual gene sets were then concatenated using the concatenate
297 alignments tool.

298 Phylogenetic estimates were performed using Bayesian inference via the Mr. Bayes plug-in ver.
299 2.2.4 in Geneious (Huelsenbeck & Ronquist, 2001; Ronquist & Huelsenbeck, 2003). For the Bayesian
300 analysis we used Metropolis-coupled MCMC and the General Time Reversible (GTR) model with gamma
301 distribution with invariant sites (Γ + I) the GTR + Γ + I model, with 5 gamma categories. We conducted
302 the run with four heated chains at a temp, of 0.2 for 500,000 generations, sampling trees every 1,000
303 generations, with a burn length of 10,000, and a random seed of 20,512. The resulting phylogenetic tree
304 was then used as the seed tree for Maximum Likelihood analyses. A maximum likelihood phylogenetic
305 tree was created in MEGA X using the Maximum Likelihood statistical method and the bootstrap method
306 for the test of phylogeny with 1,000 bootstrap replications. The substitution type used was nucleotide
307 and not a protein coding sequence of DNA, and the model used for the substitution was the GTR + Γ + I
308 with 5 discrete gamma categories. Gaps were included in the data treatment as many individual gaps
309 are created in ITS and *RPB1* sequences after alignment in the variable regions. For tree inference options
310 we used the nearest-neighbor-interchange (NNI) heuristic method, and had the initial tree be
311 automated under the default settings-Neighbor joining (NJ)/bioNJ, the resulting Bayesian tree was used
312 as the initial tree file, and no branch swap filter. The resulting tree in newick (.nwk) form with branch
313 lengths and bootstrap values was then imported into the interactive tree of live (iTOL) program ver. 6.6

314 for visualization, and edited in Adobe Illustrator to add combined posterior probabilities and bootstrap
315 values and highlight the new species (Letunic & Bork, 2021).

316 *Assemble Species by Automatic Partitioning for DNA-based Species Delimitation*

317 We used Assemble Species by Automatic Partitioning (ASAP) to confirm our species delimitation
318 that was observed in our phylogenetic analyses (Puillandre et al., 2021). We used the web-based version
319 of ASAP (https://bioinfo.mnhn.fr/abi/public/asap/) using the Kimura (K80) model on our aligned ITS-
320 only, 18S-28S-ITS gene concatenation alignment, and our 18S-28S-ITS-*RPB1* gene concatenation
321 alignment. The resulting lowest ASAP score (smallest p-value and largest relative barcode gap) was
322 chosen to be the most likely delimitation of species of that dataset.

323 *Mating Type Locus Identification*

324 Mating loci for *E. viscosa* JF 03-3F and *E. viscosa* JF 03-4F were determined using the methods
325 described by (Teixeira et al., 2017). Genes known to flank the MAT loci of most Chaetothyriales species
326 include: *APN2*, *SLA2*, *APC5*, and *COX13*. The protein sequences of these genes from *Aspergillus nidulans*
327 were used to BLASTp against the genomes of the new fungi. These gene sequences were obtained from
328 Aspergillus Genome Database (now called FungiDB https://fungidb.org/) and protein-protein BLASTed
329 using JGI's Mycocosm. Once the genes were found, analysis of upstream and downstream flanking
330 genes was performed until the mating gene MAT1-1 was located. Genes close to MAT1-1 and within the
331 span of genes listed above were considered part of the MAT locus.

332 Phenotyping Experiments:

333 Phenotyping experiments of *E. viscosa* JF 03-3F and *E. viscosa* JF 03-4F were performed to
334 characterize the new species' capabilities and differences between the strains. Experiments performed
335 were carbon utilization, nitrogen utilization, UV resistance, metal resistance, growth temperature range,
336 budding patterns, lipid profiles, and growth capabilities on various fungal medias as described below.

337 *Budding Pattern Determination*

338 Protocols for observing the budding patterns of these new strains were derived from methods in
339 Mitchison-Field et al. (2019) (**Figure S1**). A 1:1:1 ratio by weight of Vaseline, Paraffin, and Lanolin
340 (VALAP) was combined in a glass bottle and heated to 115 °C to melt completely and kept at room
341 temperature for later use. Heated solid MEA was aliquoted into a 50 mL tube for agar slab making.
342 Isolates were grown in liquid MEA for 5 days prior to inoculation of slides. First, the VALAP was brought
343 back up to 115 °C to melt completely for application. Then 5 µL of the 5-day old cells were diluted in 995

344 µL of liquid MEA. Agar slabs of MEA were made by microwaving the 50 mL tube of solid MEA until it
345 melted, then pipetting 1 mL of the hot agar into a 1 cm x 2 cm mold formed out of cut strips of silicone
346 and laid down in a sterile petri dish. This agar slab was allowed to solidify and was then cut in half to be
347 1 cm x 1 cm. Both the microscope cover slip and the microscope slide were wiped down with 70%
348 ethanol to ensure clean and sterile growth conditions for the cells. 6 µL of the diluted cells was pipetted
349 onto the center of the sterile slide, then one square of the agar slab was carefully placed on top of the
350 cells in media, 8 µL of MEA was pipetted onto the top of the agar slab, and the coverslip was placed over
351 the agar slab. Using a small paintbrush, the melted VALAP was carefully painted onto the gap between
352 the coverslip and the microscope slide to seal off the coverslip. Finally, a 23-gauge needle was used to
353 poke holes in the solidified VALAP to allow for gas exchange. The slide was then placed with the
354 microscope slide facing down onto the inverted microscope EVOS fl set to the 40x objective. Once an
355 adequate number of cells was observed in frame, the cells were allowed to settle for 2 hours before
356 imaging began. Images were then automatically taken every 30 mins for 72 hours. Videos of the budding
357 pattern were created using Adobe Premiere Pro.

358 *Growth of E. viscosa* JF 03-3F *and E. viscosa* JF 03-4F *on Different Medias*

359 Nine different fungal media were used to observe the growth of these novel fungi. These media
360 have been used for identification purposes and will be useful for future identification of this species
361 from other locations. Media used in this experiment were: MAG, MEA, MN, MNV, MN+NAG, PDA,
362 Spider, YPD, YPD+TE, and V8 (**Table 1**). Both isolates were first grown in 25 mL of liquid MEA in a 250 mL
363 Erlenmeyer flask at room temperature, shaking at 200 rpm for 5 days. Then 1 mL of each fungus was
364 aliquoted and washed 3 times with water. Washed cells were then applied to the media in three ways: 5
365 µL spotting (pipetting 5 µL of cells onto the plate), toothpick poking (poking a sterile toothpick tip into
366 the suspended cells and then onto a plate), and metal loop streaking (placing sterile metal loop into
367 suspended cells, then spreading cells onto plate in a decreasing manner). Cells were then allowed to
368 grow on the plates for 14 days. This provided us with different plating techniques that could potentially
369 yield different morphologies. Descriptions of colony color morphologies follow color nomenclature from
370 Ridgway (1912).

371 *Carbon Utilization*

372 Carbon utilization of each isolate was determined using a BioMerieux ID C32 carbon utilization
373 strip (Cat. No. 32200-1004439110). These strips have 30 different carbon sources in individual wells, one
374 well with no carbon source for a negative control, and one well with esculin ferric citrate. The esculin (β-

375 glucose-6,7-dihydroxycoumarin) ferric citrate assay is a colorimetric assay originally used to identify
376 Enterobacteria via production of a dark color in positive cultures for esculin degradation (Edberg et al.,
377 1977), and was co-opted to identify *Cryptococcus neoformans* (Edberg et al., 1980). Therefore, the dark
378 coloration that forms is due to the nature of the colorimetric assay, not due to extreme amounts of
379 melanized fungal growth. The inoculated strips were kept in a plastic box container with a lid and lined
380 with moist paper towels to reduce drying. The initial inoculum of cells was prepared in 25 mL of MEA
381 shaking at room temp for 5 days. Inoculation of the strips was done according to the instructions
382 provided by the vendor, and each strain was inoculated in three separate strips for triplicate replication.
383 Cells were diluted to the kit requirement of McFarland standard #3 (McFarland, 1907) before starting
384 the inoculum. Growth in the ID strip lasted 10 days before evaluation. Growth in each well was observed
385 and evaluated by eye. Each well was compared to the negative control (no carbon) and the positive
386 control (dextrose). Nuances of the fungal growth on individual carbon sources required a more gradual
387 scale, and so scores were adjusted to form a range of 1-5 to allow for more accurate average calculation
388 between the three replicates. For this scale: ”1” was no growth or equal to the kits “-“, ”5” was the most
389 growth and equivalent to the kit’s “+”; numbers in between allowed us to average out the replicates to
390 ensure we had a sliding scale of utilization rather than multiple variable “V” utilizations without a clear
391 idea of how variable the utilization was. Since triplicates were performed, we averaged the growth
392 results in each carbon source, and then determined the fungus’ carbon utilization profile from the
393 averages. The scale used goes as follows: no growth “-“ = 1.0-1.9, variable growth “v” = 2.0-3.6, growth
394 “+” = 3.7-5.0.

395 *Wavelength for Optical Density Determination*

396 The proper wavelength for optical density (OD) readings of these new strains was determined by
397 creating a standard curve. We performed a full spectrum analysis of serially diluted cells of these fungi
398 at their exponential growth phase. Cells were allowed to grow in 25 mL of MEA in a 250 mL Erlenmeyer
399 flask for 5 days. Then 200 µL of culture was removed, washed 3x with water, and diluted 1:1 in water
400 (100 µL of cells to 100 µL of MEA) 9 times to reach a maximum dilution of 1:256 (DF = 512). OD was
401 measured at wavelengths from 300 nm – 700 nm in 10 nm increments. Then the R^2 values for: OD to
402 percent difference at 25% dilution (DF=4) and below, OD to percent difference at 50% dilution (DF=2)
403 and below, OD to cell count at 2.19×10^6 cells/mL (DF=8) and below, OD to cell count at 4.38×10^6 cells/mL
404 (DF=4) and below, and OD to the consistency of the actual cell counts percent difference at 12.5%
405 dilution (DF=8) and below, were compared across all wavelengths to determine the most optimal

406 wavelength. The most optimal wavelength would have the highest R^2 values for all comparisons except
407 OD to the consistency of the actual cell counts percent difference at 12.5% dilution and below which
408 would have the lowest R^2 value. Optical density reads were done on the BioTek Synergy H1 hybrid
409 spectrophotometer.

410 *Nitrogen Utilization*

411 Nitrogen utilization tests were performed using ten different nitrogen conditions in MN base
412 media. 100 mM was the concentration used for all compounds that contained one nitrogen atom per
413 molecule: proline, ammonium tartrate dibasic, serine, sodium nitrate, glycine, glutamate, and aspartate;
414 50 mM was the concentration used for urea because it has two atoms of nitrogen per molecule; 1% w/v
415 of Peptone was used as a positive control and no nitrogen was added as a condition for a negative
416 control (**Table 3**). This concentration 100 mM was used because our standard growth media YPD
417 contains 20 g/L of peptone, which contains 14% total nitrogen by weight. 14% total nitrogen per gram of
418 peptone is 1.4 g of nitrogen per 100 mL of water, which if we use 1% peptone as a positive control that
419 equals 100 mM total nitrogen in 1% of peptone. Liquid minimal media (MN) with MN salts (not 20x
420 Nitrate salts) was used with the varying nitrogen sources to ensure that no alternative nitrogen source
421 would be available to the fungi. Fungi were first grown up in liquid MEA for 5 days at room temperature
422 to reach maximum density. Then, 1 mL of cells was removed and washed three times with water. 99 µL
423 of each nitrogen source-containing medium was added to six wells in a 96-well plate, for six replicates,
424 and 1 µL of the washed cells was added to each well. 100 µL of each medium was also added to one well
425 each without cells to blank each condition, because the different nitrogen sources created different
426 colors of medium. Daily growth was measured from day 0 to day 7 at 420 nm (the resulting optimal
427 wavelength for OD reads), using the BioTek Synergy H1 hybrid spectrophotometer.

428 *Optimal Growth Temperature and Range of Growth Temperatures*

429 To determine the temperature resistance range and optimal growth temperature for each
430 isolate, we grew both fungi at 4 °C, 15 °C, 23 °C (i.e., ambient room temperature), 28 °C, 37 °C, and 42
431 °C. Isolates were first grown up in 25 mL of MEA for 5 days at room temperature to maximum density.
432 Then 1 mL of cells was removed, and a 10x serial dilution was made from 0x to 100,000x, using pre-filled
433 1.5 mL tubes with 900 µL of MEA and adding 100 µL of the previous tubes each time. Then 5 µL of each
434 serial dilution was spotted onto a square MEA plate which allowed us to determine the carrying capacity
435 of each isolate at the different temperatures. Plates were kept at their respective temperatures for 7
436 days before observations were made, however the 37 °C and 42 °C plates were only kept at those

437 temperatures for two days and the incubators required cups of water inside of them to prevent the
438 plates from dehydrating. Plates grown in 42 °C and 37 °C were then allowed to grow at room temp for
439 up to a week to determine if the isolates died at these temperatures or if their growth was just arrested.

440 *UV Resistance*

441 Resistance to UV light was observed to determine if these black fungi, with highly melanized cell
442 walls and constant exposure to sunlight in their natural habitat, were UV resistant. To determine this,
443 we used the UVP HL-2000 HybriLinker UV crosslinker as our source of UV light, which has a UV
444 wavelength of 254 nm. Lower wavelengths (100-280 nm) are of the UV-C range, they are considered
445 ionizing radiation and are the most detrimental to living organisms, but are completely blocked by the
446 ozone layer (Molina & Molina, 1986; Schreier et al., 2015). Therefore, using this wavelength we are able
447 to push our organisms beyond the UV limits found in their natural habitat and test extreme amounts of
448 UV exposure.

449 The fungi were inoculated in 25 mL of MEA in a 250 mL Erlenmeyer flask and let grow under
450 shaking conditions at 200 rpm for 5 days at room temperature to reach maximum density. 100 µL of this
451 culture was then spread out onto 6 MEA plates, using a glass spreader. Three plates were kept as the
452 control growth, to compare to the three other plates which were exposed to the UV light. Experimental
453 plates were placed inside of the UV crosslinker with their lids taken off. Then the plates were exposed to
454 120 seconds of UV light from a distance of 9.5 cm to the light source at 10,000 $\mu J/cm^2$ (254 nm) (Frases
455 et al., 2007). We then wrapped all plates in aluminum foil and placed them in the Percival light incubator
456 set at 23 °C for 2 days. Placing UV-exposed cells in complete dark after exposure is essential for limiting
457 repair via photoreactivation (Weber, 2005). After 2 days the plates were removed from the aluminum
458 foil and left in the incubator for 5 more days before final observations were made. To determine
459 whether a particular isolate was resistant to UV exposure, the growth of the fungi exposed to UV was
460 compared to the control growth in imageJ, by comparing the pixel areas of the plates.

461 *Metal Resistance*

462 Metal resistance is a relatively universal trait in many polyextremotolerant fungi. Due to the
463 under-studied nature of this particular characteristic in BSCs and fungi, we decided to test if any of our
464 isolates were resistant to any heavy metals which would indicate possible bioremediation capacity. In
465 order to test metal resistance, we used the antibiotic disk method by aliquoting metal solutions onto
466 paper discs and observing zones of clearance. Metals and concentrations used are listed in **Table 4.** For
467 testing, 5 µL of each metal solution was aliquoted onto a dry autoclaved Whatman filter paper disc

468 which was created using a standard paper hole puncher. These discs were then allowed to air dry and
469 kept at 4 °C for up to a week. Initial growth of the fungi (*E. viscosa* JF 03-3F, *E. viscosa* JF 03-4F, *E.*
470 *dermatitidis*, and *S. cerevisiae* ML440) was done in 25 mL of MEA, shaking at 200 rpm for 5 days at room
471 temperature. We then spread 100 µL of each fungus onto 100 mm sized MEA plates using a glass
472 spreader to create a lawn. Using flame sterilized tongs our metal paper discs were placed onto the
473 center of the petri dish on top of the fungal lawn and lightly pressed down to ensure the metal disc was
474 touching the plate completely. These plates were then placed in the Percival light incubator at 23 °C
475 with a 12 hr light/dark cycle for up to 2 weeks. Once a zone of clearing was clearly visible amongst the
476 fungal growth (1-2 weeks), the zone of clearing was then measured in cm. Generally, large zones of
477 clearing indicated sensitivity to the metal, whereas zones of reduced size were consisted with resistance
478 to the metal.

479 *Lipid Profiles*

480 Comparison of the lipid production of *S. cerevisiae*, *E. dermatitidis*, *E. viscosa* JF 03-3F, and *E.*
481 *viscosa* JF 03-4F was performed in the presence of fermentable vs. non-fermentable sugars in high and
482 low nitrogen. To test these conditions, we grew all four fungi in four different media types. 1) MEA; 2)
483 MEA + 20 g/L of peptone instead of 2 g/L; 3) MEA with the dextrose replaced with the same weight
484 amount of glycerol; 4) MEA with glycerol instead of dextrose and 20 g/L of peptone instead of 2 g/L. All
485 four fungi were first inoculated in 25 mL of liquid MEA in a 250 mL Erlenmeyer flask and shaken at 200
486 rpm for 5 days at room temperature to reach peak density. Then 100 µL was inoculated into 5 mL of
487 each media in a size 25 mm tube, placed in a roller drum and allowed to grow at room temperature for 5
488 days.

489 To observe their lipid profile, we performed a standard Bligh Dyer lipid extraction (Bligh & Dyer,
490 1959). Equal wet weight of each organisms' cells was pelleted and re-suspended in 2 mL of methanol
491 inside of 16 mm glass tubes. Tube openings were covered in Duraseal before applying the lid of the
492 tube, then samples were boiled for 5 minutes and let cool for 10 minutes. Then 2 mL of chloroform and
493 1.6 mL of 0.9% NaCl were added, and the tubes were vortexed to fully mix. Tubes were then centrifuged
494 at 5000 rpm for 5 minutes to separate the layers. The bottom lipid layer of the suspension was removed
495 and placed in a new glass tube which was then dehydrated using nitrogen gas till the samples became
496 fully dried. Dehydrated samples were then re-suspended with 100 µL of a 9:1 ratio of chloroform :
497 methanol to run the thin layer chromatography (TLC) with.

498 For all samples except the *S. cerevisiae*, 7 µL of the lipid suspension was used to dot the TLC. For
499 *S. cerevisiae,* 10 µL of the lipid suspension was needed. The solvent systems used for TLC were
500 chloroform : methanol : glacial acetic acid: water 85:12.5:12.5:3 for the polar lipid solvent system, and
501 petroleum ether : diethyl ether : acetic acid 80:20:1 for the neutral lipid solvent system. The TLC plates
502 were loaded with 7 or 10 µL of the re-suspended samples, and they were placed in the polar solvent
503 system for approximately 30 minutes (half-way up the plate) before transferring to the neutral lipid
504 solvent system in a separate container till the solvent front reached just a few cm below the top of the
505 plate. The plate was then removed and dried for 15 minutes, until the solution on the plate was no
506 longer volatile by smell, and the plate was placed in the presence of iodine (Sigma-Aldrich cat. No.
507 207772) in a glass chamber for 5 minutes until all the lipids were visible. The plates were then
508 immediately placed in plastic covers and scanned and photographed for visualization and
509 documentation.

510 Melanin Biosynthesis and Regulation Experiments:

511 *Melanin Biosynthesis Gene Annotation*

512 Melanin biosynthesis in fungi occurs via three different pathways: the 1,8-DHN pathway which
513 creates allomelanin, the L-DOPA pathway which creates pheomelanin, and the tyrosine degradation
514 (HGA) pathway which creates pyomelanin (Cao et al., 2021; Gessler et al., 2014) (**Figure 1**). Most fungal
515 species only contain one melanin biosynthetic pathway, but there are many species in Pezizomycotina,
516 particularly in the genera *Aspergillus* and *Exophiala*, which are capable of producing two or all three
517 forms of melanin (Perez-Cuesta et al., 2020; Teixeira et al., 2017). For that reason, we decided to
518 manually annotate the *E. viscosa* JF 03-3F and *E. viscosa* JF 03-4F genome sequences to determine if
519 they too possessed multiple melanin biosynthetic pathways. In all cases, the relevant *A. niger* and *A.*
520 *fumigatus* proteins were used as queries (Chen et al., 2014; Teixeira et al., 2017). Protein sequences for
521 each gene were found using the Aspergillus genome database (AspGD) (now called FungiDB
522 https://fungidb.org/) and were tested using protein-protein BLAST against the filtered model proteins
523 database of *E. viscosa* JF 03-3F *and E. viscosa* JF 03-4F on Mycocosm. Since *A. niger* contains paralogs for
524 some melanin biosynthetic genes, all genes listed in Teixeira et al. and Chen et al. (2014; 2017) were
525 used as queries for BLAST searches. Additionally, the enzyme sequences for scytalone dehydratase
526 (Arp1) and 1,3,8-trihydroxynapthelene reductase (Arp2) are not homologous between *A. niger* and *A.*
527 *fumigatus* (Jørgensen et al., 2011), therefore both species' protein sequences were used for BLASTing
528 against *E. viscosa* JF 03-3F and *E. viscosa* JF 03-4F. Once the melanin biosynthetic genes in *E. viscosa* JF

529 03-3F and *E. viscosa* JF 03-4F were identified, their highest matching protein sequences were then
530 reverse BLASTed to the *A. niger* genome to determine the reciprocal best hit to ensure true homology.
531 Similarity scores (>40%), e-values ($<10^{-6}$), and bit scores (>50) of the protein-protein BLASTs followed
532 standards for homology laid out by Pearson (2013).

533 *Regulation of Melanin Production Using Chemical Blockers*

534 Once it was established that both isolates contain the potential for production of all three fungal
535 melanins, we wanted to determine which melanin was actively being produced using chemical blockers
536 of the 1,8-DHN and L-DOPA melanin production pathways. DHN-melanin blocker phthalide and the L-
537 DOPA melanin blocker kojic acid, were both used to determine which melanin was being actively
538 produced. Stock solutions were made according to (Pal et al., 2014): phthalide was diluted in 70%
539 ethanol, and kojic acid in DMSO. Three separate experiments were performed using these melanin
540 blockers, to determine which method would provide the most informative results.

541 The first was the disc diffusion method whereby Whatman filter paper discs were autoclaved
542 and impregnated with 5 µL of either 10 mM of phthalide or 10 mg/mL of kojic acid. Impregnated filter
543 paper discs were then placed on top of freshly spread lawns of either isolates on both MEA and YPD.
544 Lawns were of 50:50 diluted 5-day old cells grown in MEA, and 100 µL of this dilution was spread onto
545 the petri plates with a glass spreader. These plates were then grown at 23 °C with 12 hr light/dark cycles
546 for 5 days. Additionally, both a kojic acid disc and phthalide discs were placed on fungal lawns ~4 cm
547 apart simultaneously to observe their specific melanin-blocking capabilities on the same cells.

548 Next, we tried adding the melanin blockers directly to the medium as was done in Pal et al.
549 (2014). Since melanin is more universally distributed in *Exophiala* cells compared to *Aspergillus* cells, we
550 decided to use the highest concentration of both kojic acid and phthalide that was used by Pal et al.
551 (2014), which was 100 mM of each compound. This concentration of each compound was added to both
552 solid YPD and MEA after autoclaving, chemicals were added both individually and combined. These
553 plates were then used for two forms of growth experiments, serial dilutions and lawn growth. We
554 spread a lawn of either fungus onto YPD and MEA with and without kojic acid, phthalide, and both
555 compounds at 100 mM each. And we performed a 10x serial dilution of both *E. viscosa* JF 03-3F and *E.*
556 *viscosa* JF 03-4F up to 10,000x diluted, and spotted 5 µL of each dilution onto MEA plates with and
557 without Kojic acid, Phthalide, and both compounds. We let both growth experiments grow at 23 °C for 5
558 days with a 12 hr light/dark cycle.

559 *Evaluating the Cause of Melanin Excretion*

560 To assess the role of organic nitrogen levels in melanin excretion, we initially switched the
561 concentration of peptone added to YPD and MEA media such that the new media were YPD + 0.2%
562 peptone, and MEA + 2% peptone. *E. viscosa* JF 03-3F and *E. viscosa* JF 03-4F were grown in liquid MEA
563 for 5 days with shaking at room temperature and were plated onto these new media using the same
564 technique as described above for growth comparison on different media. To determine if a more
565 gradual increase in peptone would correlate with a gradual excretion of melanin, we took the base
566 media of MEA (solid) and changed the concentration of peptone to 0.1%, 0.5%, 1%, 1.5%, 2%, 2.5%, 3%,
567 3.5%, 4%, and 5%. We then spotted 5 µL of both strains onto the plates after performing a 10x serial
568 dilution up to 10,000x dilution. The plates were grown at 23° for 10 days with a 12 hr light/dark cycle.

569 Additionally, we tested if tyrosine levels (a direct precursor for L-DOPA and HGA-derived
570 melanin) were the source of the increased melanin excretion in the increased peptone experiment.
571 Growth of 5 µL spots of *E. viscosa* JF 03-3F and *E. viscosa* JF 03-4F were grown on "Tyrosine media"
572 (Jalmi et al., 2012) (2% w/v dextrose, 1% w/v peptone, 0.1% w/v yeast extract (**Table 1**)): without added
573 tyrosine, with 0.5 g/L tyrosine, with 1 g/L tyrosine, and MN-nitrate 2% w/v dextrose with 0.5 g/L tyrosine
574 as the sole nitrogen source. Colonies were allowed to grow for 19 days and then observations were
575 made to see if melanin excretion was induced by different tyrosine levels.

576 *Melanin Extraction and Spectrophotometric Measurements*

577 Extraction of melanin from a variety of sources has been performed using two different
578 approaches: chemical extraction and enzymatic extraction (Pralea et al., 2019). We performed both
579 chemical and enzymatic extractions on our fungi's melanin. The enzymatic extraction method that was
580 used came from Rosas et al. (2000), and the chemical extraction method, which has been used more
581 extensively in previous works, was derived from Pal et al. (2014). Pal et al.'s method for extraction and
582 purification of melanin from culture filtrate was adapted and used for all future melanin extractions,
583 mainly supernatant melanin extractions. Adjustments to the Pal et al. method included: the 6M HCl
584 precipitation took multiple days instead of overnight for melanin to precipitate, and the protocol was
585 stopped when 2M NaOH was added to the extracted melanin. We did not continue on to re-
586 precipitation and drying of the melanin as this product did not reprecipitate in any solvents used.

587 Exact methods are as follows. 10 mL of culture was centrifuged at 3,000x g for 5 minutes, and
588 the resulting supernatant was filter sterilized through a 2 µm filter to ensure all cells were removed. The
589 filtered supernatant was then transferred into a 50 mL centrifuge tube, and 40 mL of 6M HCl was added
590 to the tube. The filtrate was then allowed to precipitate out for up to two weeks. Precipitated solutions

591 were then centrifuged at 4000x g for 3 minutes, and the resulting supernatant was discarded. The pellet
592 was washed with 2 mL of dd H_2O, vortexed, centrifuged, and the supernatant discarded. Then 3 mL of
593 1:1:1 chloroform : ethyl acetate : ethanol was added to the samples and vortexed vigorously to ensure
594 re-distribution of the melanin. The tubes were then centrifuged at 4,000x g for 1 minute, and any
595 resulting clear layers (top and or bottom) were discarded, leaving behind the dark layer. 2 mL of water
596 was added to the sample for washing, and the tubes were centrifuged at 4,000x g for 1 minute, and the
597 entire supernatant was discarded. Finally, 1 mL of 2M NaOH was added to each sample to allow for a
598 standard volume added even if the melanin amount and therefore the final volume varied.

599 Extracted melanin samples suspended in 1 mL of 2M NaOH were then diluted 5 µL into 195 µL of
600 2M NaOH into a 96-well plate, with a 200 µL 2M NaOH blank well. These diluted samples were then read
601 using the BioTek Synergy H1 hybrid spectrophotometer. The settings were for a full spectrum read from
602 230 nm to 700 nm, with 10 nm steps. However, the machine could not read OD values above 4.0, and
603 therefore only data from 300 nm to 700 nm was used.

604 *Confirming Active Melanin Excretion from Living Cells and Determining its OD Amount in the Supernatant*

605 To confirm that *E. viscosa* JF 03-3F and *E. viscosa* JF 03-4F were actively excreting melanin, as
606 opposed to dead cells lysing and releasing it, we grew up both strains and took daily aliquots for melanin
607 extraction. We use the term excrete/excreting instead of secrete/secreting for the terminology of
608 melanin being released into the media by the fungi because we have no evidence currently that this
609 melanin release mechanism is an active process (i.e.: via Golgi, efflux pumps, or autophagy) warranting
610 active secretion. Additionally, we wanted to compare the melanin excretion capabilities of these strains
611 to *E. dermatitidis* for a baseline comparison. All three fungi were grown up in liquid MEA shaking at
612 room temperature for 5 days. Then 2 mL of cells were washed with water three times. 500 µL of washed
613 cells were then inoculated into 100 mL of MEA and YPD in 500 mL flasks. We let the cells grow at 23 °C
614 shaking at 200 rpm for 7 days, removing 11 mL of cells and supernatant daily and pipetting them into 15
615 mL centrifuge tubes. The tubes of cells were then centrifuged at 3000x g for 5 minutes, the supernatant
616 was removed, filter sterilized through a 2 µm filter, and placed into a new tube. We filter sterilized the
617 supernatant to ensure that no cells remained in the supernatant, therefore all of the melanin extracted
618 came only from excreted melanin. Melanin was then extracted using the chemical method explained
619 above. Resulting pure melanin for all samples was read with the full spectrum as stated above, and both
620 standard OD and log scale graph were created to confirm the presence of melanin with the proper R^2
621 value above 0.9 (Pralea et al., 2019).

622 Albino Mutant Creation for Genetic Analysis of Melanin Production:

623 *Creation of EMS Mutants and Annotation of their Mutations*

624 Genetic modification of *E. viscosa* has not been established yet. Therefore, random mutagenesis
625 was performed using ethyl methanesulfonate (EMS) to induce G:C to A:T mutations EMS mutagenesis
626 was performed using the method by Winston (2008). Albino mutants and other interesting pigmentation
627 or morphological mutants were isolated from the resulting mutagenesis, and their DNA was extracted
628 using the CTAB DNA extraction protocol described above. DNA was then sent to the former Microbial
629 Genome Sequencing Center (MiGS; https://www.migscenter.com/; 355 Fifth Avenue, Suite 810
630 Pittsburgh, PA 15222, now called SeqCenter (https://www.seqcenter.com/ ; 91 43rd Street, Ste. 250
631 Pittsburgh, PA 15201) for genome re-sequencing and base-called against the wild-type genome
632 sequences. Resulting mutations were then manually annotated using the JGI Mycocosm genome
633 "search" tool to identify affected genes.

634 *Recovery of Melanin Production in Albino Mutants: Modern use of the Classical Beadle and Tatum*
635 *Biochemical-Genetics Experiment*

636 Following recovery of an albino mutant, we attempted to restore melanin production via
637 chemical induction of the other melanin biosynthetic pathways. We did this using hydroxyurea (HU), L-
638 DOPA, 1,8-DHN, and tyrosine. Hydroxyurea has been shown to enhance melanin production in *E.*
639 *dermatitidis*, and L-DOPA is needed for certain fungi to produce melanized structures, including the
640 albino mutant form of *E. dermatitidis* WdPKS1 (Dadachova et al., 2007; Paolo et al., 2006; Schultzhaus et
641 al., 2020). Both YPD and MEA medium was made up and 20 mM of HU, 1 mM of L-DOPA, or 1 mM of
642 1,8-DHN was added to the medium after autoclaving. 5 µL of albino and wildtype control cells were
643 spotted onto these media with added compounds, and they were grown for 10 days at 23 °C 12 hr
644 light/dark cycle.

645 Additionally, we also tested the presence of tyrosine, the starting compound for L-DOPA and
646 HGA melanins on the albino mutant. Growth of 5 µL spots of EMS 2-11 was grown on "Tyrosine media"
647 (Jalmi et al., 2012) (2% w/v dextrose, 1% w/v peptone, 0.1% w/v yeast extract (**Table 1**)): without added
648 tyrosine, with 0.5 g/L tyrosine, with 1 g/L tyrosine, and MN-nitrate 2% w/v dextrose with 0.5 g/L tyrosine
649 as the sole nitrogen source. Colonies were allowed to grow for 19 days and then observations were
650 made to see if melanization was recovered by different tyrosine levels.

651 ***Data Availability***

652 All data generated is available through the JGI Mycocosm website under *E. viscosa* JF 03-3F and
653 *E. viscosa* JF 03-4F, or at NCBI under accession numbers JALDXI000000000 for *E. viscosa* JF 03-3F and
654 JALDXH000000000 for *E. viscosa* JF 03-4F. Transcriptomes for these fungi can be found at NCBI using the
655 SRA numbers: SRX5076261 for *E. viscosa* JF 03-3F, and SRX5077344 for *E. viscosa* JF 03-4F. All accession
656 numbers from all databases for both strains are listed in **Table 5**. The strains of *E. viscosa* JF 03-3F CBS
657 148801 and *Exophiala viscosa* JF 03-4F CBS 148802 have also been deposited to the Westerdijk institute
658 in a metabolically inactive state for access to the scientific community, but all strains used in this study
659 can also be obtained from the corresponding author upon request. Finally, if any additional details or
660 questions are required for the replication of any experiments listed above, one may reach out to the
661 corresponding author.

662

663 ## Results

664 *Fungal Isolation, ITS Alignment, and General Morphological Observations*

665 Two fungi were isolated from BSCs located near Jackman Flats Provincial Park in B.C., Canada
666 (Latitude: 52.94997°, Longitude: -119.41919°, Altitude: 738). Biological soil crust samples were diluted in
667 water, crushed with a plastic micropestle, and plated out onto MEA with antibiotics and cycloheximide,
668 and grown at 23 °C for 2 weeks to obtain the isolates. Once colonies began to form, they were picked
669 and struck out onto regular MEA to obtain pure cultures. DNA extractions were performed on liquid
670 cultures of the isolates that had been grown in liquid MEA for 5 days at 23 °C and 160 rpm of shaking.
671 PCR amplification of the isolates' ITS region was performed and then sequenced using Sanger
672 sequencing. The resulting ITS sequences placed the fungal isolates within the genus *Exophiala*, and later
673 apparent sequencing errors created nucleotide differences in their ITS sequences which initially placed
674 them as different species. Further whole genome sequencing using Illumina based sequencing allowed
675 for more accurate sequences of the ITS region for these isolates.

676 Using the Illumina-based ITS sequences of the isolates, it was determined that they have 100%
677 identity to each other's ITS sequence (**Supplementary File 1**). BLAST results to their ITS sequences using
678 the UNITE simple analysis (Nilsson et al., 2019) resulted in a 97.57% identity to "*Exophiala nigra* strain
679 CBS 535.95" accession number: MH862481.1, which was performed on September 29th, 2022. UNITE's
680 fungal species identification delineation typically separates species on ITS sequence similarity with ≥98%
681 as the cut-off (Kõljalg et al., 2013), indicating that via ITS sequence alone, our *Exophiala* isolates

682 (introduced here as *E. viscosa* JF 03-3F and JF 03-4F) were a separate species from *E. nigra*. However,
683 since that date, the UNITE database has been further curated with more strict parameters and now only
684 contains 19 *Exophiala* species, removing *E. nigra* and *E. sideris* as species in Taxon name searches.
685 Repeating this analysis on December 12th, 2022, resulted in a BLAST result of *Capronia acutiseta*
686 UDB035414 86.16% identity as the highest match.

687 Although both *E. viscosa* JF 03-3F and *E. viscosa* JF 03-4F are two strains of the same species
688 indicated via their marker gene alignment, their cellular morphology and budding patterns differ
689 drastically as described below. Both strains form smooth, shiny, sooty black colonies on PDA after 9 days
690 of growth at 23 °C. When grown on high organic nitrogen media such as YPD, they will begin to excrete
691 melanin into the agar by day 7 when grown at 23 °C, and by day 3 in liquid YPD (**Figures 4L, 5L, & 14**). On
692 MEA, they are greyish brown in color, have the consistency of sticky black tar (**Videos S1 & S2**), and an
693 iridescent rainbow shine which forms on their colonies after a week at 23 °C (**Figures 4K, 5K & S3**). These
694 fungi also fail to easily disperse when suspended in water but can be readily pelleted. These
695 observations and the prominence of lipid bodies within the cells (**Figure S4**) suggested that lipid-derived
696 compounds could cause their sticky, water repelling, iridescent nature. These isolates grow to their
697 maximum density in 7 days at 23 °C in 25 mL of MEA in a 250 mL Erlenmeyer flask shaken at 160 rpm.
698 Both *E. viscosa* JF 03-3F and *E. viscosa* JF 03-4F have been preserved in a metabolically inactive state at
699 the Westerdijk institute.

700 *Phylogenetic Placement of Exophiala viscosa Amongst the Genus Exophiala*

701 Phylogenetic analyses were performed using the marker genes 18S rDNA (1,600 bp), 28S rDNA
702 (548 bp), and ITS rDNA (547 bp), with a combined sequence length of 2,685 base pairs. These genes
703 were chosen because while they are predominant marker genes, they are also the only genes available
704 on NCBI for the species *Phaeoannellomyces elegans*, which has been identified as closely related to this
705 clade regardless of its nomenclature (Moussa et al., 2017). Bayesian analysis of the multi-locus gene tree
706 yielded the best scoring tree, with the final log likelihood value of -9,031.1. Estimated base frequencies
707 were: A = 0.242, C = 0.23, G = 0.275, and T = 0.253; with substitution rates of: AC = 0.161, AG = 0.151, AT
708 = 0.143, CG = 0.067, CT = 0.412, GT = 0.065. The shape parameter of the gamma distribution of rate
709 variation alpha was 0.141, and the total tree length was 0.574. The final average standard deviation of
710 split frequencies at the end of the total 500,000 MCMC generations was 0.002955.

711 The multi-locus combined Bayesian inference and Maximum likelihood tree placed *E. viscosa*
712 within the monophyletic clade composed of *E. nigra*, *E. sideris*, *E. bergeri*, and *P. elegans* with a posterior

713 probability of 100% (**Figure 2**). In this combined Bayesian and Maximum likelihood tree, *P. elegans* is
714 placed with 100% posterior probability and a bootstrap value of 100 as related to *E. sideris* and distinct
715 from *E. nigra*. Additionally, *E. nigra* is further separated from *E. viscosa*, placing *E. nigra* on its own node
716 beneath *E. bergeri* with 100% posterior probability and 100 bootstrap value (**Figure 2**). Both strains of
717 the new fungus *E. viscosa* form a monophyletic node separate from *E. nigra*, *E. sideris*, *E. bergeri,* and *P.*
718 *elegans* with a posterior probability of 100%, providing supporting that these strains are a novel species.

719 One additional marker gene sequence is available for *E. nigra* which is not available for *P.*
720 *elegans*, and that is *RPB1*. When *RPB1* (464 bp) is added to the gene concatenation, creating the
721 combination of 18S, 28S, ITS, and *RPB1* (3,156 bp total), *E. nigra* is again placed on its own node below *E.*
722 *bergeri* maintaining a separate position to *E. viscosa* and the *E. sideris* clade with 100% posterior
723 probability and 79 bootstrap value (**Figure S2**). This tree also shows *E. sideris* as the closest relative to *E.*
724 *viscosa* with 100% posterior probability and a bootstrap value of 100. Within the three gene
725 concatenation (18S, 28S, and ITS), the percent identical base pairs between *E. viscosa* and *E. sideris* are
726 98.436%, and 99.07% identical bases between *E. viscosa* and *E. nigra*. However, when *RPB1* is added to
727 the concatenation, the percent identical bases between *E. sideris* and *E. viscosa* remain similar at
728 98.551%; whereas percent identical bases between *E. viscosa* and *E. nigra* becomes 97.03%. Percent
729 identity matches between all species represented in the phylogenetic trees of Figure 2 and Figure S2
730 across all genes and gene concatenations are provided in **Supplemental File 1**. Further phylogenetic
731 analyses were performed on all *Exophiala* species and related fungi who have been whole genome
732 sequenced, and whose genomes are available in JGI's Mycocosm. With their whole genomes, we were
733 able to perform single-copy homologous protein sequence approximate maximum likelihood
734 phylogenetic analyses, providing additional support for *E. viscosa*'s intraspecific variation from
735 specifically the fungus *E. sideris*. Our approximate maximum likelihood single-copy homologous protein
736 phylogenetic tree shows with 100 bootstrap value, that *E. sideris* is separate from *E. viscosa* (**Figure 3**).

737 ASAP values of the marker genes allowed us to confirm our phylogenetic inferences of
738 separating *E. viscosa* from the other species in its clade. For the ITS-only ASAP analysis, the output
739 provided an ASAP score of 1.0 to 18 distinct species with a distance threshold of 1.32% (**Supplemental**
740 **File 2**). Both strains of *E. viscosa* were considered one species, and *E. sideris* and P. elegans were
741 considered one species. When ASAP was performed on the concatenated 18S-28S-ITS alignment, it
742 maintained that there should be 18 distinct species (ASAP score of 2.0), with both strains of *E. viscosa* as
743 one species and *E. sideris* and *P. elegans* as one species. However, with the three-gene concatenation,

744 the distance threshold decreased to 0.75%. Finally, the concatenation of 18S-28S-ITS-*RPB1* provided an
745 ASAP score of 2.5 which suggested that there be 16 species with a distance threshold of 2.5%,
746 combining both strains of *E. viscosa* into one species, and combining *E. aquamarina* and *E. pisciphila* into
747 one species (*E. crusticola* and *P. elegans* are not in this dataset). All three ASAP analyses suggest that
748 both strains of *E. viscosa* remain as one species, and that they are a distinct species from the other
749 *Exophiala* spp.

750 *Morphological Differences Between E. viscosa Strains JF 03-3F and JF 03-4F*

751 While these two strains of *E. viscosa*, JF 03-3F and JF 03-4F, are very similar to each other in
752 genomic content and have 100% similarity across the four marker genes 18S, 28S, ITS, and *RPB1*, they
753 vary in gene synteny, they contain multiple single nucleotide polymorphisms across their genomes, and
754 their morphologies differ. *E. viscosa* JF 03-3F is found primarily as a yeast morphology on all media
755 tested, with ellipsoidal cells 4.4 µm ± 0.34 µm wide and 5.36 µm ± 0.37 µm long (n=20 cells measured; in
756 MEA). *E. viscosa* JF 03-4F is found primarily in a pseudohyphal form on all medias tested, with more
757 elongated cells 3.6 µm ± 0.38 µm wide and 6.0 µm ± 0.67 µm long (n=20 cells measured; in MEA). *E.*
758 *viscosa* JF 03-3 will form pseudohyphae when grown for longer than 2 weeks and only on solid media,
759 whereas *E. viscosa* JF 03-4F readily forms pseudohyphae in liquid media and on solid media as a primary
760 growth from and will form a few true hyphae after 3 weeks of growth on MEA (**Figures 5N, 6, & Video**
761 **S3**). As seen in **Figures 6 & S3D**, the cellular morphology of *E. viscosa* JF 03-4F resembles that of *Hortaea*
762 *werneckii* as observed by Mitchison-Field et al. (2019). Budding of *E. viscosa* JF 03-3F cells occur at 180°
763 or 90° from the mother cell's origin, whereas JF 03-4F is almost exclusively budding 180° from the
764 mother cell. When *E. viscosa* JF 03-4F is grown up to maximum density in liquid culture, pipetting
765 becomes difficult due to large clumps of cells formed by its more filamentous growth pattern (**Figures**
766 **5N & 6**). However, *E. viscosa* JF 03-3F at maximum density in liquid culture does not form large clumps,
767 and therefore creates no pipetting issues. Notably, *E. viscosa* JF 03-4F possesses a looser pellet and is
768 less refractory to re-suspension than *E. viscosa* JF 03-3F. *E. viscosa* JF 03-4F also produces a fuller,
769 thicker biofilm at the air-liquid interface than *E. viscosa* JF 03-3F, as seen in **Figures 4I & 5I**. *E. viscosa* JF
770 03-3F is also a much more prolific melanin excreter than *E. viscosa* JF 03-4F (**Figures 14, 15, & 16**).

771 *Recognition of Novel Taxon Exophiala viscosa*

772 The new species *Exophiala viscosa* is defined based on molecular phylogenetic analyses of the
773 four marker regions: 18S, 28S, ITS, and *RPB1* resulting in the holotype and the additional strain forming
774 one monophyletic node separate from *E. sideris, P. elegans, E. bergeri* and *E. nigra* which are its closest

775 relatives, with the genes ITS and *RPB1* providing the most support for intergenic variation (**Figures 2** &
776 **S2**). Additional phylogenetic support results from the single-copy gene tree of whole genome sequenced
777 *Exophiala* spp. and related fungi, which further supports intraspecific variation of *E. viscosa* from *E.*
778 *sideris* (**Figure 3**). Whole genome sequencing and then single-copy gene phylogenetic analyses of *E.*
779 *nigra* and *P. elegans* would have been beneficial for further elucidation of this fungus, but that was not
780 feasible at this time. Additionally, ASAP values of all three gene/gene concatenations tested were in
781 consensus that *E. viscosa* is a separate species from *E. sideris*, *E. bergeri*, *P. elegans*, and *E. nigra*.

782 Morphological comparison of *E. viscosa* to *E. nigra* from images in Moussa et al. show
783 differences in colony and cell morphology (2017). Colonies of *E. nigra* on MEA showed no rainbow sheen
784 and remained olivaceous black, with irregular undulate colony edges (Moussa et al., 2017). Whereas *E.*
785 *viscosa*'s colonies are smooth to curled, are dark grayish brown in color, and have a rainbow sheen. *E.*
786 *nigra* colonies on PDA were also irregular and undulate on the edges and umbonate or lumpy on the
787 elevation morphology (Moussa et al., 2017), whereas *E. viscosa* has smooth and circular edges with a
788 flat elevation on PDA (**Figures 4E & 5E**). Cellular morphology images of *E. nigra* on MEA showed
789 pseudohyphae to hyphal formation with conidia forming on the tips of hyphae (Moussa et al., 2017).
790 Pseudohyphae are observed in *E. viscosa* on MEA, but hyphae are rarely observed except in the strain JF
791 03-4F, and no conidia were observed forming at the tips of pseudohyphae or hyphae on MEA even after
792 three weeks. No characteristic asexual or sexual structures of *Exophiala* species were observed in either
793 strain on any medias or conditions tested on *E. viscosa*.

794 The other closest relative of *E. viscosa* is *E. sideris*. Multiple strains of *E. sideris* were isolated
795 from primarily arsenate and other metal-contaminated locations, and the holotype strain is isolated
796 from *Sorbus aucuparia* berries in The Netherlands (Seyedmousavi et al., 2011). These specific locations
797 and environments are distinct from those in which *E. viscosa* has so far been recovered. The differences
798 between a BSC environment and a berry or rock surface would be the permanence of the location (in
799 reference to the berry surface) and the abundance and make-up of microbial neighbors (i.e.:
800 cyanobacteria, algae, specific lichens, and bacteria) (Couradeau et al., 2019; Nunes da Rocha et al.,
801 2015). Additionally, while arsenate was not a metal tested on *E. viscosa*, the other metals tested on both
802 strains of this fungus did not indicate increased metal resistance, and showed less resistance to $CoCl_2$,
803 $AgNO_3$, and $CuCl_2$ than *S. cerevisiae* (**Table 9**). Neither sexual nor asexual structures were observed in *E.*
804 *viscosa* on all medias and conditions tested including on PDA after 30 days, whereas *E. sideris* readily
805 forms conidia on PDA (Seyedmousavi et al., 2011). Attempts at inducing asexual or sexual development

806 for both *E. viscosa* strains were performed using established methods: Modified Leonian's agar from
807 Untereiner (1994), Untereiner & Naveau (1999), and Potato dextrose agar via methods from
808 Seyedmousavi et al. (2011), but were not successful.

809 The isolates described here are the first described instance of this fungus being cultured. This is
810 only the second instance of an *Exophiala* species being isolated from a BSC, the first being *E. crusticola*
811 (Bates et al., 2006). The ITS sequences of *E. viscosa* and *E. crusticola* have 82.904% identity
812 (**Supplemental File 1**), and therefore they are not the same species, which is supported by the
813 phylogenetic tree in **Figure 2**. It is also the first instance of an *Exophiala* species being isolated from a
814 BSC in Canada, as opposed to the Western United States where *E. crusticola* was isolated. In terms of
815 other instances of *E. viscosa*'s presence in biological samples, according to BLAST results of *E. viscosa*'s
816 ITS region on NCBI there has been one instance of another 100% identical fungal DNA from a rocks
817 surface with the accession number AY843177. Unfortunately, this fungal DNA is from an unpublished
818 article according to NCBI. Additional fungal ITS ribosomal DNA that closely matched *E. viscosa*'s via
819 BLAST on NCBI with 99.26% identity were: MZ017038, MZ016619, MZ016618, all of which were DNA
820 samples labeled "Fungal sp." from *Pinus ponderosa* either roots or needles from Arizona (USA) (Bowman
821 & Arnold, 2021).

822 *Taxonomy and Species Descriptions of E. viscosa*

823 ***Exophiala viscosa* JF 03-3F Goopy** E.C. Carr, S.D. Harris, **sp. nov.**

824 MycoBank MB845198

825 **Figure 4**

826 *Typification:* CANADA. BRITISH COLUMBIA: Adjacent to Fraser-Fort George H, Jackman Flats
827 Provincial Park (Lat.: 52.95; Long.: -119.416; Alt.: 783), in biological soil crust sample, sampled June
828 2015, *S. Harris*, isolated July 2015, *E. Carr*. Holotype culture strain JF 03-3F Goopy: CBS 148801.
829 Additional strains JF 03-4F Slimy: CBS 148802.

830 *GenBank*: Whole genome = JALDXI000000000.1

831 *NCBI Taxonomy ID*: 2486360

832 *Etymology*: *Exophiala viscosa* was colloquially referred to as "Goopy" due to the nature of its
833 yeast morphology lending to a very goopy colony. Accordingly, we have formally named it *Exophiala*
834 *viscosa* for the Latin term of viscous.

835 *Sexual and asexual morph*: not observed.

836 *Culture characteristics:* Hyphae not observed in liquid culture, aerial pseudohyphae in colonies
837 observed by day 30 in Malt Extract medium (MEA), primarily found in yeast form in liquid MEA and Yeast
838 Peptone Dextrose (YPD) mediums (23 °C) but will form pseudohyphae as well. Cells in MEA liquid culture
839 are ellipsoid in shape, 3.9 µm ± 0.55 µm wide and 5.66 µm ± 0.62 µm long (n=40 cells measured). Cell
840 walls start off thin and become thicker over time. In pseudohyphal form on solid MEA, budding occurs at
841 180° or 90° from the mother cell's origin, or at acute angles from the previous bud site. Cells either
842 maintain size and shape of yeast form as pseudophyphal cells bud out for four buds then begin to
843 elongate, or the buds begin to elongate from the first bud and continue to elongate with each linear
844 budding. Colony morphology all at 23 °C with a 12 hour light/dark cycle: on MEA colonies are initially
845 shiny dark grayish brown and smooth to curled, then develops a rainbow sheen with a colony size of 5.2-
846 6.6 mm by day 14, additionally dark supernatant is observed in liquid MEA culture starting on day 3; on
847 Malt Extract Agar with vitamins and trace elements (MAG) colonies are sooty black and glossy with
848 smooth colony edges forming a dome shape, and 6.3-8.1 mm growth is observed on day 14; on Minimal
849 media (MN; nitrate with salts) + N-acetyl Glucosamine as the carbon source, the colony is matte sooty
850 black smooth edged and grows to 2.7-2.8 mm in 14 days; on MN with vitamins added (MNV), the colony
851 is glossy raisin black with smooth edges and smooth top, colonies grow to 4.7-5.3 mm in 14 days; on
852 Potato Dextrose Agar (PDA) colonies are glossy sooty black with smooth edges and grow to 5.6-5.8 mm
853 in 14 days; on Spider media, the colonies are sooty black and irregularly shaped with a size of 3.0-4.5
854 mm in 14 days, additionally a red pigment Is observed surrounding the colonies in the media; on V8
855 medium colonies are glossy sooty black and irregularly shaped, growth reaches 7.5-8.1 mm in 14 days;
856 on YPD colonies are blackish brown (1) and matte with round to irregular side morphologies and
857 undulate top morphology, dark excretions are observed coming from the colonies and excessively dark
858 supernatant is observed in liquid culture starting on day 2, colony growth reaches 6.1-6.2 mm in 14
859 days. Color descriptions used above come from Ridgway (1912).

860 *Cardinal temperatures*: Growth is capable at temperatures from 4 °C to 28 °C, and optimal
861 growth is at 23 °C, growth is not capable at or above 37 °C.

862 *Additional specimen examined*: CANADA. BRITISH COLUMBIA: Fraser-Fort George H, Jackman
863 Flats Provincial Park, in biological soil crust sample, sampled June 2015, *S. Harris*, isolated July 2015, *E.*
864 *Carr*. Culture *Exophiala viscosa* Slimy JF 03-4F CBS 148802.

865 *Notes*: Support for *E. viscosa* as a novel species stems from molecular multi-locus phylogenetic
866 analyses both for marker genes and single-copy genes, morphological comparisons of micro- and
867 macromorphology to phylogenetically related species, ecology, and biogeography of the novel species.
868 *E. viscosa* is phylogenetically placed on all analyses as related to but separate from *E. sideris* with 100%
869 posterior probability in all Bayesian analyses, and bootstrap values above 95 in all Maximum likelihood
870 analyses (**Figures 2, 3, & S2**). The highest matching species to *E. viscosa*'s ITS sequence was *E. nigra*,
871 however, marker gene phylogenies place it as polyphyletic to *E. viscosa* (**Figures 2 & S2**).
872 Morphologically, *E. viscosa* is distinct in that it excreted melanin into its surrounding environment,
873 especially on high organic nitrogen substrates such as YPD or on MEA if grown for longer than 2 weeks,
874 which is not noted in other *Exophiala* species. Additionally, it forms a rainbow sheen when grown on
875 MEA, which is not observed in *E. sideris* or *E. nigra* (Moussa et al., 2017; Seyedmousavi et al., 2011).
876 Sexual or asexual structures were not observed in *E. viscosa* on all medias and conditions tested,
877 whereas *E. sideris* readily forms conidia on PDA (Seyedmousavi et al., 2011). Both strains of *E. viscosa*
878 are also the first instances of *Exophiala* species being isolated from Canadian soils and biological soil
879 crusts, and the only other *Exophiala* species that has been previously isolated from a biological soil crust
880 was *E. crusticola* (Bates et al., 2006).

881

882 *Genome Description and Gene Content*

883 Genome sequencing, assembly, and annotation was performed by DOE JGI and their genomes
884 and transcriptomes are deposited on the Mycocosm website under their genus species names. All
885 accession numbers for both strains are listed in **Table 5**. The genome assembly sizes of these two novel
886 *Exophiala* strains are: 28.29 Mbp for *E. viscosa* JF 03-3F and 28.23 Mbp for *E. viscosa* JF 03-4F (**Table 6**).
887 These sizes are similar to other yeasts in the genus *Exophiala* and are only a bit smaller than their closest
888 relative *E. sideris* (29.51 Mbp). Their predicted gene contents are 11,344 for *E. viscosa* JF 03-3F and
889 11,358 for *E. viscosa* JF 03-4F (**Table 6**). *E. sideris* appears to possess longer genes, transcripts, exons,
890 and introns compared to *E. viscosa* JF 03-4F and *E. viscosa* JF 03-3F, which could also contribute to the
891 gene number to genome size differences (**Table 6**). *E. viscosa* JF 03-3F contains the highest GC%
892 amongst the *Exophiala* species listed in **Table 6**. *E. viscosa* JF 03-3F's GC content is even higher than *E.*
893 *viscosa* JF 03-4F by 2.65%.

894 Although the morphology and development of *E. viscosa* is seemingly much less complex
895 compared to other Eurotiomycete fungi (e.g., *Aspergillus nidulans*), there are few differences in the

896 complement of genes that are assigned to these processes when these fungi are compared. For
897 example, compared to *A. nidulans*, differences include losses of a velvet regulator (VosA) as well as a
898 class of hydrophobins (RodA, DewA), along with the gains of additional cryptochrome/photolyases
899 (CryA) and an NADPH oxidase (NoxB) (**Supplemental File 3**). This pattern suggests that *E. viscosa* might
900 harbor additional morphological or developmental complexity that has yet to observed. Notably, results
901 from automated and manual annotation of the genome sequences reveal no striking differences in
902 numerous traits (e.g., morphogenetic or developmental functions, gene clusters associated with
903 secondary metabolism, CAZymes, transcription factors, cytochrome p450 complement) compared to
904 other sequenced and annotated genomes from the members of Chaetothyriales (Teixeira et al., 2017).
905 Additional details of both species' genome sequences, including results from automated annotation
906 (e.g., GO, KEGG, PFAM domains, etc.) can be found on their respective pages on the JGI Mycocosm
907 website (https://mycocosm.jgi.doe.gov/mycocosm/home).

908 *Mating Type*

909 *Exophiala* species are one of the many fungal genera whose mating capabilities remain
910 incompletely understood and vary across the genus (Teixeira et al., 2017). The closest species to *E.*
911 *viscosa* JF 03-3F and *E. viscosa* JF 03-4F with its mating type identified is *E. sideris,* within which both
912 mating types have been characterized as a single fused gene (Teixeira et al., 2017). Given the known
913 order of genes in regions flanking the *MAT* locus in *Exophiala* species, we used comparative approaches
914 to determine the mating identities of the sequenced *E. viscosa* JF 03-3F and *E. viscosa* JF 03-4F isolates,
915 and to look for possible evidence of homothallism that is also presumed in *E. sideris*. Homologues of the
916 genes *APN2*, *SLA2*, *APC5*, *COX13*, and *MAT1* (*MAT1-1/alpha*) in *E. viscosa* JF 03-3F and *E. viscosa* JF 03-4F
917 were identified via BLAST searches. We found that *APN2* and *SLA2* flank the *MAT* locus of both species,
918 and they also contain the Herpotrichielleaceae-specific mating gene *MAT1-1-4* (**Figure S5**). These results
919 are not surprising, in that this is the exact same order of these genes in *E. sideris*. Interestingly, as
920 Teixeira et al. indicate, in *E. sideris* the *MAT* gene is a fused *MAT1-1/MAT1-2* gene with the HMG domain
921 in the middle splitting the α-box in half (2017). When the MAT protein sequences of *E. viscosa* JF 03-3F
922 and *E. viscosa* JF 03-4F are aligned with the *MAT* gene of *E. sideris*, we see 83.79% homology between
923 their protein sequences indicating that these fungi also contain a fused *MAT* gene (**Figure S5**). We were
924 able to confirm that the HMG domain was inserted within the α-box of *E. viscosa* via NCBI's conserved
925 domains visualizer, where residues 75 to 206 were the HMG domain within the *MAT1-1* protein
926 sequence. This fused *MAT* gene (*MAT1-1-1*) presumably confers homothallic mating behavior, although

927 this has not been confirmed experimentally in any of these three fungi. Additionally, neither *E. viscosa* JF
928 03-3F nor *E. viscosa* JF 03-4F contain an additional gene between *APN2* and the *MAT1-1-4* as is found in
929 *E. sideris* (Teixeira et al., 2017). Furthermore, *COX13* and *APC5* are about 7,000 bp downstream of the
930 MAT locus in both species, but *COX13* is on the reverse strand in *E. viscosa* JF 03-4F compared to being
931 on the forward strand in *E. viscosa* JF 03-3F (**Figure S5**).

932 Phenotyping of *E. viscosa* JF 03-3F and *E. viscosa* JF 03-4F:

933 To further understand the morphology, growth capabilities, and stress responses of *E. viscosa* JF
934 03-3F and *E. viscosa* JF 03-4F, we performed multiple phenotyping experiments. The intent of these
935 experiments was to provide a broader perspective on the potential adaptations that would support the
936 ability of these fungi to successfully colonize BSCs and other extreme niches.

937 *Budding Patterns*

938 Due to similarities in their colony morphologies, the extent to which this was reflected in their
939 respective budding patterns was assessed. Using protocols adapted from Mitchison-Field et al. (2019)
940 we were able to perform more detailed time-lapse microscopy of their budding patterns (**Figure S1**).
941 From this we were able to observe dramatic differences in the budding types of *E. viscosa* JF 03-3F and
942 *E. viscosa* JF 03-4F.

943 *E. viscosa* JF 03-3F buds with round cells in initially a distal fashion where the new bud forms
944 180° from the mother cell origination site, but also forms new buds at a ~90° angle from where the
945 mother bud was formed in a proximal manner (**Figure 6; Video S4**). *E. viscosa* JF 03-4F on the other hand
946 forms elongated cells in a distal manner, forming longer chains of cells instead of clusters, with axial
947 buds forming at later timepoints (**Figure 6; Video S2**). These morphological differences in budding
948 patterns influences the way these two strains grow in a shaking flask. For example, *E. viscosa* JF 03-4F
949 forms more elongated cells and buds distally which although it does not result in the formation of
950 hyphae, still creates larger clumps of cells which are not easily pipetted. However, because *E. viscosa* JF
951 03-3F forms rounder cells and buds with both distal and proximal patterns, it does not form extensive
952 clumps in a shaking flask and is more easily pipetted. *E. viscosa* JF 03-4F also forms more extensive
953 biofilms at the liquid-air interface than *E. viscosa* JF 03-3F, likely also due to the elongated cell
954 morphology (**Figures 4I & 5I**).

955 *Growth of E. viscosa* JF 03-3F *and E. viscosa* JF 03-4F *on Different Media:*

956 Growth of *E. viscosa* JF 03-3F and *E. viscosa* JF 03-4F on a variety of different media was done to
957 evaluate growth requirements and their impact on pigmentation (**Figures 7 & 8**). The media used are
958 described in **Table 1**, and include MAG, MEA, MN+NAG, MNV, PDA, Spider, YPD, YPD+TE, and V8. The
959 addition of Vitamin mix (**Table 1**) to any medium, but specifically to MAG and MNV, caused the colonies
960 of both isolates to become much shinier, blacker (vs. browner), and more yeast morphology. Growth on
961 MEA caused the formation of a rainbow iridescent sheen (**Figures 7, 8, 4K and 5K**), which is not seen on
962 any other medium. Spider medium and YPD caused the formation of a colored halo around colonies of
963 both strains. However, the halo around colonies grown on YPD is much darker and extends further than
964 on Spider medium, and *E. viscosa* JF 03-3F showed a more extensive halo than *E. viscosa* JF 03-4F. When
965 trace elements (TE) are added to YPD, the formation of a dark halo is inhibited in both strains. The ability
966 of both strains to grow on V8 medium implies that they can use cellulosic material as a carbon source.
967 Overall, colony growth and pigmentation were similar across of media types for both strains (**Figures 7**
968 **& 8**).

969 *Optimal Wavelength for OD Measurements*

970 Serial dilutions (1:1 to DF=512) of both *E. viscosa* JF 03-3F and *E. viscosa* JF 03-4F were read in a
971 wavelength range of 300-700 nm at 10 nm intervals. The OD results of those dilutions were then
972 compared to: the percent difference at 25% dilution and below, the percent difference at 50% and
973 below, cell counts at $2.19x10^6$ cells/mL and below, cell counts at $4.38x10^6$ cells/mL and below, and the
974 consistency of the actual percent difference at 12.5% dilution and below. The resulting R^2 values showed
975 that the optimal wavelength range for reading ODs for these strains is between 410-420nm
976 (**Supplemental Table 1**). To reduce the potential effect pure melanin in the supernatant might be having
977 on the OD results, we decided to choose the higher wavelength of 420 nm for our OD reads.

978 *Carbon and Nitrogen Utilization*

979 Carbon source utilization was determined using Biomerieux C32 carbon strips, which are
980 typically used for identification of human pathogens (Tragiannidis et al., 2012). Following the protocols
981 provided by the vendor, we were able to show that *E. viscosa* JF 03-3F and *E. viscosa* JF 03-4F can utilize
982 a wide range of carbon sources. Triplicates were performed on these strips to ensure results were
983 uniform and representative. Overall, a variety of carbon sources supported robust growth of both strain
984 (e.g., D-glucose, L-sorbose, D-galactose, N-acetyl glucosamine, D-sorbitol, D-xylose, glycerol, L-
985 rhamnose, L-arabinose, D-cellobiose, and maltose), and there are only a few quantitative differences in
986 utilization patterns (**Figure 9; Tables 7 & 8**). Carbon sources that could not support growth of either

987 strain included D-raffinose, D-melibiose, methyl-aD-glucopyranoside, and D-lactose. Genome annotation
988 did not provide an obvious explanation for this observation (**Supplemental File 3**). Both strains were
989 resistant to cycloheximide and were capable of producing a black color in the presence of esculin ferric
990 citrate (positive for esculin metabolism) (**Figure 9**). Notably, for both *E. viscosa* JF 03-3F and *E. viscosa* JF
991 03-4F, growth on some carbon sources, particularly sorbose, levulinic acid, and N-acetyglucosamine,
992 lead to enhanced pigmentation (**Figure 9**).

993 We were particularly interested in patterns of nitrogen utilization for *E. viscosa* JF 03-3F and *E.*
994 *viscosa* JF 03-4F given their isolation from a nutrient depleted niche with extensive nitrogen-fixing
995 bacterial populations. Nine different nitrogen sources were tested: five amino acids (aspartate,
996 glutamate, glycine, proline, serine), ammonium tartrate, sodium nitrate, urea, peptone (mixed short
997 chain amino acids) as a positive control, and no nitrogen as a negative control. Both strains are
998 incapable of utilizing aspartate and glutamate as nitrogen sources; *E. viscosa* JF 03-3F having a p-value of
999 0.012 (n=6) for aspartate and 0.0005 (n=6) for glutamate; *E. viscosa* JF 03-4F having a p-value of 0.0003
1000 (n=6) for aspartate and .00005 (n=6) for Glutamate (all compared to peptone) (**Figure 10**). E. viscosa JF
1001 03-3F and E. viscosa JF 03-4F differed in their preferred nitrogen sources. Both preferred proline, p-value
1002 for *E. viscosa* JF 03-3F 0.024 (n=6), p-value for E. viscosa JF 03-4F is 0.0012 (n=6), over peptone.
1003 However, they differ in that *E. viscosa* JF 03-3F most prefers urea p-value 0.009 (n=6), while *E. viscosa* JF
1004 03-4F had additional significantly preferred nitrogen sources including serine (p-value 0.0064 (n=6)),
1005 ammonium (p-value 0.0007 (n=6)), and nitrate (p-value 0.022 (n=6) (**Figure 10**).

1006 *Optimal Growth Temperature and Range of Growth Temperatures*

1007 *E. viscosa* JF 03-3F and *E. viscosa* JF 03-4F were isolated from an environment that experiences
1008 wide seasonal and diurnal temperature changes. As such, we determined the optimal growing
1009 temperature for these strains, as well as the limits at which they are capable of survival (cardinal
1010 temperatures). Both isolates were serial diluted and spotted onto MEA plates to determine the carrying
1011 capacity at different temperatures. Both *E. viscosa* JF 03-3F *and E. viscosa* JF 03-4F were capable of
1012 growth at 4 °C, 15 °C, 23 °C, and 27 °C, but could not grow at 37 °C and 42 °C (**Figure 11**). Optimal growth
1013 temperature of both *E. viscosa* JF 03-3F and *E. viscosa* JF 03-4F was 23 °C (**Figure 11**). Growth at 4 °C was
1014 slow, but after a year the isolates both strains formed extensive colonies and flooded the agar with
1015 melanin (**Figure S6**). Although neither strain grew at 37 °C, they retained viability as they were able to
1016 resume growth following return to 23 °C after two days of exposure to 37 °C (**Figure S6**). In contrast, the
1017 same experiment showed that incubation at 42 °C is lethal.

1018 *UV and Metal Resistance*

1019 Melanized fungi are recognized for their resistance to UV light, and the possibility of using
1020 ionizing radiation as an energy source (Dadachova et al., 2007). To assess the response of *E. viscosa* JF
1021 03-3F and *E. viscosa* JF 03-4F to UV radiation, they were each exposed to a dose (120 seconds of 10,000
1022 $\mu J/cm^2$ at 254 nm) that was lethal to *S. cerevisiae* and *E. dermatitidis* (data not shown). The same level of
1023 exposure did not kill either *E. viscosa* JF 03-3F or *E. viscosa* JF 03-4F (**Figure 12**) but did significantly
1024 reduce the number of viable colonies. Strikingly, surviving colonies showed no evidence of induced
1025 mutagenesis based on the absence of altered morphologies or pigmentation (**Figure 12**).

1026 Polyextremotolerant fungi have been previously noted as having increased metal resistances as
1027 a result of their melanized cell wall and other adaptations to harsh environments (Gadd & de Rome,
1028 1988). To test if these two new *Exophiala* spp. possess increased metal resistances when compared to *E.*
1029 *dermatitidis* and *S. cerevisiae*, we impregnated Whatman filter discs with various metals of different
1030 concentrations. Diameters of zones of clearing revealed no evidence for enhanced metal resistance to
1031 the metals tested (**Table 9**). On the other hand, both strains appear to be moderately more sensitive to
1032 $NiCl_2$ and $CdCl_2$ (**Table 9**).

1033 *Lipid Profiles*

1034 Both *E. viscosa* JF 03-3F and *E. viscosa* JF 03-4F appear to possess abundant lipid bodies (**Figure**
1035 **S4**). This observation along with the unique sticky morphology of both strains led us to the idea that
1036 they might contain unique or copious amounts of lipids. We performed a Bligh and Dyer lipid extraction
1037 followed by thin layer chromatography (TLC) to observe patterns of lipid accumulation in *E. viscosa* JF
1038 03-3F and *E. viscosa* JF 03-4F grown on media that contained fermentable or non-fermentable sugars,
1039 both with high nitrogen and low nitrogen. These iterations creating four unique media types would
1040 allow us to cover as much of a spread of lipid changes as possible. *S. cerevisiae* and *E. dermatitidis* were
1041 also similarly analyzed. Results from this lipid extraction showed that our two new strains did not seem
1042 to produce any unique or novel amounts or types of lipids when compared to *S. cerevisiae* and *E.*
1043 *dermatitidis* (**Figure S7**).

1044 Melanin Production and Regulation in *E. viscosa* JF 03-3F and *E. viscosa* JF 03-4F

1045 *Melanin Biosynthesis Gene Annotation*

1046 A defining feature of black yeasts is their pigmentation caused by the accumulation of melanin
1047 (Bell & Wheeler, 1986). Given the presumed importance of melanin to a polyextremotolerant lifestyle,

1048 we are interested in understanding how melanin production is regulated. A first step in this process is to
1049 determine the types of melanin that *E. viscosa* JF 03-3F and *E. viscosa* JF 03-4F are capable of producing.
1050 To accomplish this, the sequenced and automatically annotated genomes of *E. viscosa* JF 03-3F and *E.*
1051 *viscosa* JF 03-4F were manually annotated using protein sequences for all three melanin biosynthetic
1052 pathways in *Aspergillus niger* (Teixeira et al., 2017). The list of *A. niger* (and two *A. fumigatus*) proteins
1053 and their homologs in both *E. viscosa* JF 03-3F and *E. viscosa* JF 03-4F are summarized in **Table 10**.
1054 Manual annotation and reverse BLASTP of the melanin biosynthesis pathway genes showed that both *E.*
1055 *viscosa* JF 03-3F and *E. viscosa* JF 03-4F have the genetic capability to produce all three forms of known
1056 fungal melanins: DOPA-melanin (pheomelanin), DHN-melanin (allomelanin), and L-tyrosine/HGA derived
1057 pyomelanin. Two *A. fumigatus* proteins, hydroxynaphthalene reductase (Arp2) and scytalone
1058 dehydratase (Arp1) were also separately BLASTPed against the sequences of *E. viscosa* JF 03-3F and *E.*
1059 *viscosa* JF 03-4F because those protein sequences are not homologous between *A. niger* and *A.*
1060 *fumigatus* (Jørgensen et al., 2011). Both *E. viscosa* JF 03-3F and *E. viscosa* JF 03-4F were found to have
1061 homologous proteins to both *A. fumigatus* and *A. niger*'s Arp1 and Arp2 (**Table 10**).

1062 *Regulation of Melanin Production Using Chemical Blockers*

1063 Because *E. viscosa* JF 03-3F and *E. viscosa* JF 03-4F possess the genetic capability to produce all
1064 three forms of fungal melanin, we asked whether they were all being produced simultaneously or if one
1065 was preferred for production versus excretion. We used chemical blockers for both L-DOPA-melanin and
1066 DHN-melanin to determine the predominant type of melanin produced on MEA and YPD. Kojic acid
1067 blocks the production of L-DOPA melanin, whereas phthalide inhibits the synthesis of DHN-melanin;
1068 both are effective at doses of 1, 10, and 100 µg/mL in various fungi (Pal et al., 2014).

1069 First, we used 100 mM of phthalide and 100 mg/mL of kojic acid in a filter disc assay. Placing
1070 drug-impregnated filter discs on freshly spread lawns of cells either individually or with both drugs
1071 combined did not block melanin production even though the concentrations of the drugs were higher
1072 than that of previous studies (**Figure S8**). Then using Pal et al.'s (2014) method of melanin blocking , we
1073 added the highest dosage (100 µg/mL) of phthalide and kojic acid individually and combined to agar-
1074 solidified MEA, and both spread a lawn of cells and spotted serially diluted cells onto the plates. Neither
1075 assay resulted in blockage of melanin production in *E. viscosa* JF 03-3F or *E. viscosa* JF 03-4F (**Figures 13**
1076 **& S8**). However, addition of 100 µg/mL of phthalide alone did result in their apparent excretion of a dark
1077 substance into MEA (**Figure 13**). Overall, chemical inhibition of L-DOPA-melanin or DHN-melanin

1078 production did not qualitatively reduce colony pigmentation, possibly suggesting that the tyrosine-
1079 derived pyomelanin is still being produced.

1080 *Evaluating the Cause of Melanin Excretion*

1081 The appearance of a dark pigment surrounding colonies of *E. viscosa* JF 03-3F and *E. viscosa* JF
1082 03-4F under specific conditions raised the idea that these fungi are able to excrete melanin into their
1083 local environment. The presence of dark pigments in the supernatants of liquid cultures lent further
1084 support to this.

1085 Initial studies were performed to determine which media triggered the release of melanin. Both
1086 *E. viscosa* JF 03-3F and *E. viscosa* JF 03-4F were capable of releasing the most melanin and in the
1087 shortest growth time on YPD, with *E. viscosa* JF 03-3F seemingly excreting more than *E. viscosa* JF 03-4F
1088 (**Figures 7 & 8**). Because YPD and MEA only differ by the presence of yeast vs. malt extract as well as the
1089 percentage of peptone (2% in YPD, 0.2% in MEA), we first determined if the peptone differences
1090 impacted melanin excretion. By switching the peptone amounts in YPD and MEA, we demonstrated that
1091 *E. viscosa* JF 03-3F acquired the ability to excrete melanin on MEA if it was supplemented with 2%
1092 peptone (**Figure S9**). To extend this observation, we added progressively higher amounts of peptone to
1093 MEA media (i.e., 10 different concentrations of peptone ranging from 0.1% to 5%). We observed that *E.*
1094 *viscosa* JF 03-3F starts excreting melanin on MEA at a peptone amount of 2%, and *E. viscosa* JF 03-4F
1095 starts excreting melanin at about 4% peptone (**Figure 14**).

1096 To determine if it was tyrosine (the precursor to L-DOPA and HGA/tyrosine-derived melanins) in
1097 the peptone that was inducing melanin excretion at higher peptone levels, we tested differing tyrosine
1098 amounts on our fungi. When 0.5 g/L of tyrosine is added to the media, *E. viscosa* JF 03-3F and *E. viscosa*
1099 JF 03-4F are capable of melanin excretion, whereas increasing the tyrosine amount to 1 g/L melanin
1100 excretion is stopped completely in *E. viscosa* JF 03-4F and is greatly reduced in *E. viscosa* JF 03-3F.
1101 Additionally, when tyrosine in the only source of nitrogen at 0.5 g/L, no melanin excretion is observed in
1102 the wild type strains (**Figure S10**). Additional tests of added amino acids and ammonium chloride's effect
1103 on melanin excretion were also performed. A summarized description of the media variants and their
1104 results on these fungi's ability to excrete melanin can be found in **Table S3.** Additional details and
1105 further understanding of these results are to be described at a later date.

1106 *Confirmation of Melanin Excretion from Living Cells and Determining its OD Amount in the Supernatant*

1107 To confirm that the dark pigment in culture supernatants is indeed melanin, we performed a
1108 melanin extraction using previously described methods (Pal et al., 2014; Pralea et al., 2019). Although
1109 both enzymatic and chemical extraction of melanin was attempted, the chemical extraction process
1110 proved to be more efficient at recovering excreted melanin from the supernatant (**Figure S11**).
1111 Therefore, all extractions going forward were performed using the chemical extraction method to
1112 ensure all melanin was extracted from the solution.

1113 Growth of *E. viscosa* JF 03-3F, *E. viscosa* JF 03-4F, and *E. dermatitidis* on YPD and MEA were
1114 observed daily for melanin excretion; 11 mL aliquots of their supernatant were removed daily, and the
1115 melanin was extracted from each sample. As the experiment progressed, it was obvious that *E. viscosa*
1116 JF 03-3F and *E. viscosa* JF 03-4F began excreting melanin on day 3 and excreted more in YPD than in
1117 MEA (**Figure 15**). *E. dermatitidis* on the other hand seemed to have a slower build-up of melanin, and
1118 melanin wasn't truly obvious in the medium until day 6 in MEA though it can be seen in MEA day 3 in
1119 **Figure 15**. Analysis of the optical density (OD) of the final extracted melanin revealed that melanin
1120 amount increased over the course of the experiment, and that greater amounts of melanin are released
1121 in YPD for *E. viscosa* JF 03-3F and *E. viscosa* JF 03-4F compared to MEA for *E. dermatitidis* (**Figures S12,**
1122 **S13, & S14**). Interestingly, for both *E. viscosa* JF 03-3F and *E. viscosa* JF 03-4F, their peak melanin
1123 excretion was on day 6 and not on day 7 when grown in YPD (**Figure 16**). There was less melanin on day
1124 7 for both strains, indicating that the melanin after day 6 was either degrading, or was being taken back
1125 up by the cells. This was only obvious with reading the OD results of the extracted melanin, as the
1126 supernatants themselves past day 5 all strikingly dark and hard to differentiate visually (**Figure 15**).
1127 Extracted melanin from all *E. viscosa* JF 03-3F, *E. viscosa* JF 03-4F, and *E. dermatitidis* samples (except *E.*
1128 *dermatitidis* in MEA on day 3) displayed the typical results from a full spectrum read on pure melanin
1129 (**Figures S12, S13, & S14; Table S2**). When graphed, absorbance to Wavelength, the sample should have
1130 an exponentially decreasing OD as wavelength increases, and when the log10 of the OD absorbance
1131 reads is calculated, the full spectrum reads should become be a linear regression with an R^2 value of
1132 0.97 or higher (Pralea et al., 2019). All *E. viscosa* JF 03-3F, *E. viscosa* JF 03-4F, and *E. dermatitidis*
1133 supernatant samples displayed these features (**Table S2**), and therefore we can confirm that the dark
1134 nature of their supernatants is caused by excreted melanin.

1135 <u>Genetic Analysis of Melanin Production</u>

1136 *Creation of an Albino Mutant Using Chemical Mutagenesis*

1137 At this time, molecular tools for the manipulation of *E. viscosa* JF 03-3F and *E. viscosa* JF 03-4F
1138 are not yet available. Therefore, we combined classical genetics with genome re-sequencing to initially
1139 investigate the regulation of melanin production. Following mutagenesis with the alkylating agent ethyl
1140 methanesulfonate (EMS), four distinct phenotypic classes of mutants were recovered: pink/albino,
1141 crusty, brown, and melanin over-excretion (data not shown). At this time, the most important of these
1142 phenotypes was the pink/albino phenotype found in a mutant of *E. viscosa* JF 03-4F, a mutant we
1143 named EMS 2-11 (**Figure 17**). Genome re-sequencing of high molecular weight DNA from mutant EMS 2-
1144 11 and comparison to the reference *E. viscosa* JF 03-4F genome revealed a deleterious SNP causing a
1145 nonsense mutation in the gene polyketide synthase 1 (*pks1*). This mutation was on position 2,346,590 in
1146 scaffold 3, located in the *pks1* gene, which caused a C -> T mutation on the first position of the codon
1147 such that it became a stop codon, Q814STOP. Interestingly, *pks1* only functions in one of the three
1148 melanin biosynthetic pathways found in *E. viscosa* JF 03-4F, specifically the DHN/allomelanin pathway,
1149 which is typically known as the main melanin produced by polyextremotolerant fungi. Only two of the
1150 other random mutations found in EMS 2-11 were missense or nonsense mutations. One is a mutation in
1151 a transcriptional repressor EZH1, and another is in alcohol dehydrogenase GroES-like/polyketide
1152 synthase enolreductase. Although either of these mutations could theoretically contribute to the pink
1153 phenotype, it is more likely that a nonsense mutation in *pks1* is solely responsible for the loss of melanin
1154 production despite the lack of mutations in the other melanin biosynthetic pathways. This mutant is
1155 considered albino but is colored pink because of carotenoid production (Noack-Schönmann et al., 2014;
1156 Tesei et al., 2017). It has already been shown that blockage of melanin production in *E. dermatitidis* by
1157 mutations in *pks1* results in pink instead of white albino colonies because they also produce carotenoids
1158 and by-products such as flavolin that are normally masked by melanin (Geis & Szaniszlo, 1984; Geis et
1159 al., 1984).

1160 *Recovery of melanin Production in an Albino Mutant: Modern use of the Classical Beadle and Tatum*
1161 *Biochemical-Genetics Experiment*

1162 Pks1 is a polyketide synthase that is essential for the first step in the DHN-melanin/allomelanin
1163 production pathway. However, both *E. viscosa* JF 03-4F and *E. viscosa* JF 03-3F are shown to have the
1164 genetic capabilities to produce all three forms of fungal melanins, which means theoretically any of the
1165 three pathways could be activated to produce melanin if the fungi are given the proper chemical
1166 precursors. To test if "activation" of any of the three melanin production pathways could restore
1167 melanin production to the EMS 2-11 mutant, we performed the classical Beadle and Tatum biochemical-

1168 genetics experiment (Beadle & Tatum, 1941) and substituted either 1 mM of L-DOPA, 20 mM
1169 hydroxyurea (HU), tyrosine (additive of 0.5 g/L, 1 g/L, or 0.5 g/L sole nitrogen source), or 1 mM of 1,8-
1170 DHN into the medium. L-DOPA was previously shown to recover melanization in a *pks1* deletion mutant
1171 of *E. dermatitidis*, thus we presumed that it would be taken up by our EMS 2-11 mutant and activate the
1172 DOPA melanin/pheomelanin biosynthesis pathway (Dadachova et al., 2007; Paolo et al., 2006).
1173 However, substitution of 1 mM L-DOPA into either MEA or YPD did not induce melanin production in the
1174 EMS 2-11 *pks1* mutant (**Figure 17**). These plates were grown in the dark for 10 days, as L-DOPA will auto
1175 polymerize into a melanin precursor in the presence of light, and still no melanin production was
1176 observed.

1177 Addition of tyrosine, a melanin precursor molecule for L-DOPA and HGA-based melanins, also
1178 did not recover EMS 2-11's melanin production in any of the media iterations tested (**Figure S10**).
1179 Hydroxyurea is another compound that in other *Exophiala* species induced melanin production
1180 (Schultzhaus et al., 2020) , however addition of 20 mM of HU also did not activate melanin production in
1181 our EMS 2-11 albino mutant (**Figure 17**). Finally, addition to the media of 1 mM of 1,8-DHN, which is the
1182 immediate precursor to the final DHN-melanin/allomelanin molecule and is downstream of *pks1*, did
1183 result in recovery of melanized colonies. The colonies that grew on MEA+ 1 mM 1,8-DHN did not form
1184 extensive growth, but their cells were still dark, and on YPD + 1,8-DHN active dark colony growth is
1185 observed (**Figure 17**). These results suggest that the DHN-melanin produced by the Pks1 polyketide
1186 synthase is responsible for the bulk of melanin production by *E. viscosa* JF 03-4F.

1187

1188 ## Discussion

1189 A major limitation to our understanding of the roles played by BSCs in semi-arid ecosystems is
1190 our lack of insight into the microbial components of these biofilms and the nature of their functional
1191 interactions (Carr et al., 2021). As photoautotrophs, the roles of cyanobacteria and algae in BSCs are
1192 clear (Belnap, 2002), but the importance of other residents such as fungi and heterotrophic bacteria is
1193 less so. Here, we identify two isolates of a novel species of black yeasts from BSCs; *E. viscosa* two strains
1194 JF 03-3F and JF 03-4F. In addition to presenting the complete annotated genome sequence for both
1195 strains, we also provide a relatively detailed profile of their ability to utilize diverse carbon and nitrogen
1196 sources, as well as their response to different forms of stress. Most importantly, we demonstrate that *E.*
1197 *viscosa* JF 03-3F and *E. viscosa* JF 03-4F are capable of producing excessive amounts of melanin,
1198 including melanin that is excreted at high levels. Our results suggest that by making melanin

1199 extracellularly available as a public good, polyextremotolerant fungi provide a critical service to the
1200 broader BSC community.

1201 *E. viscosa and its Closest Relatives*

1202 *E. viscosa* JF 03-3F and *E. viscosa* JF 03-4F are two strains of a novel fungus from the family
1203 Herpotrichielleaceae that we isolated from a lichen-dominated BSC. Distinguishing features of these
1204 isolates includes their yeast-dominated morphology, pronounced melanization, and production of
1205 extracellular material that leads to the formation of "goopy" or "slimy" colonies. Notably, numerous
1206 other melanized fungi with filamentous or polymorphic characteristics were also isolated from the same
1207 BSC communities. These fungi, which will be described in detail elsewhere, grow much more slowly than
1208 *E. viscosa* JF 03-3F or *E. viscosa* JF 03-4F and also release much less or no melanin.

1209 Phylogenetic comparisons suggest that the closest relatives of *E. viscosa* JF 03-3F and *E. viscosa*
1210 JF 03-4F are *E. sideris*, *E. bergeri*, *P. elegans*, and *E. nigra*. However, through extensive phylogenetic
1211 analyses we can confirm that *E. viscosa* is a distinct species separate from these related fungi.
1212 Comparison of the two strains respective annotated genome sequences revealed that overall gene
1213 content and characteristics are similar to *E. sideris*. *E. sideris* belongs to the *jeanselmei*-clade of
1214 *Exophiala*; it is typically recovered from highly arsenate-polluted environments and is not known to be
1215 pathogenic (Seyedmousavi et al., 2011). The failure of *E. viscosa* JF 03-3F and *E. viscosa* JF 03-4F to grow
1216 at 37 ^{o}C reinforces the point that species within this clade are less likely to possess the capacity of
1217 causing disease in mammals.

1218 Organization of the *MAT* locus between both strains of *E. viscosa* and *E. sideris* is very similar, as
1219 they possess a fused *MAT* gene, although they differ in the transcript directionality for the flanking
1220 *COX13* and *APC5* genes. Many *Exophiala* species are considered heterothallic, even species closely
1221 related to *E. sideris* such as *E. oligosperma* and *E. spinifera* are heterothallic (Teixeira et al., 2017;
1222 Untereiner & Naveau, 1999). As previously proposed by Teixeira et al., the proposed homothallic
1223 behavior of *E. sideris*, *E. viscosa* JF 03-3F, and *E. viscosa* JF 03-4F, may have resulted from an ancestral
1224 parasexual recombination event that altered the organization of the *MAT* locus (2017). Further
1225 investigation of these ideas will require demonstration that these *Exophiala* species undergo sexual
1226 development. Additional investigations will also be performed to determine the environmental factors
1227 for triggering sexual or asexual development in *E. viscosa*, as past attempts of established methods have
1228 failed but do not constitute evidence for absence of development.

1229 *Phenotypic Characterization of E. viscosa* JF 03-3F *and E. viscosa* JF 03-4F

1230 Our results show that *E. viscosa* JF 03-3F and *E. viscosa* JF 03-4F are capable of using a diverse
1231 array of carbon sources. These include mannitol, ribitol, and glucose, which are considered the main
1232 carbon sources exchanged between photobionts and their mycobiont partners in lichens (Richardson et
1233 al., 1967; Yoshino et al., 2020). Although, *E. viscosa* JF 03-3F and *E. viscosa* JF 03-4F are able to use most
1234 nitrogen sources provided, glutamate and aspartate are clearly not being taken up or used, unlike in
1235 yeasts such as *S. cerevisiae* where glutamate is a more favorable nitrogen source used for multiple core
1236 metabolism and amino acid production processes (Ljungdahl & Daignan-Fornier, 2012). Because
1237 peptone is a favorable nitrogen source for *E. viscosa* JF 03-3F and *E. viscosa* JF 03-4F, it is likely that this
1238 species can import peptides and degrade them as organic nitrogen sources. In the BSC soil
1239 environment, organic nitrogen has been shown to be the more abundant form of nitrogen (Delgado-
1240 Baquerizo et al., 2010), but whether cyanobacteria and other nitrogen-fixing bacteria in BSCs are
1241 contributing organic or inorganic nitrogen sources is not understood (Belnap, 2002). However, since
1242 these fungi can use both inorganic and organic forms of nitrogen, they can use their metabolic flexibility
1243 to benefit them when either are present.

1244 A characteristic feature of BSCs is the inherently stressful nature of these ecosystems. Of note,
1245 *E. viscosa* JF 03-3F and *E. viscosa* JF 03-4F were isolated from a site that can experience extremes in
1246 temperature, UV exposure, and soil wetness/osmotic pressure. Although the optimal growth range for
1247 these strains is from 15 °C to 27 °C, they are capable of slow growth at 4 °C and while they do not grow
1248 at 37 °C, they do remain viable after 72 consecutive hours of exposure to this temperature. The ability to
1249 grow at 4 °C, albeit slowly, presumably contributes to the success of fungi such *E. viscosa* JF 03-3F and *E.*
1250 *viscosa* JF 03-4F in adapting to BSCs in colder drylands. A broader comparison of microbiomes and
1251 associated functional traits between cold-adapted BSCs and those found in hot deserts would be an
1252 informative approach to identifying microbial species and/or physiological factors that underlie
1253 temperature adaptation.

1254 As for resistance to UV radiation, *E. viscosa* JF 03-3F and *E. viscosa* JF 03-4F were both able to
1255 survive the high exposure of UV-C and were uniquely resistant to standard UV mutagenesis conditions.
1256 Potential mechanisms that might contribute to UV resistance include the presence of melanin or other
1257 defensive compounds (i.e., carotenoids), some of which could be public goods provided by other
1258 constituents of the BSC community, or an enhanced capacity to repair damaged DNA. This will
1259 ultimately be an interesting topic to investigate in the future.

1260 One feature we expected to find in *E. viscosa* JF 03-3F and *E. viscosa* JF 03-4F, but we did not
1261 necessarily observe was higher metal resistance. Melanin is known to enhance resistances to metals
1262 (Bell & Wheeler, 1986; Gadd, 1994; Gorbushina, 2007; Purvis et al., 2004), and their closest relative *E.*
1263 *sideris* is primarily isolated from arsenate-contaminated soils (Seyedmousavi et al., 2011), so we
1264 predicted that this species would have increased metal tolerance when compared to non-melanized
1265 fungi. However, of the metals tested, only $AgNO_3$ and $CuCl_2$ showed a decreased zone of clearing (higher
1266 resistance) in *E. viscosa* JF 03-3F and *E. viscosa* JF 03-4F, compared to *S. cerevisiae* and *E. dermatitidis*. A
1267 potential explanation for the latter observation is that melanin has a higher affinity for copper due to
1268 the phenolic compounds within the polymer (Gadd & de Rome, 1988).

1269 *Production and Excretion of Melanin by E. viscosa* JF 03-3F *and E. viscosa* JF 03-4F

1270 Melanin is considered an expensive secondary metabolite to produce because it is made up of
1271 conglomerates of polyphenols and as such contains many carbons (Schroeder et al., 2020). Therefore, it
1272 would be assumed that an organism would not want to create melanin just to export it out of the cell.
1273 Either this excreted melanin is an evolutionary trait that is beneficial to the fungi in some way, or this
1274 melanin excretion is a form of overflow metabolism in which melanin is the most streamlined way to
1275 remove an excessive buildup of precursors (De Deken, 1966). Additionally, there are not many fungi
1276 known to excrete melanin and few in the genus *Exophiala* (Romsdahl et al., 2021), so the possibility of a
1277 novel species that excretes such extreme amounts of melanin into their surroundings was intriguing.

1278 Both fungi have the genetic makeup to produce all three types of fungal melanin: allomelanin
1279 (DHN-derived), pyomelanin (HGA/L-tyrosine derived), and pheomelanin (L-DOPA-derived); but it is still
1280 unknown how these melanin biosynthetic pathways are regulated. We were able to confirm through
1281 genetic means that they are producing DHN-derived allomelanin, but we were unable to definitively
1282 confirm the production of the other two forms of melanin. Additionally, we can speculate that tyrosine-
1283 derived melanins are not being directly produced for excretion under conditions we have tested, since
1284 using tyrosine as a sole nitrogen source did not induce melanin excretion. However, tyrosine used as an
1285 additive did induce melanin excretion at 0.5 g/L but not at 1 g/L, implying a possible tyrosine-dependent
1286 regulation of melanin production/excretion that is not entirely understood. We hope to eventually
1287 elucidate the melanin(s) that are produced by these fungi by combining genetic approaches with mass
1288 spectrometry and NMR in the future.

1289 In our attempts to understand the regulation of melanin production by *E. viscosa* JF 03-3F and *E.*
1290 *viscosa* JF 03-4F we tried blocking individual pathways using known chemical blockers of DHN and L-

1291 DOPA-melanin, phthalide and kojic acid respectively. Neither blocker, nor their combination at the
1292 highest amounts used were able to block the production of melanin in either strain. If this species has
1293 the capability to produce all three melanins, then it is possible that they are producing more than one at
1294 the same time. This could be the case here, since the combination of both kojic acid and phthalide still
1295 resulted in melanized cells which would indicate that tyrosine-derived pyomelanin was the cause of
1296 melanization. Alternatively, since these fungi are fully melanized, it could be that the concentrations
1297 used on fungi that use melanin in asexual structures only was not strong enough to block melanin
1298 production in these fungi. Additionally, our melanin gene annotation revealed that both fungi contain
1299 homologs to *A. niger* and *A. fumigatus'* Arp1 and Arp2, which could be causing a bifurcation of the DHN
1300 melanin pathway and prevent phthalide from being an effective blocker of melanin production
1301 (Jørgensen et al., 2011; Wheeler & Klich, 1995).

1302 Linked regulation of potentially multiple forms of melanin, was observed with an EMS-induced
1303 mutant in which the *pks1* gene was disrupted. Although *pks1* is the first enzyme involved in only the
1304 production of DHN-derived allomelanin, the cells that resulted from this mutation were albino.
1305 Theoretically, these cells should have still been capable of producing the two other melanins as their
1306 pathways were seemingly not disrupted by any mutations, but this was not the case. Addition of L-DOPA
1307 has been shown to induce melanization in a *pks1* deletion mutant of *E. dermatitidis* (Paolo et al., 2006),
1308 which would indicate that it is capable of producing both pheomelanin and allomelanin. However, the
1309 same experiment did not restore melanization to the *E. viscosa* JF 03-4F's *pks1* nonsense mutant.
1310 Therefore, it is possible that; (i) *E. viscosa* JF 03-3F and *E. viscosa* JF 03-4F only produce DHN-derived
1311 allomelanin and disruption of *pks1* causes all melanin production to shut down, (ii) *pks1* (or downstream
1312 creation of DHN-derived allomelanin) is essential for the regulation of other melanin productions, or (iii)
1313 pheomelanin and pyomelanin are only produced under specific conditions that were not tested during
1314 analysis of the mutants.

1315 Our experiments also showed that *E. viscosa* JF 03-3F and *E. viscosa* JF 03-4F actively excrete
1316 melanin when they are viable and growing. We observed that melanin began to accumulate starting as
1317 early as day 2 (by OD reads), therefore suggesting live cells are excreting melanin and not melanin
1318 coming out of dead lysed cells. However, at this time we do not have a mechanism for how melanin is
1319 being released from the cells, and something to be investigated later. We also observed a decrease in
1320 melanin concentrations after day 6 in both YPD and MEA, which raises the intriguing potential for
1321 melanin uptake or degradation by *E. viscosa* JF 03-3F and *E. viscosa* JF 03-4F. Additionally, we observed

1322 that increasing organic nitrogen in the media induced melanin excretion from both fungi, but we do not
1323 know how this phenomenon is regulated or which melanin is being excreted.

1324 *Insights into the Niche of Polyextremotolerant Fungi Within the Biological Soil Crust Consortium*

1325 Fungal residents of BSC communities include lichenized mycobionts, lichenicolous fungi,
1326 endolichenic fungi, and free-living fungi. Although the latter are likely not directly associated with
1327 lichens themselves, they are surrounded by algae, cyanobacteria, and other bacteria in the same way
1328 that lichen-associated fungi are surrounded by a similar community of microbes. This raises the
1329 intriguing possibility that fungi such as *E. viscosa* JF 03-3F and *E. viscosa* JF 03-4F might transiently
1330 associated with autotrophs in response to specific environmental conditions. Members of the genus
1331 *Exophiala* (Class Eurotiomycetes) are phylogenetically related to the lichen-forming Verrucariales, and
1332 reside between Lecanoromycetes and Lichinomycetes (James et al., 2006). Additionally, the lifestyle of
1333 the ancestral state of Eurotiomycetes is currently debated as to whether it is lichenized or not.
1334 Originally, it was thought that the ancestral state of Eurotiomycetidae was lichenized (Lutzoni et al.,
1335 2001), but recent literature has shown that the ancestral state was more likely non-lichenized (Lücking &
1336 Nelsen, 2018; Nelsen et al., 2020). However, many have recognized the similarities between taxa
1337 residing in Eurotiomycetes that are non-lichenized to their lichenized relatives. Particularly, members of
1338 Eurotiomycetes and Lecanoromycetes share commonality in their ecological locations (Gostinčar et al.,
1339 2012; Muggia et al., 2013) and in their type 1 polyketide synthase (PKS) genes (Boustie & Grube, 2005),
1340 which are thought to be acquired by lichen-forming fungi via horizontal gene transfer from
1341 actinobacteria (Schmitt & Lumbsch, 2009). As such, it is likely that *E. viscosa* JF 03-3F and *E. viscosa* JF
1342 03-4F and other related fungi have lichen-like qualities, which allow them to interact with algae,
1343 cyanobacteria, and other bacteria to form lichen-like symbioses. The idea that polyextremotolerant
1344 fungi can engage in lichen-like associations with microbes has been postulated (Gostinčar et al., 2012;
1345 Muggia et al., 2013), but direct experimentation is still needed to confirm these ideas. As these are two
1346 strains of a newly identified species, more extensive ecological and molecular investigation is needed to
1347 determine the extent to which this taxon is found in BSCs and to elucidate their species interaction
1348 networks.

1349 Correlation between environmental organic nitrogen availability and excreted melanin amounts
1350 could have strong implications for interactions between these fungi found in BSCs and their nitrogen-
1351 fixing community partners. The presumed source of nitrogen used to enhance the excretion of melanin
1352 would be from nitrogen-fixing prokaryotes such as cyanobacteria, other bacteria, and archaea in the

1353 community. Additionally, organic nitrogen was found to be more abundant than inorganic nitrogen in
1354 BSC soils, and more abundant than in other soil ecosystems (Delgado-Baquerizo et al., 2010). However,
1355 the nitrogen source that is released into the environment by nitrogen-fixing bacteria in BSCs is not
1356 known. It could be ammonia/ammonium, or it could be an organic form of nitrogen since cyanobacteria
1357 and diazotrophs are known to release both forms of nitrogen (Berthelot et al., 2015; Gimenez et al.,
1358 2016; Vitousek et al., 2002). Our results suggest that the availability of these nitrogen-fixers to produce
1359 a pool of organic nitrogen could subsequently induce the excretion of melanin that then provides
1360 protective services to the broader BSC community. Excreted melanin could function at the community-
1361 level to maintain respiration and growth under varying temperature conditions while also mitigating the
1362 effects of desiccation and exposure to UV, extending the window of time allotted for optimal
1363 photosynthetic capabilities (Carr et al., 2021; Honegger, 1997; Honegger & Haisch, 2001; Lange &
1364 Tenhunen, 1981; Nybakken et al., 2004). Moreover, the excreted melanin could simultaneously serve as
1365 an external source of carbon used by the fungi and possibly others when the environment does not
1366 allow for photosynthesis. In either scenario, the seemingly wasteful excretion of melanin by *E. viscosa* JF
1367 03-3F and *E. viscosa* JF 03-4F instead represents the optimal sharing of an expensive public good for the
1368 overall betterment of the BSC community in which they reside.

1369 The availability of complete, annotated genome sequences for *E. viscosa* JF 03-3F and *E. viscosa*
1370 JF 03-4F will enable more detailed investigations of the mechanisms that support the adaptation of
1371 these fungi to extreme environments. This in turn should provide greater insight into the roles that
1372 these fungi play in the BSC community. Of particular interest will be the regulatory mechanisms that
1373 coordinate the production of different types of melanin in response to environmental and chemical
1374 inputs. Moreover, the broad applicability of melanin as a bioproduct has triggered growing interest in
1375 microorganisms that excrete this polymer. In this context, *E. viscosa* JF 03-3F and *E. viscosa* JF 03-4F
1376 could potentially serve as excellent platforms for additional engineering focused on optimizing or
1377 tailoring the type of melanin produced in responses to specific applications.

1378

1379 ## Acknowledgements

1380 The authors would like to acknowledge Dr. Rajib Saha for providing a pre-print review of this
1381 work, with his guidance we were able to make this manuscript as clear and concise as possible, Dr.
1382 Christian Elowsky for acquiring beautiful microscopic and plate photos of these new strains, Dr. Tania
1383 Kurbessoian for assistance with phylogenetic analyses, and Darwyn S. Coxson for assistance in obtaining

soil samples for isolation of these fungi. The work (proposal: 10.46936/10.25585/60001081) conducted by the U.S. Department of Energy Joint Genome Institute (https://ror.org/04xm1d337), a DOE Office of Science User Facility, is supported by the Office of Science of the U.S. Department of Energy under Contract No. DE-AC02-05CH11231. Funding for this work was provided by NASA grant number 80NSSC17K0737, and NSF PRFB fellowship number 2209217.

Citations

Altschul, S. F., Gish, W., Miller, W., Myers, E. W., & Lipman, D. J. (1990). Basic local alignment search tool. *J Mol Biol*, *215*(3), 403-410. https://doi.org/10.1016/S0022-2836(05)80360-2

Ametrano, C. G., Selbmann, L., & Muggia, L. (2017). A standardized approach for co-culturing Dothidealean rock-inhabiting fungi and lichen photobionts in vitro. *Symbiosis*, *73*(1), 35-44.

Ashburner, M., Ball, C. A., Blake, J. A., Botstein, D., Butler, H., Cherry, J. M., . . . Sherlock, G. (2000). Gene ontology: tool for the unification of biology. The Gene Ontology Consortium. *Nat Genet*, *25*(1), 25-29. https://doi.org/10.1038/75556

Bairoch, A. (2000). The ENZYME database in 2000. *Nucleic Acids Res*, *28*(1), 304-305. https://doi.org/10.1093/nar/28.1.304

Bairoch, A., Apweiler, R., Wu, C. H., Barker, W. C., Boeckmann, B., Ferro, S., . . . Yeh, L. S. (2005). The Universal Protein Resource (UniProt). *Nucleic Acids Res*, *33*(Database issue), D154-159. https://doi.org/10.1093/nar/gki070

Bateman, A., Coin, L., Durbin, R., Finn, R. D., Hollich, V., Griffiths-Jones, S., . . . Eddy, S. R. (2004). The Pfam protein families database. *Nucleic Acids Res*, *32*(Database issue), D138-141. https://doi.org/10.1093/nar/gkh121

Bates, S. T., Garcia-Pichel, F., & Nash III, T. (2010). Fungal components of biological soil crusts: insights from culture-dependent and culture-independent studies. *Bibliotheca Lichenologica*, *105*, 197-210.

Bates, S. T., Reddy, G. S., & Garcia-Pichel, F. (2006). Exophiala crusticola anam. nov.(affinity Herpotrichiellaceae), a novel black yeast from biological soil crusts in the Western United States. *International journal of systematic and evolutionary microbiology*, *56*(11), 2697-2702.

Beadle, G. W., & Tatum, E. L. (1941). Genetic Control of Biochemical Reactions in Neurospora. *Proceedings of the National Academy of Sciences*, *27*(11), 499-506. https://doi.org/10.1073/pnas.27.11.499

Bell, A. A., & Wheeler, M. H. (1986). Biosynthesis and functions of fungal melanins. *Annual review of phytopathology*, *24*(1), 411-451.

Belnap, J. (2002). Nitrogen fixation in biological soil crusts from southeast Utah, USA. *Biology and fertility of soils*, *35*(2), 128-135.

Belnap, J. (2003). The world at your feet: desert biological soil crusts. *Frontiers in Ecology and the Environment*, *1*(4), 181-189.

Belnap, J., Büdel, B., & Lange, O. L. (2001). Biological soil crusts: characteristics and distribution. In *Biological soil crusts: structure, function, and management* (pp. 3-30). Springer.

Belnap, J., & Eldridge, D. (2001). Disturbance and recovery of biological soil crusts. In *Biological soil crusts: structure, function, and management* (pp. 363-383). Springer.

Belnap, J., & Lange, O. L. (2003). *Biological soil crusts: structure, function, and management* (Vol. 150). Springer.

Berthelot, H., Bonnet, S., Camps, M., Grosso, O., & Moutin, T. (2015). Assessment of the dinitrogen released as ammonium and dissolved organic nitrogen by unicellular and filamentous marine diazotrophic cyanobacteria grown in culture. *Frontiers in Marine Science*, *2*, 80.

Birney, E., & Durbin, R. (2000). Using GeneWise in the Drosophila annotation experiment. *Genome Res*, *10*(4), 547-548. https://doi.org/10.1101/gr.10.4.547

Bligh, E. G., & Dyer, W. J. (1959). A rapid method of total lipid extraction and purification. *Canadian journal of biochemistry and physiology*, *37*(8), 911-917.

Boustie, J., & Grube, M. (2005). Lichens—a promising source of bioactive secondary metabolites. *Plant Genetic Resources*, *3*(2), 273-287. https://doi.org/10.1079/pgr200572

Bowker, M. A., Reed, S., Belnap, J., & Phillips, S. (2002). Temporal variation in community composition, pigmentation, and Fv/Fm of desert cyanobacterial soil crusts. *Microbial Ecology*, 13-25.

Bowker, M. A., Soliveres, S., & Maestre, F. T. (2010). Competition increases with abiotic stress and regulates the diversity of biological soil crusts. *Journal of Ecology*, *98*(3), 551-560.

Bowman, E. A., & Arnold, A. E. (2021). Drivers and implications of distance decay differ for ectomycorrhizal and foliar endophytic fungi across an anciently fragmented landscape. *The ISME Journal*, *15*(12), 3437-3454. https://doi.org/10.1038/s41396-021-01006-9

Cao, W., Zhou, X., McCallum, N. C., Hu, Z., Ni, Q. Z., Kapoor, U., . . . Mantanona, A. J. (2021). Unraveling the structure and function of melanin through synthesis. *Journal of the American Chemical Society*, *143*(7), 2622-2637.

Carr, E. C., Harris, S. D., Herr, J. R., & Riekhof, W. R. (2021). Lichens and biofilms: Common collective growth imparts similar developmental strategies. *Algal Research*, *54*, 102217.

Castresana, J. (2000). Selection of conserved blocks from multiple alignments for their use in phylogenetic analysis. *Molecular biology and evolution*, *17*(4), 540-552.

Chen, Z., Martinez, D. A., Gujja, S., Sykes, S. M., Zeng, Q., Szaniszlo, P. J., . . . Cuomo, C. A. (2014). Comparative Genomic and Transcriptomic Analysis of Wangiella dermatitidis, A Major Cause of Phaeohyphomycosis and a Model Black Yeast Human Pathogen. *G3 Genes|Genomes|Genetics*, *4*(4), 561-578. https://doi.org/10.1534/g3.113.009241

Cordero, R. J., & Casadevall, A. (2017). Functions of fungal melanin beyond virulence. *Fungal Biology Reviews*, *31*(2), 99-112.

Couradeau, E., Giraldo-Silva, A., De Martini, F., & Garcia-Pichel, F. (2019). Spatial segregation of the biological soil crust microbiome around its foundational cyanobacterium, Microcoleus vaginatus, and the formation of a nitrogen-fixing cyanosphere. *Microbiome*, *7*(1). https://doi.org/10.1186/s40168-019-0661-2

Cubero, O. F., Crespo, A., Fatehi, J., & Bridge, P. D. (1999). DNA extraction and PCR amplification method suitable for fresh, herbarium-stored, lichenized, and other fungi. *Plant Systematics and Evolution*, *216*(3), 243-249.

Dadachova, E., Bryan, R. A., Huang, X., Moadel, T., Schweitzer, A. D., Aisen, P., . . . Casadevall, A. (2007). Ionizing radiation changes the electronic properties of melanin and enhances the growth of melanized fungi. *PloS one*, *2*(5), e457.

De Deken, R. H. (1966). The Crabtree Effect: A Regulatory System in Yeast. *Journal of General Microbiology*, *44*(2), 149-156. https://doi.org/10.1099/00221287-44-2-149

De Hoog, G., Vicente, V., Caligiorne, R., Kantarcioglu, S., Tintelnot, K., Gerrits van den Ende, A., & Haase, G. (2003). Species diversity and polymorphism in the Exophiala spinifera clade containing opportunistic black yeast-like fungi. *Journal of Clinical Microbiology*, *41*(10), 4767-4778.

Delgado-Baquerizo, M., Castillo-Monroy, A. P., Maestre, F. T., & Gallardo, A. (2010). Plants and biological soil crusts modulate the dominance of N forms in a semi-arid grassland. *Soil Biology and Biochemistry*, *42*(2), 376-378. https://doi.org/https://doi.org/10.1016/j.soilbio.2009.11.003

1474 Donlan, R. M., & Costerton, J. W. (2002). Biofilms: survival mechanisms of clinically relevant
1475 microorganisms. *Clinical microbiology reviews*, *15*(2), 167-193.
1476 Edberg, S., Chaskes, S., Alture-Werber, E., & Singer, J. (1980). Esculin-based medium for isolation and
1477 identification of Cryptococcus neoformans. *Journal of Clinical Microbiology*, *12*(3), 332-335.
1478 Edberg, S. C., Pittman, S., & Singer, J. (1977). Esculin hydrolysis by Enterobacteriaceae. *Journal of Clinical*
1479 *Microbiology*, *6*(2), 111-116.
1480 Edgar, R. C. (2004). MUSCLE: multiple sequence alignment with high accuracy and high throughput.
1481 *Nucleic Acids Research*, *32*(5), 1792-1797. https://doi.org/10.1093/nar/gkh340
1482 Frases, S., Salazar, A., Dadachova, E., & Casadevall, A. (2007). Cryptococcus neoformans can utilize the
1483 bacterial melanin precursor homogentisic acid for fungal melanogenesis. *Applied and*
1484 *environmental microbiology*, *73*(2), 615-621.
1485 Gadd, G. M. (1994). Interactions of fungi with toxic metals. *The Genus Aspergillus*, 361-374.
1486 Gadd, G. M., & de Rome, L. (1988). Biosorption of copper by fungal melanin. *Applied microbiology and*
1487 *biotechnology*, *29*(6), 610-617.
1488 Geis, P. A., & Szaniszlo, P. J. (1984). Carotenoid pigments of the dematiaceous fungus Wangiella
1489 dermatitidis. *Mycologia*, *76*(2), 268-273.
1490 Geis, P. A., Wheeler, M. H., & Szaniszlo, P. J. (1984). Pentaketide metabolites of melanin synthesis in the
1491 dematiaceous fungus Wangiella dermatitidis. *Archives of microbiology*, *137*(4), 324-328.
1492 Gessler, N., Egorova, A., & Belozerskaya, T. (2014). Melanin pigments of fungi under extreme
1493 environmental conditions. *Applied Biochemistry and Microbiology*, *50*(2), 105-113.
1494 Gimenez, A., Baklouti, M., Bonnet, S., & Moutin, T. (2016). Biogeochemical fluxes and fate of diazotroph-
1495 derived nitrogen in the food web after a phosphate enrichment: modeling of the VAHINE
1496 mesocosms experiment. *Biogeosciences*, *13*(17), 5103-5120. https://doi.org/10.5194/bg-13-
1497 5103-2016
1498 Gnerre, S., MacCallum, I., Przybylski, D., Ribeiro, F. J., Burton, J. N., Walker, B. J., . . . Jaffe, D. B. (2011).
1499 High-quality draft assemblies of mammalian genomes from massively parallel sequence data.
1500 *Proceedings of the National Academy of Sciences*, *108*(4), 1513-1518.
1501 https://doi.org/10.1073/pnas.1017351108
1502 Gorbushina, A. A. (2007). Life on the rocks. *Environmental microbiology*, *9*(7), 1613-1631.
1503 Gostinčar, C., Grube, M., De Hoog, S., Zalar, P., & Gunde-Cimerman, N. (2009). Extremotolerance in
1504 fungi: evolution on the edge. *FEMS microbiology ecology*, *71*(1), 2-11.
1505 Gostinčar, C., Grube, M., & Gunde-Cimerman, N. (2011). Evolution of fungal pathogens in domestic
1506 environments? *Fungal biology*, *115*(10), 1008-1018.
1507 Gostinčar, C., Muggia, L., & Grube, M. (2012). Polyextremotolerant black fungi: oligotrophism, adaptive
1508 potential, and a link to lichen symbioses. *Frontiers in Microbiology*, *3*, 390.
1509 Grabherr, M. G., Haas, B. J., Yassour, M., Levin, J. Z., Thompson, D. A., Amit, I., . . . Zeng, Q. (2011). Full-
1510 length transcriptome assembly from RNA-Seq data without a reference genome. *Nature*
1511 *biotechnology*, *29*(7), 644-652.
1512 Grigoriev, I. V., Nikitin, R., Haridas, S., Kuo, A., Ohm, R., Otillar, R., . . . Shabalov, I. (2014). MycoCosm
1513 portal: gearing up for 1000 fungal genomes. *Nucleic Acids Research*, *42*(D1), D699-D704.
1514 https://doi.org/10.1093/nar/gkt1183
1515 Grigoriev, I. V., Nordberg, H., Shabalov, I., Aerts, A., Cantor, M., Goodstein, D., . . . Dubchak, I. (2012).
1516 The genome portal of the Department of Energy Joint Genome Institute. *Nucleic Acids Res*,
1517 *40*(Database issue), D26-32. https://doi.org/10.1093/nar/gkr947
1518 Grube, M., Cernava, T., Soh, J., Fuchs, S., Aschenbrenner, I., Lassek, C., . . . Sensen, C. W. (2015).
1519 Exploring functional contexts of symbiotic sustain within lichen-associated bacteria by
1520 comparative omics. *The ISME journal*, *9*(2), 412-424.

1521 Haase, G., Sonntag, L., Melzer-Krick, B., & de Hoog, G. S. (1999). Phylogenetic inference by SSU-gene
1522 analysis of members of the Herpotrichiellaceae with special reference to human pathogenic
1523 species. *Stud Mycol*, *43*, 80-97.
1524 Hom, E. F., & Murray, A. W. (2014). Niche engineering demonstrates a latent capacity for fungal-algal
1525 mutualism. *Science*, *345*(6192), 94-98.
1526 Honegger, R. (1997). Metabolic interactions at the mycobiont-photobiont interface in lichens. In *Plant*
1527 *relationships* (pp. 209-221). Springer.
1528 Honegger, R., & Haisch, A. (2001). Immunocytochemical location of the (1→ 3)(1→ 4)-β-glucan lichenin
1529 in the lichen-forming ascomycete Cetraria islandica (Icelandic moss). *New phytologist*, *150*(3),
1530 739-746.
1531 Huelsenbeck, J. P., & Ronquist, F. (2001). MRBAYES: Bayesian inference of phylogenetic trees.
1532 *Bioinformatics*, *17*(8), 754-755.
1533 Jalmi, P., Bodke, P., Wahidullah, S., & Raghukumar, S. (2012). The fungus Gliocephalotrichum simplex as
1534 a source of abundant, extracellular melanin for biotechnological applications. *World Journal of*
1535 *Microbiology and Biotechnology*, *28*(2), 505-512. https://doi.org/10.1007/s11274-011-0841-0
1536 James, T. Y., Kauff, F., Schoch, C. L., Matheny, P. B., Hofstetter, V., Cox, C. J., . . . Miadlikowska, J. (2006).
1537 Reconstructing the early evolution of Fungi using a six-gene phylogeny. *Nature*, *443*(7113), 818-
1538 822.
1539 Jurka, J. (2000). Repbase update: a database and an electronic journal of repetitive elements. *Trends*
1540 *Genet*, *16*(9), 418-420. https://doi.org/10.1016/s0168-9525(00)02093-x
1541 Jørgensen, T. R., Park, J., Arentshorst, M., van Welzen, A. M., Lamers, G., vanKuyk, P. A., . . . Ram, A. F. J.
1542 (2011). The molecular and genetic basis of conidial pigmentation in Aspergillus niger. *Fungal*
1543 *Genetics and Biology*, *48*(5), 544-553. https://doi.org/https://doi.org/10.1016/j.fgb.2011.01.005
1544 Katoh, K., Misawa, K., Kuma, K. i., & Miyata, T. (2002). MAFFT: a novel method for rapid multiple
1545 sequence alignment based on fast Fourier transform. *Nucleic acids research*, *30*(14), 3059-3066.
1546 Kearse, M., Moir, R., Wilson, A., Stones-Havas, S., Cheung, M., Sturrock, S., . . . Drummond, A. (2012).
1547 Geneious Basic: an integrated and extendable desktop software platform for the organization
1548 and analysis of sequence data. *Bioinformatics*, *28*(12), 1647-1649.
1549 https://doi.org/10.1093/bioinformatics/bts199
1550 Kobayashi, N., Muramatsu, T., Yamashina, Y., Shirai, T., Ohnishi, T., & Mori, T. (1993). Melanin reduces
1551 ultraviolet-induced DNA damage formation and killing rate in cultured human melanoma cells.
1552 *Journal of investigative dermatology*, *101*(5), 685-689.
1553 Koonin, E. V., Fedorova, N. D., Jackson, J. D., Jacobs, A. R., Krylov, D. M., Makarova, K. S., . . . Natale, D. A.
1554 (2004). A comprehensive evolutionary classification of proteins encoded in complete eukaryotic
1555 genomes. *Genome Biol*, *5*(2), R7. https://doi.org/10.1186/gb-2004-5-2-r7
1556 Krogh, A., Larsson, B., von Heijne, G., & Sonnhammer, E. L. (2001). Predicting transmembrane protein
1557 topology with a hidden Markov model: application to complete genomes. *J Mol Biol*, *305*(3),
1558 567-580. https://doi.org/10.1006/jmbi.2000.4315
1559 Kumar, S., Stecher, G., Li, M., Knyaz, C., & Tamura, K. (2018). MEGA X: Molecular Evolutionary Genetics
1560 Analysis across Computing Platforms. *Mol Biol Evol*, *35*(6), 1547-1549.
1561 https://doi.org/10.1093/molbev/msy096
1562 Kuo, A., Bushnell, B., & Grigoriev, I. V. (2014). Fungal genomics: sequencing and annotation. *Advances in*
1563 *Botanical Research*, *70*, 1-52.
1564 Kõljalg, U., Nilsson, R. H., Abarenkov, K., Tedersoo, L., Taylor, A. F. S., Bahram, M., . . . Larsson, K.-H.
1565 (2013). Towards a unified paradigm for sequence-based identification of fungi. *Molecular*
1566 *Ecology*, *22*(21), 5271-5277. https://doi.org/10.1111/mec.12481

Lan, S., Wu, L., Zhang, D., & Hu, C. (2012). Successional stages of biological soil crusts and their microstructure variability in Shapotou region (China). *Environmental Earth Sciences*, *65*(1), 77-88.

Lange, O., & Tenhunen, J. (1981). Moisture content and CO2 exchange of lichens. II. Depression of net photosynthesis in Ramalina maciformis at high water content is caused by increased thallus carbon dioxide diffusion resistance. *Oecologia*, *51*(3), 426-429.

Letunic, I., & Bork, P. (2021). Interactive Tree Of Life (iTOL) v5: an online tool for phylogenetic tree display and annotation. *Nucleic acids research*, *49*(W1), W293-W296.

Ljungdahl, P. O., & Daignan-Fornier, B. (2012). Regulation of amino acid, nucleotide, and phosphate metabolism in Saccharomyces cerevisiae. *Genetics*, *190*(3), 885-929.

Lutzoni, F., Pagel, M., & Reeb, V. (2001). Major fungal lineages are derived from lichen symbiotic ancestors. *Nature*, *411*(6840), 937-940.

Lücking, R., & Nelsen, M. P. (2018). Chapter 23 - Ediacarans, Protolichens, and Lichen-Derived Penicillium: A Critical Reassessment of the Evolution of Lichenization in Fungi. In M. Krings, C. J. Harper, N. R. Cúneo, & G. W. Rothwell (Eds.), *Transformative Paleobotany* (pp. 551-590). Academic Press. https://doi.org/https://doi.org/10.1016/B978-0-12-813012-4.00023-1

Maier, S., Muggia, L., Kuske, C. R., & Grube, M. (2016). Bacteria and non-lichenized fungi within biological soil crusts. In *Biological Soil Crusts: An Organizing Principle in Drylands* (pp. 81-100). Springer.

McFarland, J. (1907). The nephelometer: an instrument for estimating the number of bacteria in suspensions used for calculating the opsonic index and for vaccines. *Journal of the American Medical Association*, *49*(14), 1176-1178.

Mitchison-Field, L. M. Y., Vargas-Muñiz, J. M., Stormo, B. M., Vogt, E. J. D., Van Dierdonck, S., Pelletier, J. F., . . . Gladfelter, A. S. (2019). Unconventional Cell Division Cycles from Marine-Derived Yeasts. *Current Biology*, *29*(20), 3439-3456.e3435. https://doi.org/10.1016/j.cub.2019.08.050

Molina, L., & Molina, M. (1986). Absolute absorption cross sections of ozone in the 185-to 350-nm wavelength range. *Journal of Geophysical Research: Atmospheres*, *91*(D13), 14501-14508.

Moussa, T. A., Al-Zahrani, H. S., Kadasa, N. M., Moreno, L. F., Gerrits van den Ende, A., de Hoog, G. S., & Al-Hatmi, A. M. (2017). Nomenclatural notes on Nadsoniella and the human opportunist black yeast genus Exophiala. *Mycoses*, *60*(6), 358-365.

Muggia, L., Gueidan, C., Knudsen, K., Perlmutter, G., & Grube, M. (2013). The Lichen Connections of Black Fungi. *Mycopathologia*, *175*(5-6), 523-535. https://doi.org/10.1007/s11046-012-9598-8

Nelsen, M. P., Lücking, R., Boyce, C. K., Lumbsch, H. T., & Ree, R. H. (2020). No support for the emergence of lichens prior to the evolution of vascular plants. *Geobiology*, *18*(1), 3-13. https://doi.org/10.1111/gbi.12369

Nielsen, H., Brunak, S., & von Heijne, G. (1999). Machine learning approaches for the prediction of signal peptides and other protein sorting signals. *Protein Eng*, *12*(1), 3-9. https://doi.org/10.1093/protein/12.1.3

Nilsson, R. H., Larsson, K. H., Taylor, A. F. S., Bengtsson-Palme, J., Jeppesen, T. S., Schigel, D., . . . Abarenkov, K. (2019). The UNITE database for molecular identification of fungi: handling dark taxa and parallel taxonomic classifications. *Nucleic Acids Res*, *47*(D1), D259-D264. https://doi.org/10.1093/nar/gky1022

Noack-Schönmann, S., Bus, T., Banasiak, R., Knabe, N., Broughton, W. J., Den Dulk-Ras, H., . . . Gorbushina, A. A. (2014). Genetic transformation of Knufia petricola A95-a model organism for biofilm-material interactions. *Amb Express*, *4*(1), 1-6. https://doi.org/https://doi.org/10.1186/s13568-014-0080-5

1613 Nunes da Rocha, U., Cadillo-Quiroz, H., Karaoz, U., Rajeev, L., Klitgord, N., Dunn, S., . . . Garcia-Pichel, F.
1614 (2015). Isolation of a significant fraction of non-phototroph diversity from a desert biological soil
1615 crust. *Frontiers in microbiology*, *6*, 277.
1616 Nybakken, L., Solhaug, K. A., Bilger, W., & Gauslaa, Y. (2004). The lichens Xanthoria elegans and Cetraria
1617 islandica maintain a high protection against UV-B radiation in Arctic habitats. *Oecologia*, *140*(2),
1618 211-216.
1619 Ogata, H., Goto, S., Sato, K., Fujibuchi, W., Bono, H., & Kanehisa, M. (1999). KEGG: Kyoto Encyclopedia of
1620 Genes and Genomes. *Nucleic Acids Res*, *27*(1), 29-34. https://doi.org/10.1093/nar/27.1.29
1621 Pal, A. K., Gajjar, D. U., & Vasavada, A. R. (2014). DOPA and DHN pathway orchestrate melanin synthesis
1622 in Aspergillus species. *Medical mycology*, *52*(1), 10-18.
1623 Paolo, W. F., Dadachova, E., Mandal, P., Casadevall, A., Szaniszlo, P. J., & Nosanchuk, J. D. (2006). Effects
1624 of disrupting the polyketide synthase gene WdPKS1 in Wangiella [Exophiala] dermatitidis on
1625 melanin production and resistance to killing by antifungal compounds, enzymatic degradation,
1626 and extremes in temperature. *BMC microbiology*, *6*(1), 1-16.
1627 https://doi.org/https://doi.org/10.1186/1471-2180-6-55
1628 Pearson, W. R. (2013). An Introduction to Sequence Similarity ("Homology") Searching. *Current Protocols*
1629 *in Bioinformatics*, *42*(1), 3.1.1-3.1.8. https://doi.org/10.1002/0471250953.bi0301s42
1630 Perez-Cuesta, U., Aparicio-Fernandez, L., Guruceaga, X., Martin-Souto, L., Abad-Diaz-de-Cerio, A.,
1631 Antoran, A., . . . Rementeria, A. (2020). Melanin and pyomelanin in Aspergillus fumigatus: from
1632 its genetics to host interaction. *International Microbiology*, *23*(1), 55-63.
1633 Pralea, I.-E., Moldovan, R.-C., Petrache, A.-M., Ilieș, M., Hegheș, S.-C., Ielciu, I., . . . Radu, M. (2019). From
1634 extraction to advanced analytical methods: The challenges of melanin analysis. *International*
1635 *journal of molecular sciences*, *20*(16), 3943.
1636 Price, A. L., Jones, N. C., & Pevzner, P. A. (2005). De novo identification of repeat families in large
1637 genomes. *Bioinformatics*, *21 Suppl 1*, i351-358. https://doi.org/10.1093/bioinformatics/bti1018
1638 Price, M. N., Dehal, P. S., & Arkin, A. P. (2009). FastTree: computing large minimum evolution trees with
1639 profiles instead of a distance matrix. *Molecular biology and evolution*, *26*(7), 1641-1650.
1640 Puillandre, N., Brouillet, S., & Achaz, G. (2021). ASAP: assemble species by automatic partitioning.
1641 *Molecular Ecology Resources*, *21*(2), 609-620. https://doi.org/10.1111/1755-0998.13281
1642 Purvis, O. W., Bailey, E. H., McLean, J., Kasama, T., & Williamson, B. J. (2004). Uranium biosorption by
1643 the lichen Trapelia involuta at a uranium mine. *Geomicrobiology Journal*, *21*(3), 159-167.
1644 Pócs, T. (2009). Cyanobacterial crust types, as strategies for survival in extreme habitats. *Acta Botanica*
1645 *Hungarica*, *51*(1-2), 147-178.
1646 Płonka, P., & Grabacka, M. (2006). Melanin synthesis in microorganisms: biotechnological and medical
1647 aspects. *Acta Biochimica Polonica*, *53*(3).
1648 Rajeev, L., Da Rocha, U. N., Klitgord, N., Luning, E. G., Fortney, J., Axen, S. D., . . . Kerfeld, C. A. (2013).
1649 Dynamic cyanobacterial response to hydration and dehydration in a desert biological soil crust.
1650 *The ISME journal*, *7*(11), 2178-2191.
1651 Richardson, D., Smith, D., & Lewis, D. (1967). Carbohydrate movement between the symbionts of
1652 lichens. *Nature*, *214*(5091), 879-882.
1653 Ridgway, R. (1912). *Color standards and color nomenclature*. The author.
1654 Romsdahl, J., Schultzhaus, Z., Cuomo, C. A., Dong, H., Abeyratne-Perera, H., Hervey, W. J., & Wang, Z.
1655 (2021). Phenotypic Characterization and Comparative Genomics of the Melanin-Producing Yeast
1656 Exophiala lecanii-corni Reveals a Distinct Stress Tolerance Profile and Reduced Ribosomal
1657 Genetic Content. *Journal of Fungi*, *7*(12), 1078. https://doi.org/10.3390/jof7121078
1658 Ronquist, F., & Huelsenbeck, J. P. (2003). MrBayes 3: Bayesian phylogenetic inference under mixed
1659 models. *Bioinformatics*, *19*(12), 1572-1574.

Rosas, Á. L., Nosanchuk, J. D., Gómez, B. L., Edens, W. A., Henson, J. M., & Casadevall, A. (2000). Isolation and serological analyses of fungal melanins. *Journal of immunological methods*, *244*(1-2), 69-80.

Salamov, A. A., & Solovyev, V. V. (2000). Ab initio gene finding in Drosophila genomic DNA. *Genome Res*, *10*(4), 516-522. https://doi.org/10.1101/gr.10.4.516

Schmitt, I., & Lumbsch, H. T. (2009). Ancient Horizontal Gene Transfer from Bacteria Enhances Biosynthetic Capabilities of Fungi. *PLoS ONE*, *4*(2), e4437. https://doi.org/10.1371/journal.pone.0004437

Schreier, W. J., Gilch, P., & Zinth, W. (2015). Early events of DNA photodamage. *Annual review of physical chemistry*, *66*, 497-519.

Schroeder, W. L., Harris, S. D., & Saha, R. (2020). Computation-driven analysis of model polyextremo-tolerant fungus exophiala dermatitidis: defensive pigment metabolic costs and human applications. *IScience*, *23*(4), 100980.

Schultzhaus, Z., Romsdahl, J., Chen, A., Tschirhart, T., Kim, S., Leary, D., & Wang, Z. (2020). The response of the melanized yeast Exophiala dermatitidis to gamma radiation exposure. *Environmental microbiology*, *22*(4), 1310-1326.

Seyedmousavi, S., Badali, H., Chlebicki, A., Zhao, J., Prenafeta-Boldu, F. X., & De Hoog, G. S. (2011). Exophiala sideris, a novel black yeast isolated from environments polluted with toxic alkyl benzenes and arsenic. *Fungal biology*, *115*(10), 1030-1037.

Teixeira, M. M., Moreno, L. F., Stielow, B. J., Muszewska, A., Hainaut, M., Gonzaga, L., . . . de Hoog, G. S. (2017). Exploring the genomic diversity of black yeasts and relatives (Chaetothyriales, Ascomycota). *Studies in mycology*, *86*, 1-28. https://doi.org/https://doi.org/10.1016/j.simyco.2017.01.001

Ter-Hovhannisyan, V., Lomsadze, A., Chernoff, Y. O., & Borodovsky, M. (2008). Gene prediction in novel fungal genomes using an ab initio algorithm with unsupervised training. *Genome Res*, *18*(12), 1979-1990. https://doi.org/10.1101/gr.081612.108

Tesei, D., Tafer, H., Poyntner, C., Piñar, G., Lopandic, K., & Sterflinger, K. (2017). Draft Genome Sequences of the Black Rock Fungus Knufia petricola and Its Spontaneous Nonmelanized Mutant. *Genome Announc*, *5*(44). https://doi.org/10.1128/genomeA.01242-17

Tragiannidis, A., Fegeler, W., Rellensmann, G., Debus, V., Müller, V., Hoernig-Franz, I., . . . Groll, A. (2012). Candidaemia in a European Paediatric University Hospital: a 10-year observational study. *Clinical Microbiology and Infection*, *18*(2), E27-E30.

Untereiner, W. A. (1994). A simple method for the in vitro production of pseudothecia in species of Capronia. *Mycologia*, *86*(2), 290-295. https://doi.org/10.1080/00275514.1994.12026410

Untereiner, W. A., & Naveau, F. A. (1999). Molecular systematics of the Herpotrichiellaceae with an assessment of the phylogenetic positions of Exophiala dermatitidis and Phialophora americana. *Mycologia*, *91*(1), 67-83.

Untereiner, W. A., & Naveau, F. A. (1999). Molecular systematics of the Herpotrichiellaceae with an assessment of the phylogenetic positions of*Exophiala dermatitidis*and*Phialophora americana*. *Mycologia*, *91*(1), 67-83. https://doi.org/10.1080/00275514.1999.12060994

Vitousek, P. M., Cassman, K., Cleveland, C., Crews, T., Field, C. B., Grimm, N. B., . . . Sprent, J. I. (2002). *Biogeochemistry*, *57*(1), 1-45. https://doi.org/10.1023/a:1015798428743

Weber, S. (2005). Light-driven enzymatic catalysis of DNA repair: a review of recent biophysical studies on photolyase. *Biochimica et Biophysica Acta (BBA)-Bioenergetics*, *1707*(1), 1-23.

Wheeler, M. H., & Klich, M. A. (1995). The Effects of Tricyclazole, Pyroquilon, Phthalide, and Related Fungicides on the Production of Conidial Wall Pigments by Penicillium and Aspergillus Species. *Pesticide Biochemistry and Physiology*, *52*(2), 125-136. https://doi.org/https://doi.org/10.1006/pest.1995.1037

1707 White, T. J., Bruns, T., Lee, S., & Taylor, J. (1990). 38 - AMPLIFICATION AND DIRECT SEQUENCING OF
1708 FUNGAL RIBOSOMAL RNA GENES FOR PHYLOGENETICS. In M. A. Innis, D. H. Gelfand, J. J.
1709 Sninsky, & T. J. White (Eds.), *PCR Protocols* (pp. 315-322). Academic Press.
1710 https://doi.org/https://doi.org/10.1016/B978-0-12-372180-8.50042-1
1711 Winston, F. (2008). EMS and UV mutagenesis in yeast. *Current protocols in molecular biology*, *82*(1),
1712 13.13 B. 11-13.13 B. 15. https://doi.org/https://doi.org/10.1002/0471142727.mb1303bs82
1713 Yoshino, K., Yamamoto, K., Masumoto, H., Degawa, Y., Yoshikawa, H., Harada, H., & Sakamoto, K. (2020).
1714 Polyol-assimilation capacities of lichen-inhabiting fungi. *The Lichenologist*, *52*(1), 49-59.
1715 Zanne, A. E., Abarenkov, K., Afkhami, M. E., Aguilar-Trigueros, C. A., Bates, S., Bhatnagar, J. M., . . .
1716 Crowther, T. W. (2020). Fungal functional ecology: bringing a trait-based approach to
1717 plant-associated fungi. *Biological Reviews*, *95*(2), 409-433.
1718 Zdobnov, E. M., & Apweiler, R. (2001). InterProScan--an integration platform for the signature-
1719 recognition methods in InterPro. *Bioinformatics*, *17*(9), 847-848.
1720 https://doi.org/10.1093/bioinformatics/17.9.847
1721 Zeng, J. S., & De Hoog, G. S. (2008). *Exophiala spinifera*and its allies: diagnostics from morphology to
1722 DNA barcoding. *Medical Mycology*, *46*(3), 193-208.
1723 https://doi.org/10.1080/13693780701799217
1724 Zerbino, D. R., & Birney, E. (2008). Velvet: algorithms for de novo short read assembly using de Bruijn
1725 graphs. *Genome research*, *18*(5), 821-829.
1726 Zhou, K., Salamov, A., Kuo, A., Aerts, A. L., Kong, X., & Grigoriev, I. V. (2015). Alternative splicing acting as
1727 a bridge in evolution. *Stem Cell Investig*, *2*, 19. https://doi.org/10.3978/j.issn.2306-
1728 9759.2015.10.01
1729 Zupančič, J., Novak Babič, M., Zalar, P., & Gunde-Cimerman, N. (2016). The black yeast Exophiala
1730 dermatitidis and other selected opportunistic human fungal pathogens spread from dishwashers
1731 to kitchens. *PLoS One*, *11*(2), e0148166.

1732

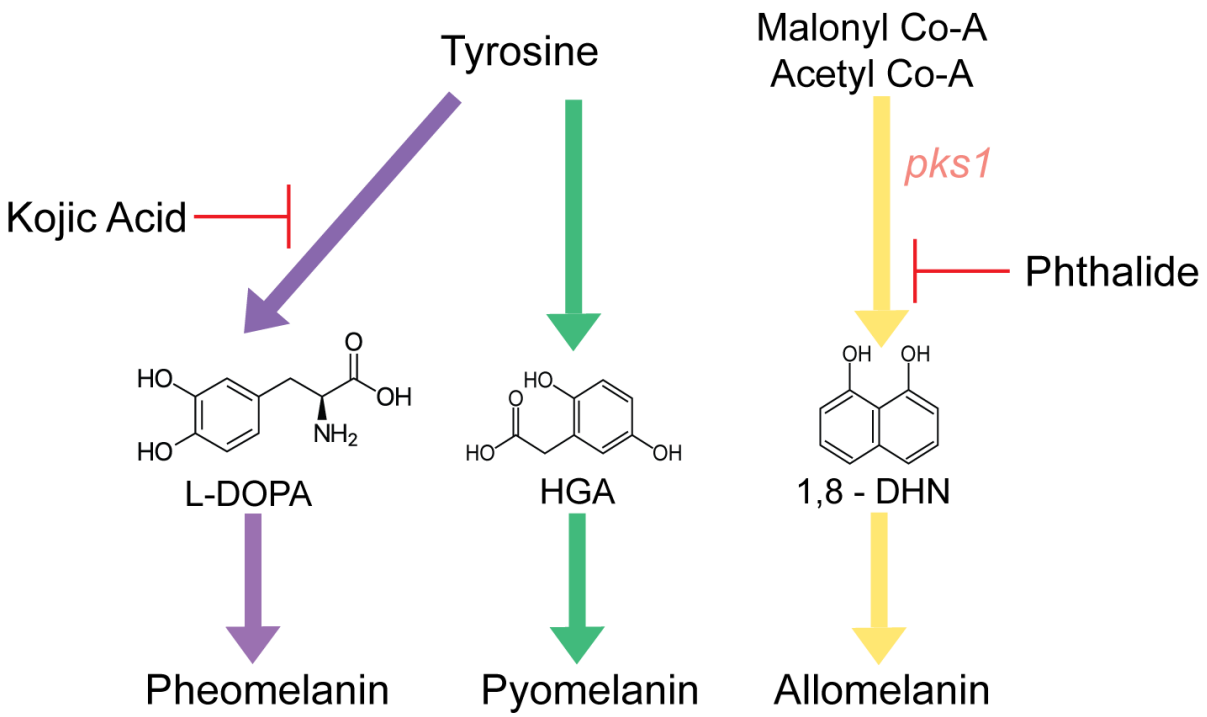

Figure 1: Visual summary of generalized fungal melanin production and the chemicals that block each pathway. Pheomelanin and Pyomelanin both use tyrosine as their starting reagent but have different biosynthesis pathways. Pheomelanin uses L-DOPA as a precursor to the final product and pyomelanin uses HMG as a precursor. Allomelanin's starting components are malonyl co-A and acetyl co-A, and its immediate precursor is 1,8-DHN. The gene *pks1* is the first gene in the biosynthetic pathway for allomelanin. Kojic acid is a chemical blocker that blocks production of pheomelanin, and phthalide blocks production of allomelanin. Additionally, the chemical precursors of the final melanin product are provided, final melanin compound structures are still unknown and therefore the precursors are used in place of melanin structure itself. Detailed descriptions of these pathways can be found in: Perez-Cuesta et al. and Płonka & Grabacka (2020; 2006).

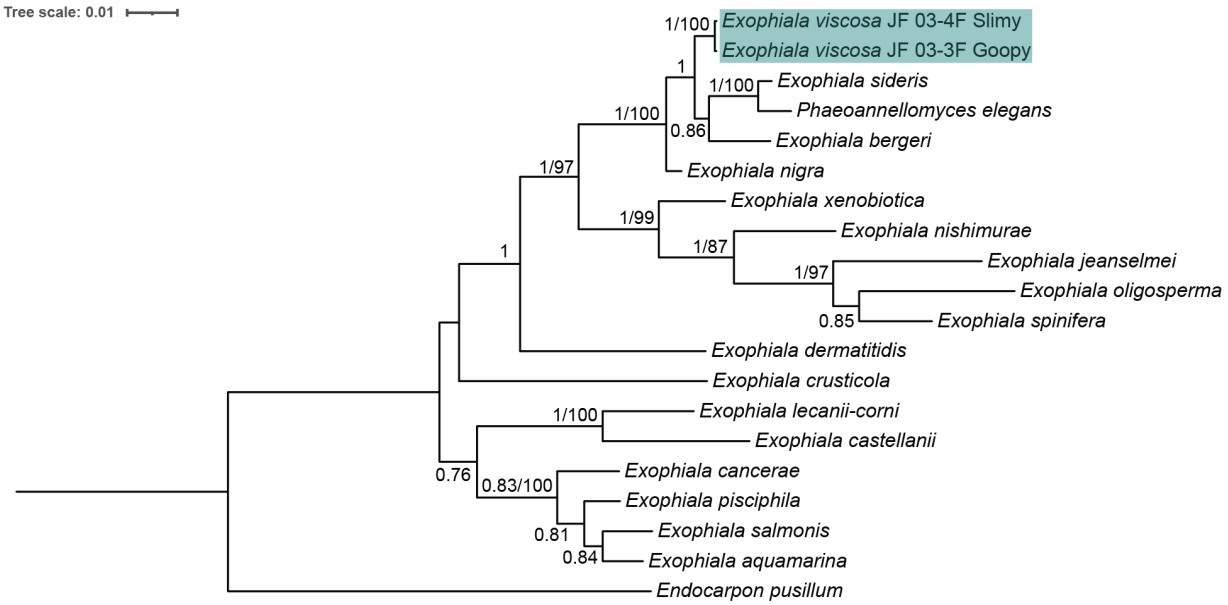

Figure 2*:* Rooted Bayesian phylogenetic tree of the concatenation of the 18S rDNA, 28S rDNA, and ITS rDNA regions of available *Exophiala* species with the addition of *E. viscosa* JF 03-3F and *E. viscosa* JF 03-4F to identify the phylogenetic location of these new species within the genus *Exophiala*. The tree with the highest log likelihood is shown. The numbers above the branches are the Bayesian posterior probability/maximum likelihood bootstrap values, with posterior probabilities > 75% and bootstrap values > 80 shown. Location of *E. viscosa* JF 03-3F and *E. viscosa* JF 03-4F within *Exophiala* places them closest to *E. bergeri, P. elegans, and E. sideris.*

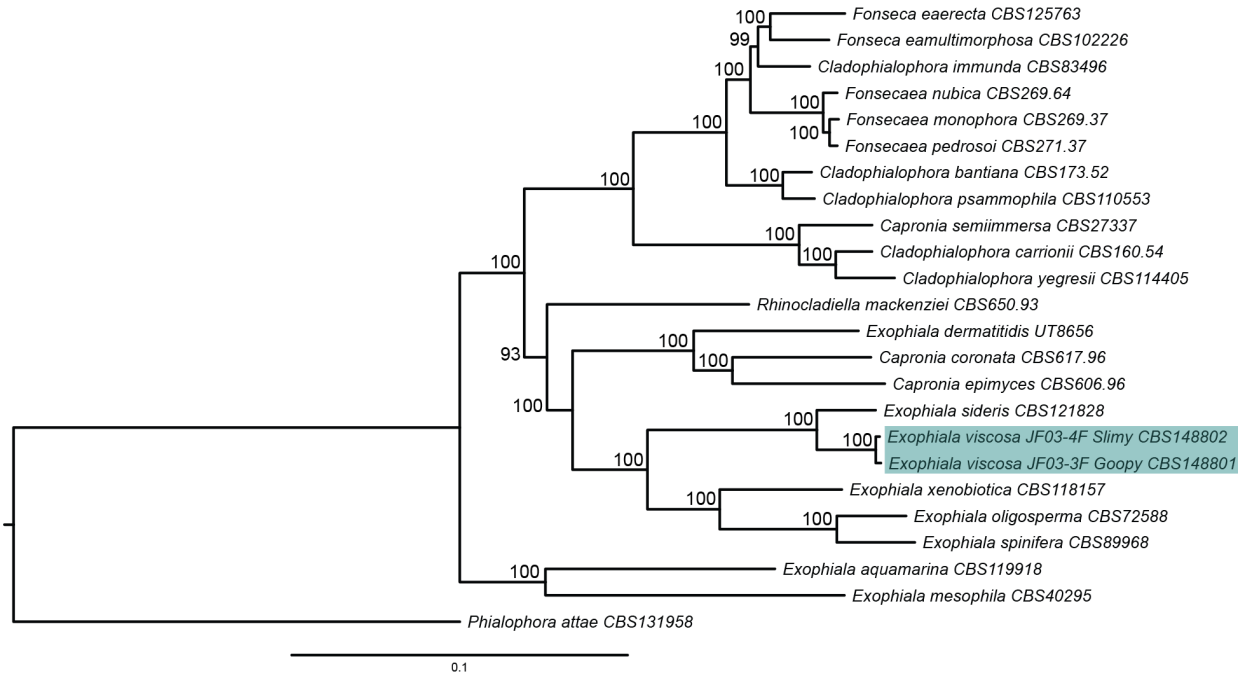

Figure 3: Single-copy homologous protein sequence approximate maximum likelihood phylogenetic tree of taxa of the family Herpotrichielleaceae all of which have been whole genome sequenced and annotated. *E. viscosa* JF 03-3F and *E. viscosa* JF 03-4F are shown to be most closely related to *E. sideris*. Node values represent bootstrap values.

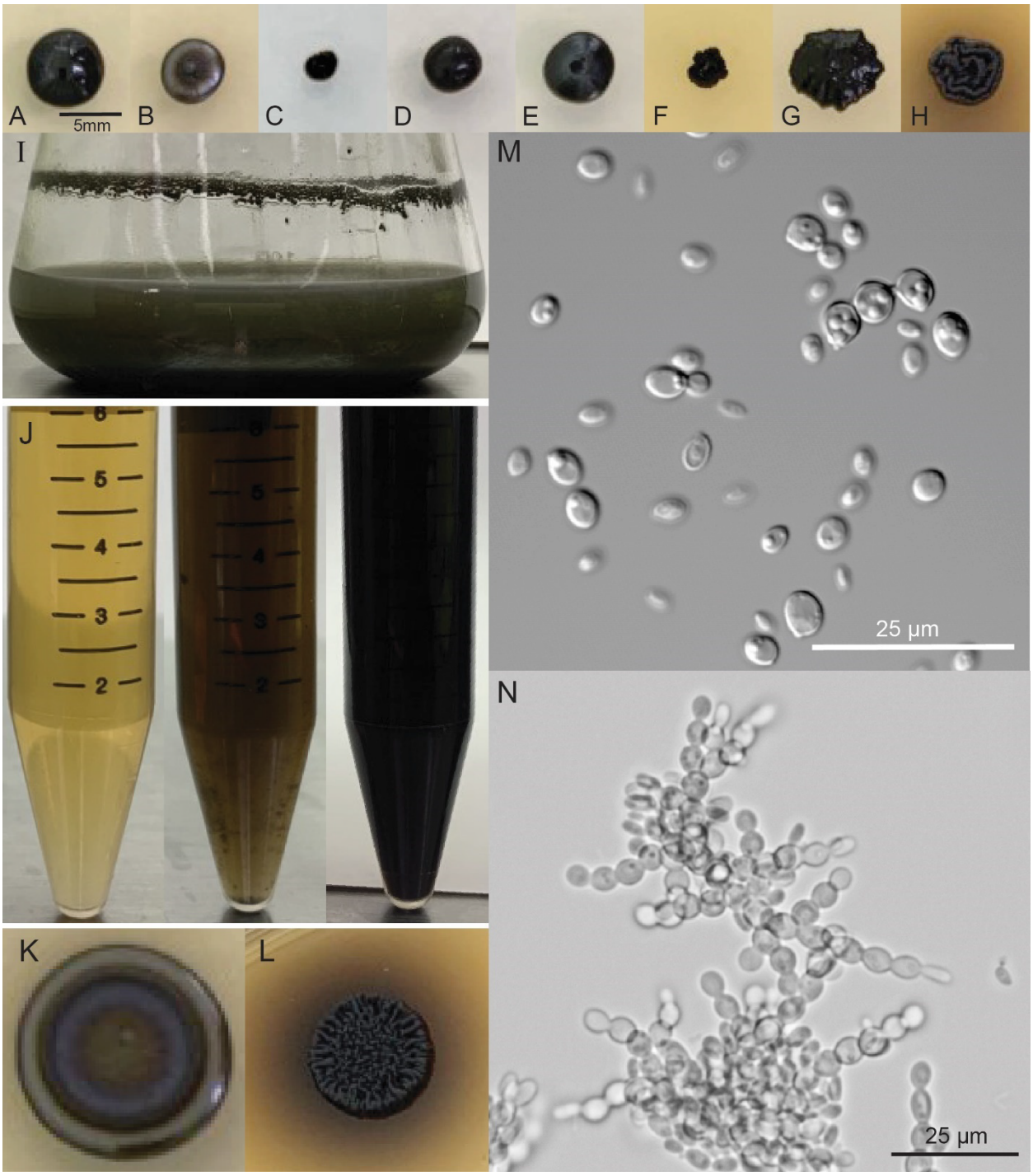

Figure 4: *E. viscosa* JF 03-3F's description summary figure. All colonies: day 14 grown at 23° C) A) Colony on MAG; B) Colony on MEA; C) Colony on MN-NAG; D) Colony on MNV; E) Colony on PDA; F) Colony on Spider media; G) Colony on V8; H) Colony on YPD; I) Biofilm at air-liquid Interface of growth in MEA day 3; J) Supernatant when grown in YPD; Day 0, 3, 6; K) Colony growth from 5 µL of liquid culture on MEA after 14 days with rainbow sheen; L) Colony growth from 5 µL of liquid culture on YPD after 14 days with dark excretions; M) Cellular growth in liquid MEA, shaking at room temp. day 5; N) Cellular growth on solid MEA, room temp. hour 65, using VALAP method.

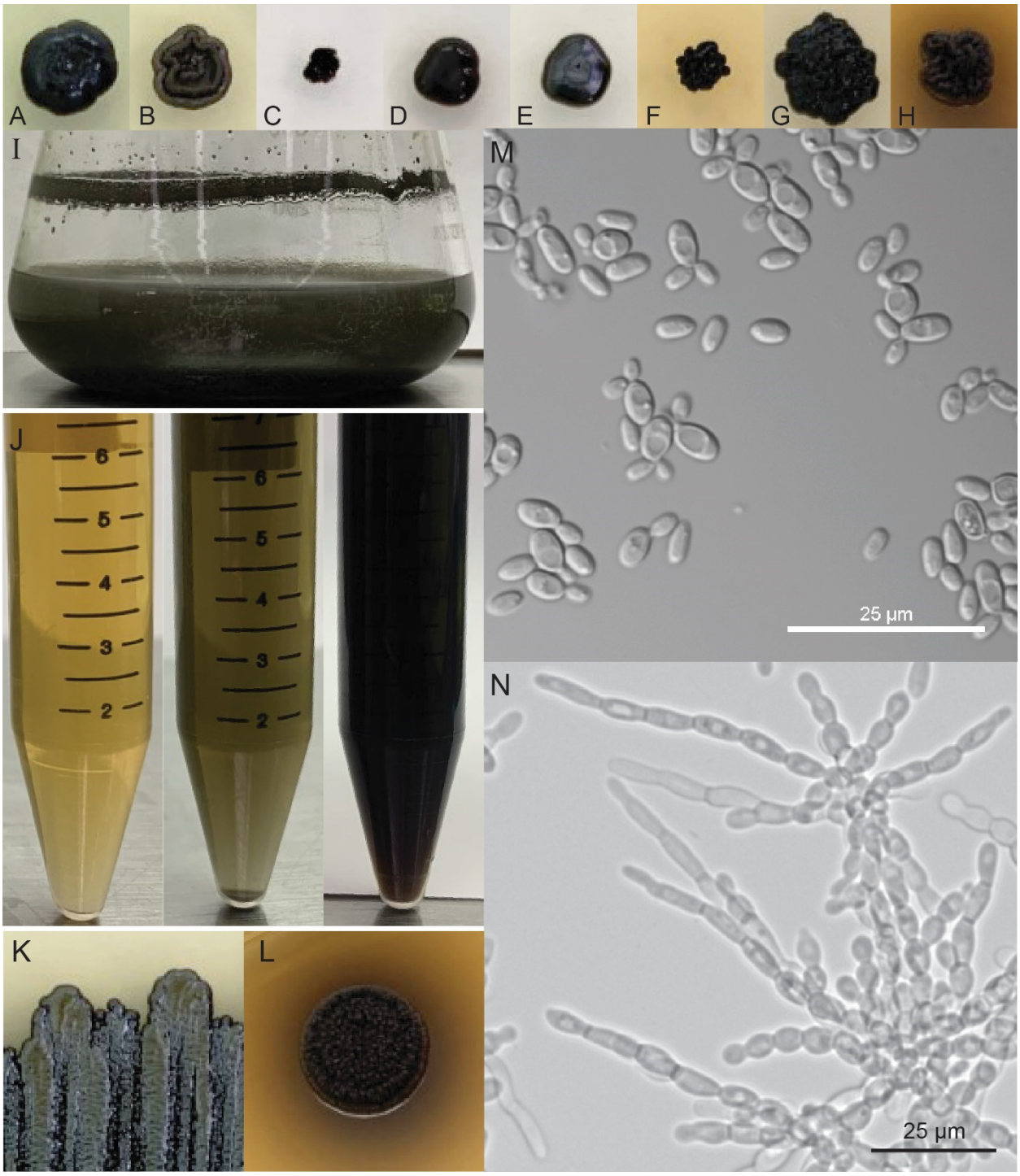

Figure 5: *E. viscosa* JF 03-4F's description summary figure. All colonies: day 14 grown at 23° C A) Colony on MAG; B) Colony on MEA; C) Colony on MN-NAG; D) Colony on MNV; E) Colony on PDA; F) Colony on Spider; G) Colony on V8; H) Colony on YPD; I) Biofilm at air-liquid interface of growth in MEA day 3; J) Supernatant when grown in YPD; Day 0, 3, 6; K) Colony growth from 5 µL of liquid culture on MEA after 14 days with rainbow sheen; L) Colony growth from 5 µL of liquid culture on YPD after 14 days with dark excretions; M) Cellular growth in liquid MEA, shaking at room temp. day 5; N) Cellular growth on solid MEA, room temp. hour 60, using VALAP method.

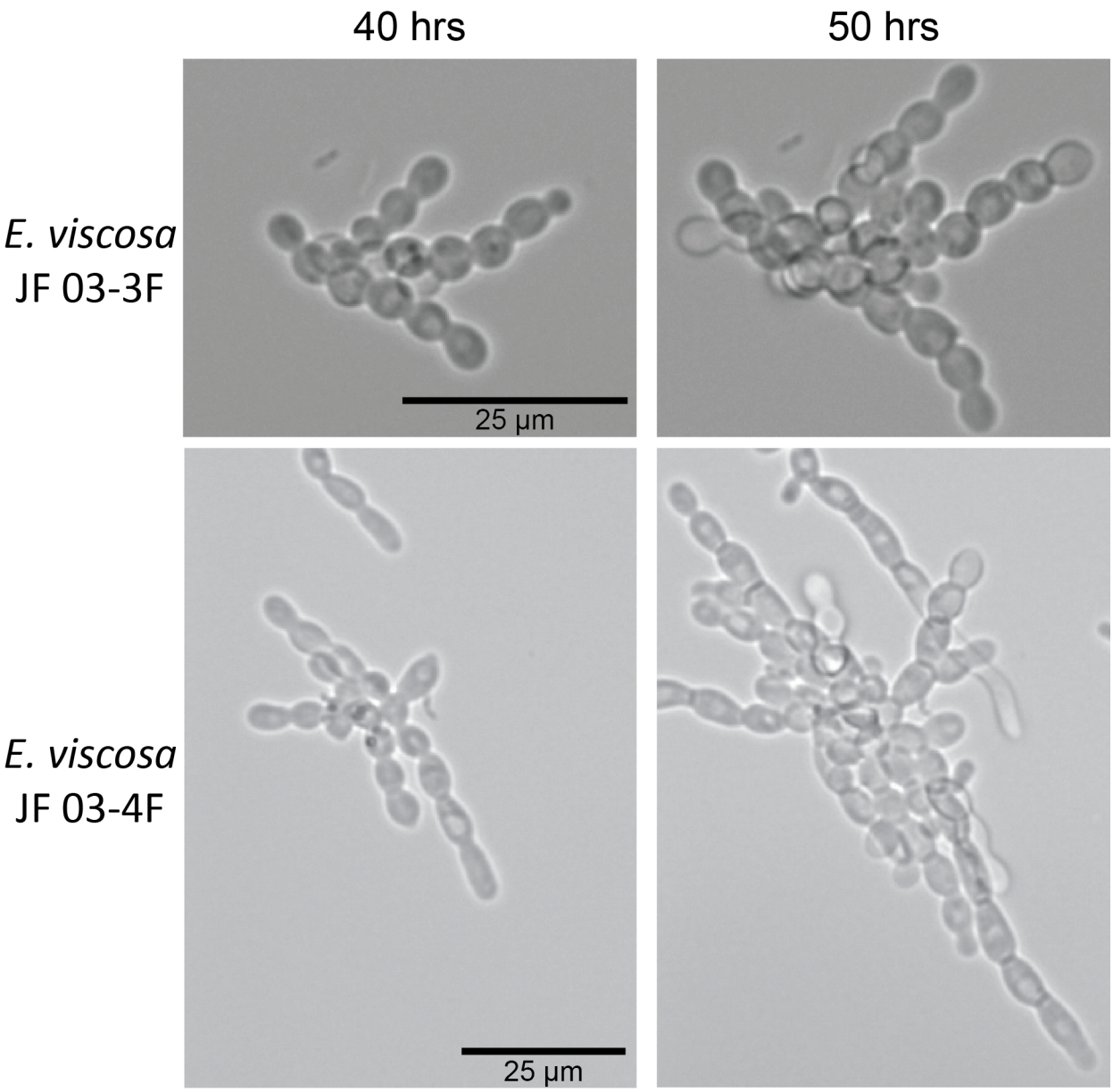

Figure 6: Budding styles of *E. viscosa* JF 03-3F and *E. viscosa* JF 03-4F pseudohyphae. Rate of budding is higher in *E. viscosa* JF 03-4F than in *E. viscosa* JF 03-3F, as seen at the 50 hrs mark. Budding style is also different between the species, *E. viscosa* JF 03-3F buds both distal polarly and proximal at close to a 90° angle, whereas *E. viscosa* JF 03-4F buds almost exclusively as a distal polar. *E. viscosa* JF 03-4F's cells also elongate with every bud, forming almost hyphal-like structures at the 50 hr timepoint (scale bars apply to side-by-side images).

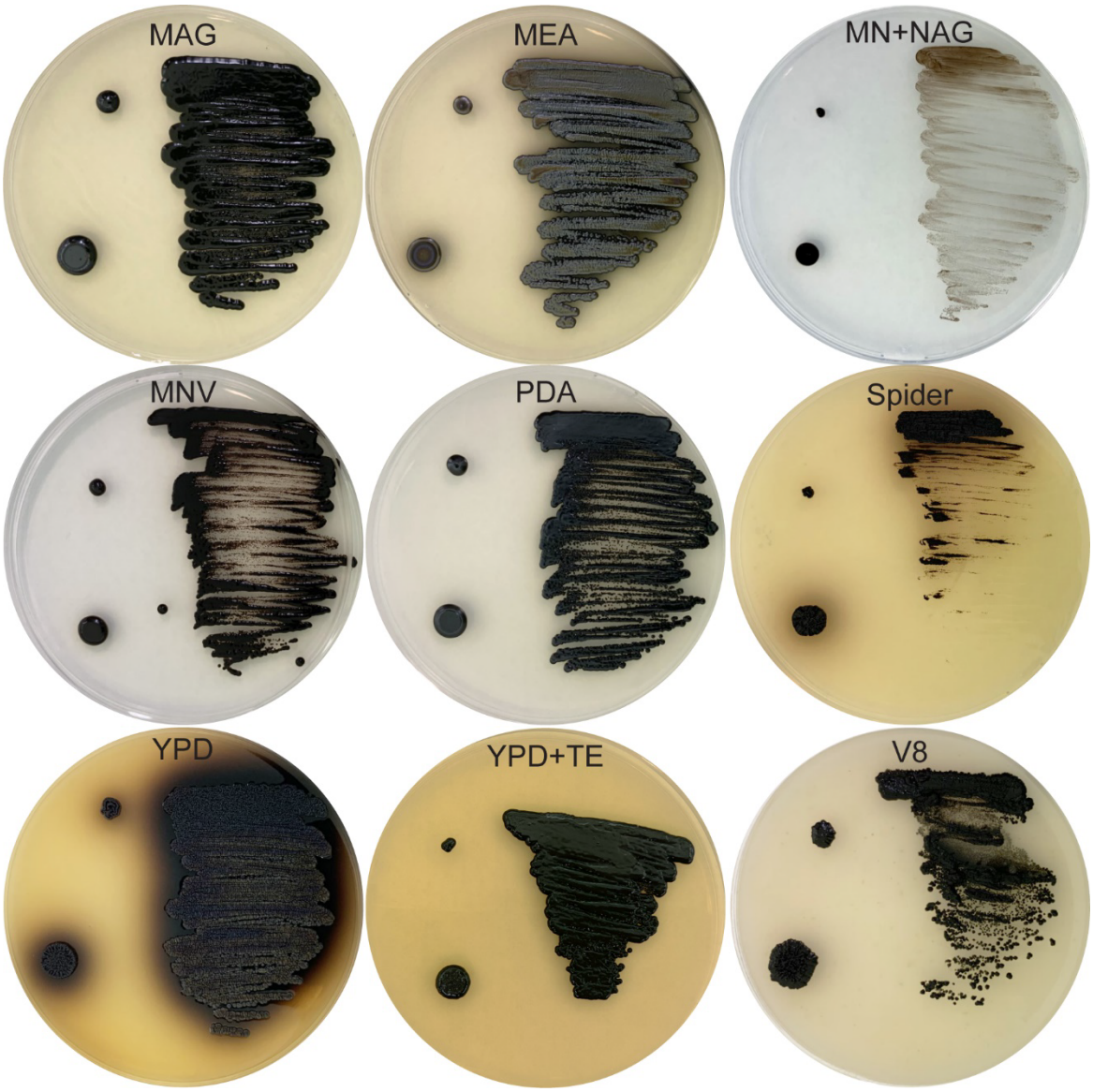

Figure 7: Growth of *E. viscosa* JF 03-3F on different media types grown at 22 °C for 14 days, plated as a toothpick prick (top left), 5 µL spot (bottom left), and loop streak patterns (pictures reduced in contrast and lightened to see details; see **Figure S15** for originals). *E. viscosa* JF 03-3Fwas capable of growth on all medias tested, but growth on MN+NAG showed the least amount of growth. PDA, MAG, and MNV allowed for very shiny and dark black colony growth. Growth on V8 medium shows potential for saprotrophic growth on plant material. Colorful red excretion was observed on Spider media and a lot of dark brownish-black excretion on YPD. Addition of trace elements (TE) to YPD prevents excretion of melanin into the media. Growth on MEA resulted in a rainbow iridescent shine on both the streaked-out growth and the 5 µL spot. Images adjusted for brightness and contrast for easier visualization, original images in **Figure S15**.

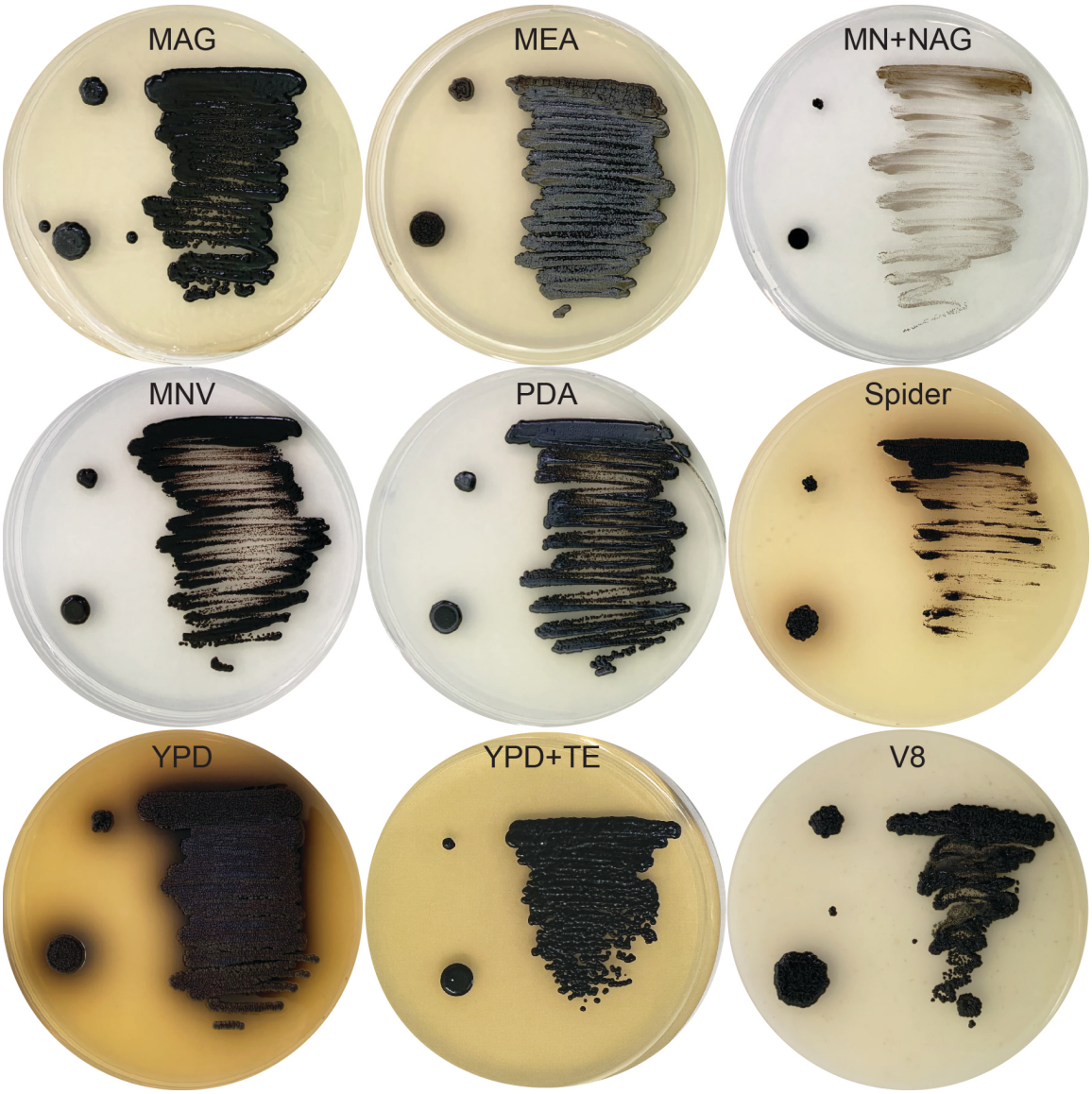

Figure 8: Growth of *E. viscosa* JF 03-4F on different media types grown at 22 °C for 14 days, plated as a toothpick prick (top left), 5 µL spot (bottom left), and loop streak patterns (pictures reduced in contrast and lightened to see details; see supplementary for originals). *E. viscosa* JF 03-4F was capable of growth on all medias tested, but growth on MN+NAG showed the least amount of growth. PDA, MAG, and MNV allowed for very shiny and dark colonies to form. Growth on V8 medium shows potential for saprotrophic growth. Colorful excretions were observed on both Spider media and YPD. Addition of trace elements (TE) to YPD prevents excretion of melanin into the media. Growth on MEA shows an iridescent shine on the streaked-out growth. Images adjusted for brightness and contrast for easier visualization, original images in **Figure S15**.

Figure 9: Growth of (A) *E. viscosa* JF 03-3F and (B) *E. viscosa* JF 03-4F on C32 strips for determining carbon utilization. Both species were capable of using the same carbon sources, though some variations are seen. *E. viscosa* JF 03-4F was better at growing on palatinose (PLE), trehalose (TRE), potassium 2-ketogluconate (2KG), and mannitol (MAN) than *E. viscosa* JF 03-3F. *E. viscosa* JF 03-3F was not better at growing on any carbon sources than *E. viscosa* JF 03-4F.

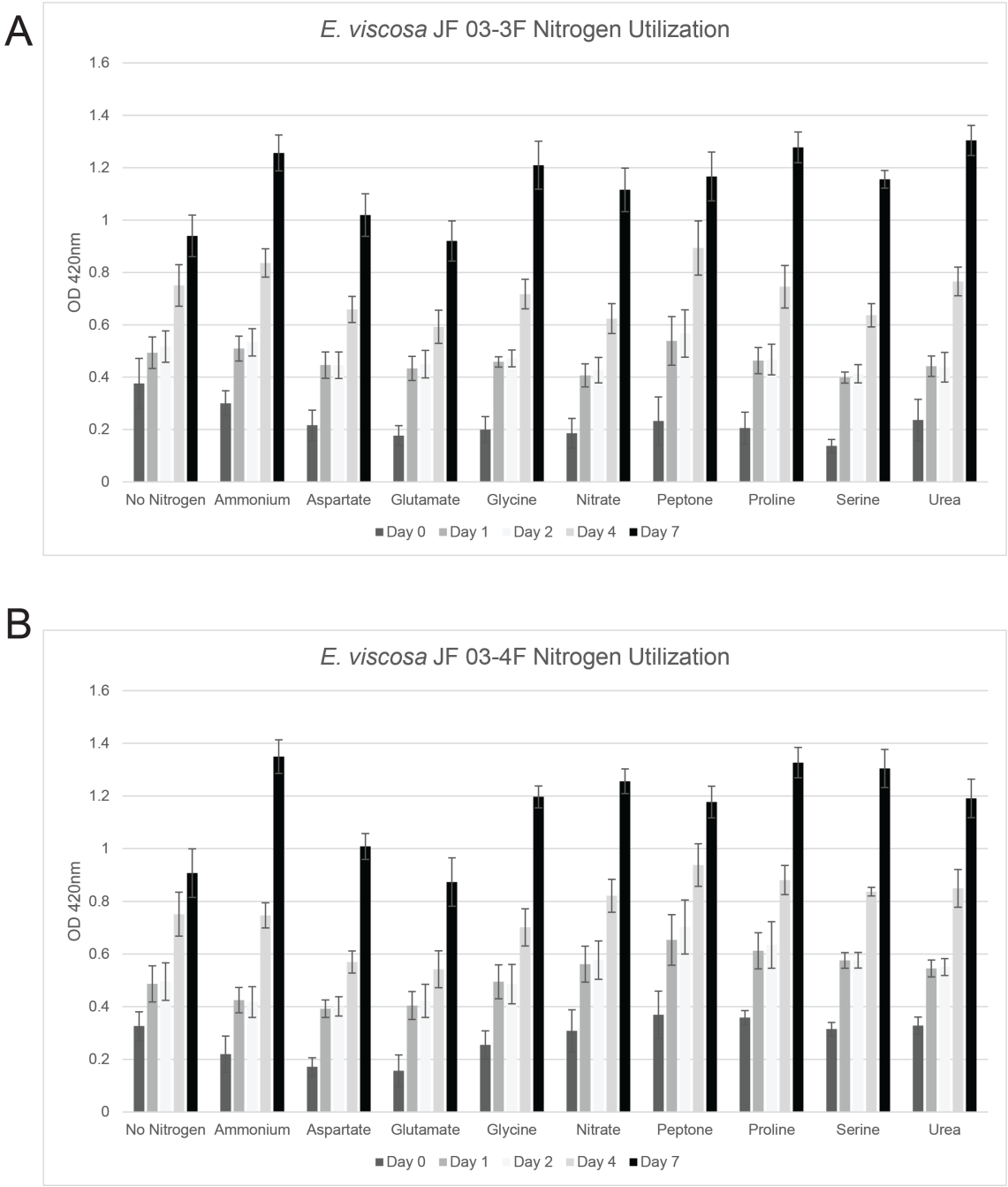

Figure 10: Nitrogen source utilization of (A) *E. viscosa* JF 03-3F and (B) *E. viscosa* JF 03-4F in liquid culture. Neither species was capable of using aspartate or glutamate as a nitrogen source, as their growth amount were equivalent to no nitrogen. All other nitrogen sources tested were used by both species with varying preference. Ammonium was the preferred nitrogen source for *E. viscosa* JF 03-4F (p-value = 0.0007 compared to peptone (n=6)), and *E. viscosa* JF 03-3F preferred urea for a nitrogen source (p-value = 0.009 compared to peptone (n=6)). *E. viscosa* JF 03-3F was unable to use aspartate or glutamate as nitrogen sources, but *E. viscosa* JF 03-4F was able to use aspartate as a nitrogen source (p-value = 0.03 compared to no nitrogen (n=6)). * = p-value of 0.05 > (n=6) compared to peptone positive control, ** = p-value of 0.01 > (n=6) compared to peptone positive control, + = p-value of 0.05 > (n=6) compared to no nitrogen negative control.

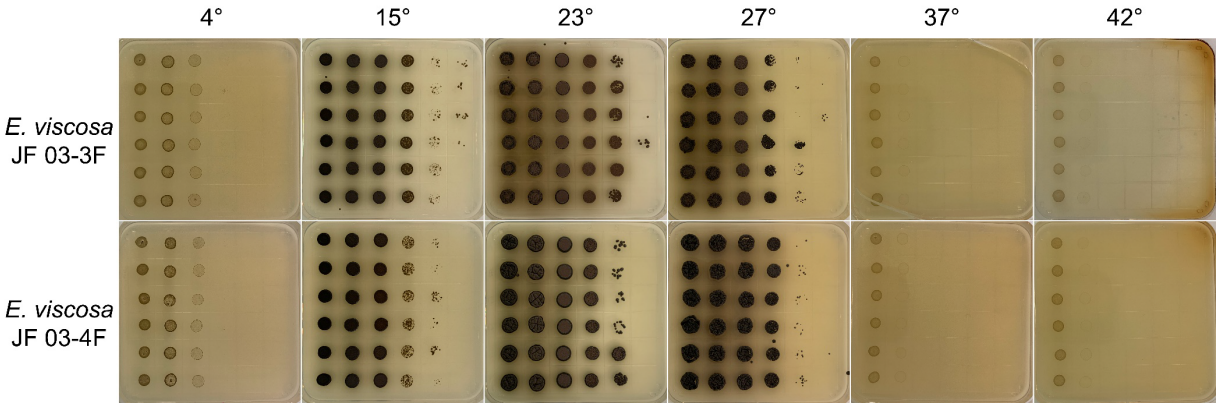

Figure 11: Growth of *E. viscosa* JF 03-3F and *E. viscosa* JF 03-4F at varying temperatures. Neither species was capable of growth at or above 37 °C, implying they are not human pathogens. Both species optimally grew at 23 °C, but were capable of growth down to 4 °C.

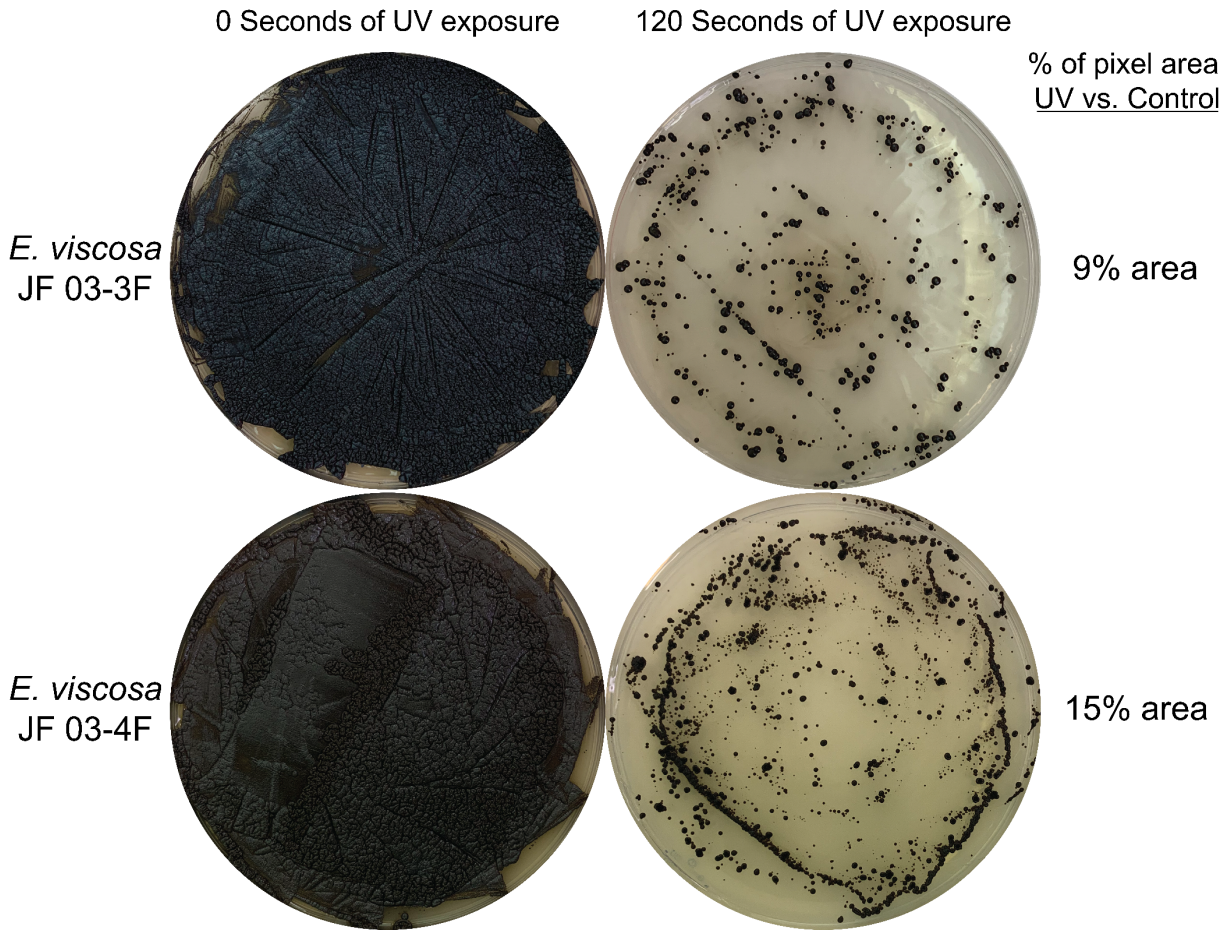

Figure 12: Difference in growth of *E. viscosa* JF 03-3F and *E. viscosa* JF 03-4F with and without exposure to UV light. *E. viscosa* JF 03-3F showed slightly less resistance to the UV exposure than *E. viscosa* JF 03-4F. Neither species was mutated from 120 seconds of UV exposure, normally *S. cerevisiae* and *E. dermatitidis* are incapable of growth after the same amount of UV exposure (data not shown).

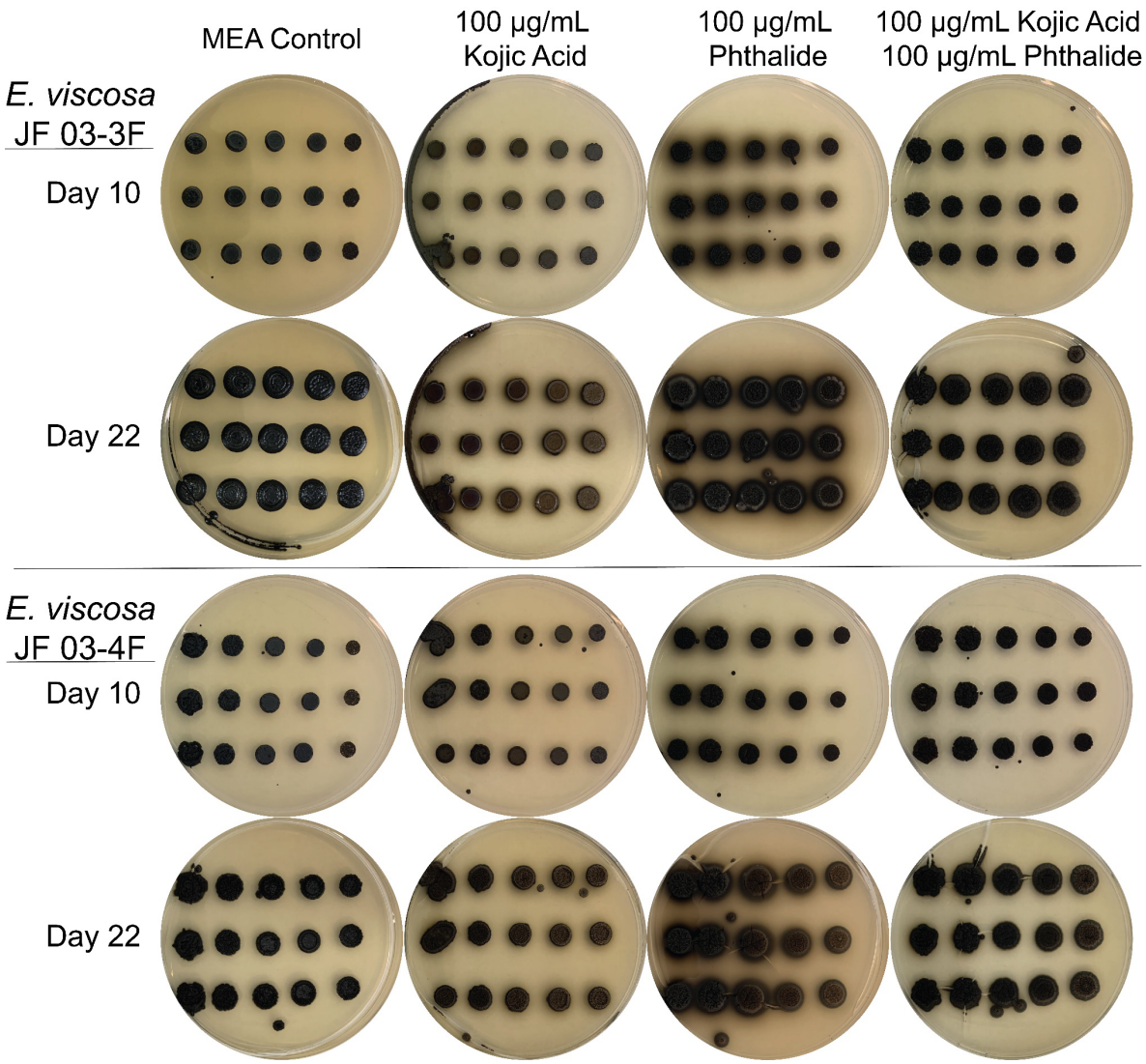

Figure 13: Growth of serial diluted (0x-10,000x with 10x steps) *E. viscosa* JF 03-3F and *E. viscosa* JF 03-4F in the presence of melanin blockers kojic acid and phthalide. Neither chemical melanin blocker was capable of blocking melanin production in either fungus, even when both chemical blockers were used simultaneously. Additionally, use of phthalide on *E. viscosa* JF 03-3F induced melanin secretion on a medium where this does not usually occur. The melanin halo around *E. viscosa* JF 03-3F's colonies on medium containing phthalide was replaced with hyphal growth after 22 days.

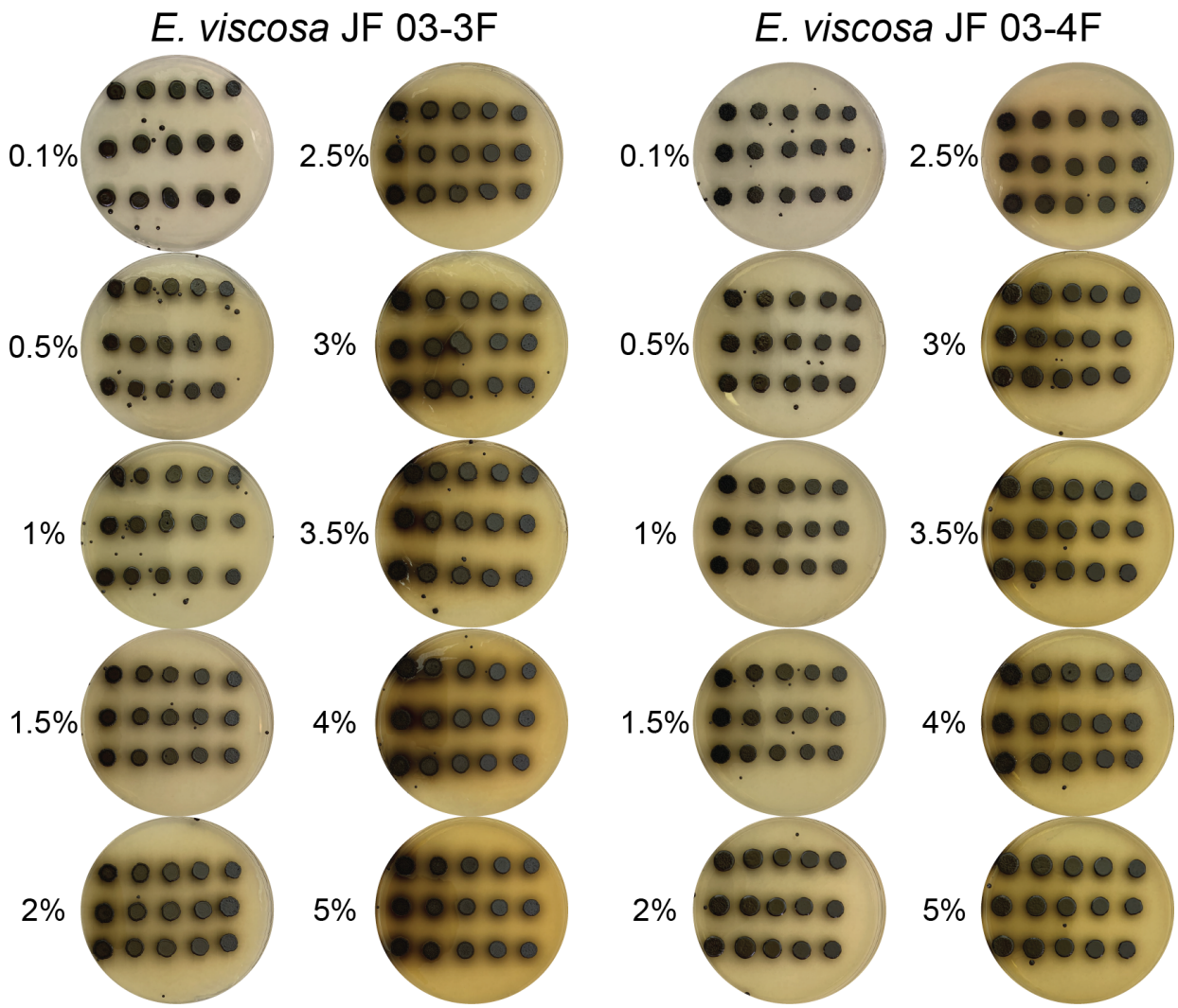

Figure 14: *E. viscosa* JF 03-3F and *E. viscosa* JF 03-4F grown on MEA with increasing amounts of peptone. The higher the amount of peptone in the medium, the more melanin was secreted. *E. viscosa* JF 03-3F started secreting melanin at 2%, and *E. viscosa* JF 03-4F at 4%.

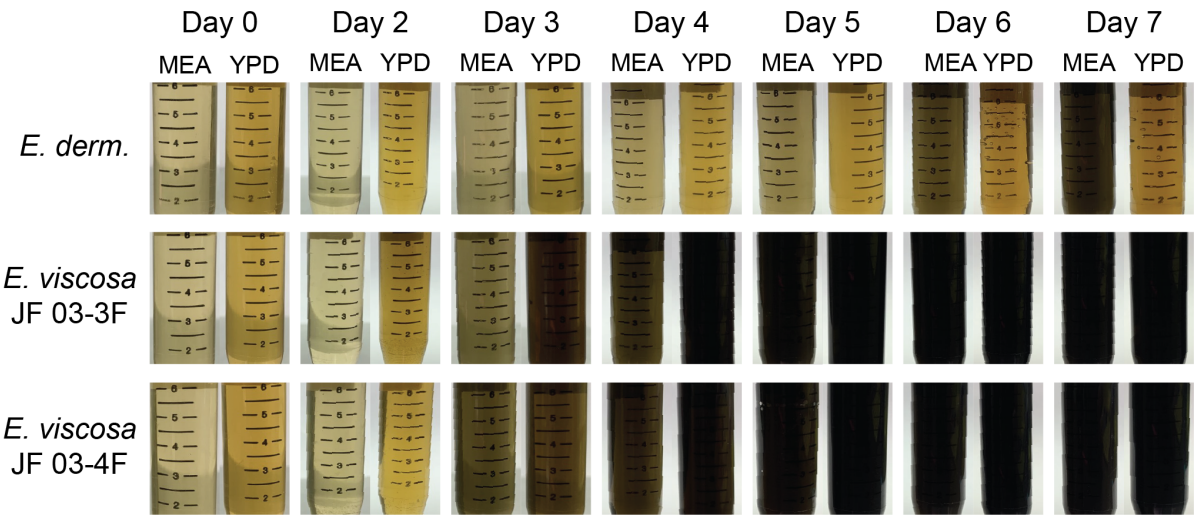

Figure 15: Supernatants of *E. dermatitidis (E. derm.)*, *E. viscosa* JF 03-3F, and *E. viscosa* JF 03-4F for each day to observe their accumulation of external melanin. Melanin began to accumulate in the supernatant of *E. viscosa* JF 03-3F and *E. viscosa* JF 03-4F on day 3, with a steep increase in melanin in YPD. *E. dermatitidis* began melanin secretion at day 6, and only in MEA.

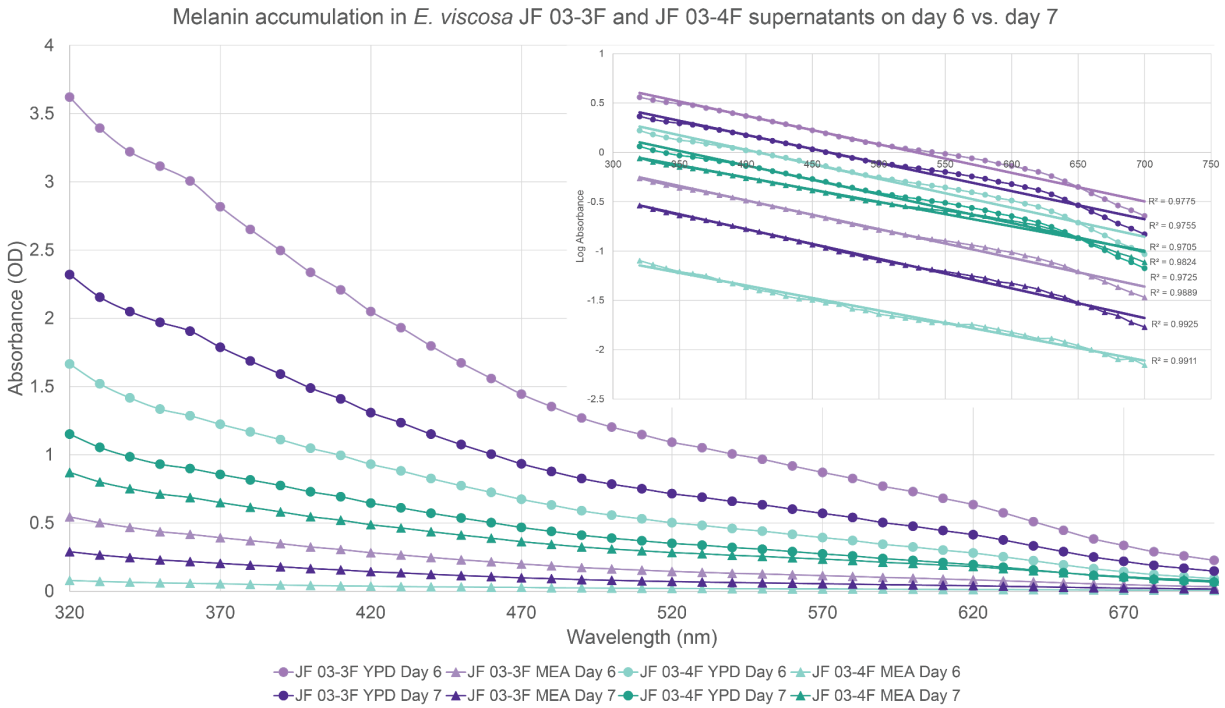

Figure 16: Day 6 and 7 results of daily melanin extraction from *E. viscosa* JF 03-3F and *E. viscosa* JF 03-4F. Both samples display typical melanin properties with full spectrum light, in that all samples have a linear regression when their Log Absorbance is plotted against wavelength, with an R^2 value of 0.97 or higher (Pralea et al., 2019). The sample with the highest amount of secreted melanin was *E. viscosa* JF 03-3F in YPD on day 6. Both *E. viscosa* JF 03-3F and *E. viscosa* JF 03-4F had more secreted melanin when grown on YPD as opposed to MEA which showed lower melanin secretion for both species. Interestingly, both species had a decrease in melanin on day 7 when grown on YPD.

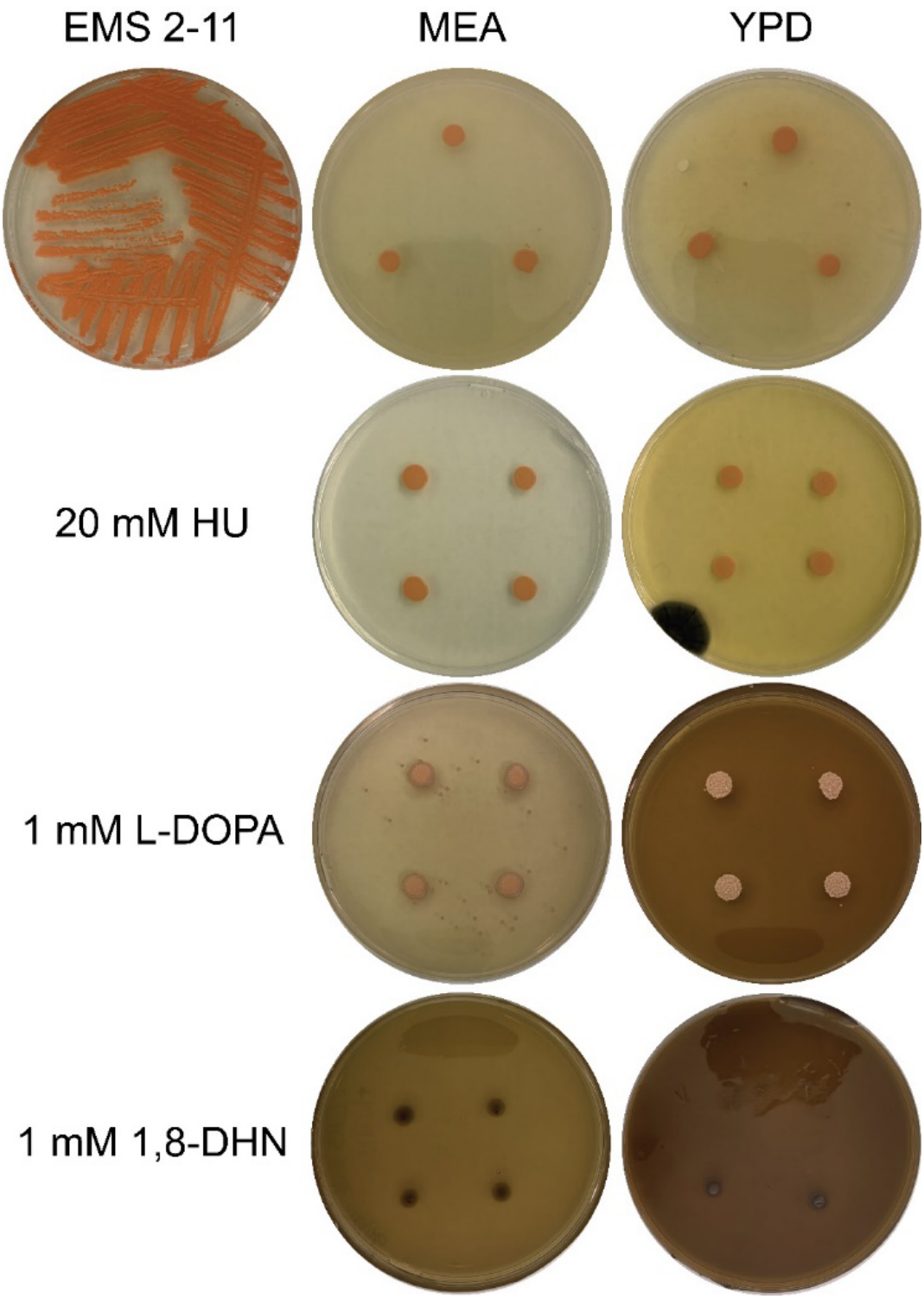

Figure 17: Phenotype of the EMS 2-11 mutant of *E. viscosa* JF 03-4F with *pks1* nonsense mutation Q814STOP, causing melanin production to be stopped hence the pink coloration. Attempts to recover melanin production were done with Hydroxyurea (HU), L-DOPA, and 1,8-DHN. Neither HU nor L-DOPA were able to recover melanin production in the mutant, however 1,8-DHN was able to recover melanin production in this mutant.

Table 1: Medias used and their compositions

Media Name	Acronym	Composition (L^{-1})
Malt Extract Agar Glucose	MAG	20 g Dextrose 20 g Malt Extract (Sigma 70167) 2 g Peptone (Fisher BP1420) 1 mL Hutner's Trace Elements 1 mL Vitamin Mix 15 g Agar
Malt Extract Agar	MEA	20 g Dextrose 20 g Malt Extract 2 g Peptone 15 g Agar
Minimal	MN	10 g Dextrose 50 mL 20x Nitrate salts 1 mL Hutner's Trace Elements
Minimal + Vitamins	MNV	10 g Dextrose 50 mL 20x Nitrate salts 1 mL Hutner's Trace Elements 1 mL Vitamin Mix
Minimal + N-acetyl Glucosamine	MN+NAG	10 g Dextrose 50 mL 20x Nitrate salts 1 mL Hutner's Trace Elements 4.74 g N-Acetyl Glucosamine (21.43 mM)
Potato Dextrose Agar	PDA	24 g BD Difco Potato dextrose Broth powder 15 g agar (if not in powder)
Spider	Spider	20 g Nutrient Broth 20 g Mannitol 4 g K_2HPO_4 27 g Agar pH adjusted to 7.2 with NaOH
Yeast Extract Peptone Dextrose	YPD	20 g Dextrose 20 g Peptone 10 g Yeast Extract 20 g Agar
V8	V8	200 mL V8 Juice 2 g $CaCO_3$ 15 g Agar
Tyrosine Media	Tyr	20 g Dextrose 10 g Peptone 1 g Yeast Extract 20 g Agar
Additives	**Volume**	**Composition**
20X Nitrate Salts/MN salts	1 L	120 g $NaNO_3$ (remove for "MN salts") 10.4 g KCl 10.4 g $MgSO_4$-$7H_2O$ 30.4 g KH_2PO_4

Hutner's Trace Elements (TE)	100 mL	2.2 g $ZnSO_4$-$7H_2O$ 1.1 g H_3BO_3 0.5 g $MnCl_2$-$4H_2O$ 0.5 g $FeSO_4$-$7H_2O$ 0.17 g $CoCL_2$-$6H_2O$ 0.16 g $CuSO_4$-$5H_2O$ 0.15 g Na_2MoO_4-$2H_2O$ 5 g EDTA (Disodium salt)
Vitamin Mix	100 mL	10 mg biotin 10 mg pyridoxin 10 mg thiamine 10 mg riboflavin 10 mg p-aminobenzoic acid (PABA) 10 mg nicotinic acid

Table 2: List of NCBI accession numbers of genes and strains of each fungal species used for concatenated phylogenetic analyses. If alternative strain was used for a gene the strain is listed under the accession number.

Fungal species and predominant strain used	18S	ITS	*rpb1*	28S
Exophiala aquamarina CBS 119918	NG 062075	NR 111626	XM 013403745	KX712347
				Sutton R-3685
Exophiala bergeri CBS 353.52	NG 062764	NR 165997	FJ358371	NG_059199
			PW2468	
Exophiala cancerae CBS 120420	KF155198	NR 137766	JX498928	MH874540
			PW2463	CBS 115142
Exophiala castellanii CBS 158.58	NG 062076	NR 121460	FJ358372	NG_070513
Exophiala dermatitidis CBS 207.35	X79312	NR 121268	JX498937	NG_059225
			PW 2643	
Exophiala jeanselmei CBS 507.90	NG 062765	NR 111129	JX498921	NG_070514
			CBS 677.76	
Exophiala lecanii-corni CBS 123.33	NG 062766	NR 145351	JX498934	NG_059200
			PW2534	
Exophiala nigra CBS 535.94	NG 062119	MH862481	FJ358375	NG_059253
			dh 12296	
Exophiala nishimurae CBS 101538	NG 063073	NR 137092	JX498925	KX712351
Exophiala oligosperma CBS 725.88	AY554287	NR 111134	JX498935	NG_059201
			PW2535	
Exophiala pisciphila CBS 537.73 rpb1	JN856018	NR 121269	DQ840556	DQ823101
				AFTOL-ID 669
Exophiala salmonis CBS 157.67	NG 061119	NR 121270	EF413610	AY213702
			no strain listed	
Exophiala sideris CBS 121828	NG 062072	NR 111553	Mycococsm BLAST	MH875856
				CBS:127096
Exophiala spinifera CBS 899.68	KF155201	NR 111131	JX498922	KF155182

	CBS 101534		CBS 101644	CBS 101534
Exophiala xenobiotica CBS 118157	KF155202	NR 111203	JX498920	XR_001230708
			CBS 117753	
Endocarpon pusillum AFTOLID 2279	EF689837	JQ927447	EF689756	EF643754
Phaeoannellomyces elegans CBS 101597	X80708	NR 155687	N/A	KF928507

Table 3: Nitrogen sources, concentrations, and providers

Nitrogen Source	Concentration	Catalog number
No Nitrogen	N/A	N/A
Peptone	1% w/v	Fisher Brand: BP1420
L-Proline	100 mM	Sigma: P-0380
Ammonium tartrate	100 mM	Sigma: A2956
L-Serine	100 mM	Sigma: S4500
Sodium Nitrate	100 mM	Fisher Brand: S343
Glycine	100 mM	Fisher BioReagents: BP381
L-Glutamic acid	100 mM	Sigma: G1251
L-Aspartic acid	100 mM	Sigma: A9256
Urea	50 mM	Alfa Aesar: A12360

Table 4: Metals used and their concentration

Metal	Concentration	Catalog Number
$Fe(III)SO_4$	0.6 M	Fisher: I146
$CoCl_2$	0.5 M	Sigma: C-2644
$NiCl_2$	1.5 M	Sigma-aldrich: 223387
$CuCl_2$	1.5 M	Sigma: 203149
$CdCl_2$	10 mM	Fisher: 7790-84-3
$AgNO_3$	0.47 M	Alfa Aesar: 7761-88-8

Table 5: Accession numbers for all databases containing *E. viscosa* JF 03-3F and JF 03-4F's data.

Database ID numbers	***Exophiala viscosa JF 03-3F***	***Exophiala viscosa JF 03-4F***
WGS Accession GenBank	JALDXI000000000	JALDXH000000000
WGS Accession version used	JALDXI010000001.1	JALDXH000000001.1
Transcriptome Accession	PRJNA501636	PRJNA501637
BioProject	PRJNA500555	PRJNA500554
BioSample	SAMN10366861	SAMN10366859
SRA	SRS4089839	SRS4090708
DOE JGI GOLD project ID	Gp0220461	Gp0220460
CBS strain number	148801	148802
MycoBank number	MB845198	MB845199

Table 6: Genome descriptions of the novel *Exophiala* species and related taxa. Information gathered from JGI's Mycocosm.

	E. viscosa JF 03-3F CBS148801	*E. viscosa* JF 03-4F CBS148802	*E. sideris* CBS121828	*E. spinifera* CBS89968	*E. xenobiotica* CBS118157	*E. oligosperma* CBS72588	*E. dermatitidis* UT8565
Accession #s	PRJNA500555	PRJNA500554	PRJNA325799	PRJNA325800	PRJNA325801	PRJNA325798	PRJNA225511
Genome Assembly statistics							
Genome Assembly size (Mbp)	28.29	28.23	29.51	32.91	31.41	38.22	26.35
Number of contigs	35	27	69	143	64	287	10
Number of scaffolds	30	17	5	28	15	143	10
Number of scaffolds >= 2Kbp	25	17	5	20	11	129	10
Scaffold N50	4	5	2	4	3	5	4
Scaffold L50 (Mbp)	2.24	2.89	7.9	3.79	5.04	3.39	3.62
Number of gaps	5	10	64	115	49	144	0
% of scaffold length in gaps	0.00%	0.00%	0.10%	0.10%	0.10%	0.80%	0.00%
Three largest Scaffolds (Mbp)	5.39, 4.56, 2.49	4.57, 3.58, 2.93	9.94, 7.90, 7.15	6.18, 3.93, 3.92	5.55, 5.20, 5.04	4.47, 4.29, 4.12	4.25, 4.22, 3.71
GC content (%)	51.91	49.26	49.73	49.42	51.89	50.99	51.74
Gene statistics							
Number of genes	11344	11358	11120	12049	13187	13234	9562
Gene length (bp, Average)	1840	1844	2044	1593	2072	2090	2237

Gene length (bp, Median)	1666	1671	1823	1415	1845	1879	1923
Transcript length (bp, Average)	1740	1746	1933	1483	1941	1949	2122
Transcript length (bp, Median)	1564	1574	1710	1311	1710	1735	1794
Exon length (bp, Average)	705	707	776	621	738	743	896
Exon length (bp, Median)	410	414	452	339	430	426	513
Intron length (bp, Average)	70	69	74	81	80	85	85
Intron length (bp, Median)	56	56	56	61	57	61	62
Protein length (aa, Average)	488	489	500	494	492	488	501
Protein length (aa, Median)	428	430	434	437	431	429	429
Exons per gene (Average)	2.47	2.47	2.49	2.39	2.63	2.62	2.37
Exons per gene (Median)	2	2	2	2	2	2	2

Table 7: Carbon source utilization values of *E. viscosa* JF 03-3F

***E. viscosa* JF 03-3F**		***# 1***	***# 2***	***# 3***	***Average***	***Score***
D-galactose	GAL	4	5	4	4.3	+
D-sorbitol	SOR	4	4	4	4.0	+
actidione (cycloheximide)	ACT	5	4	4	4.3	+
D-xylose	XYL	4	4	4	4.0	+
D-saccharose (sucrose)	SAC	1	1	1	1.0	-
D-ribose	RIB	2	2	2	2.0	V
N-acetyl-glucosamine	NAG	4	5	4	4.3	+
glycerol	GLY	4	4	4	4.0	+
lactic acid	LAT	3	3	3	3.0	V
L-rhamnose	RHA	4	4	4	4.0	+
L-arabinose	ARA	4	4	4	4.0	+
palatinose	PLE	3	3	3	3.0	V
D-cellobiose	CEL	4	4	4	4.0	+
erythritol	ERY	2	2	2	2.0	V
D-raffinose	RAF	1	1	1	1.0	-
D-melibiose	MEL	1	1	1	1.0	-
D-maltose	MAL	4	4	4	4.0	+
sodium glucuronate	GRT	2	2	2	2.0	V
D-trehalose	TRE	3	3	3	3.0	V
D-melezitose	MLZ	2	2	2	2.0	V
potassium 2-ketogluconate	2KG	4	3	4	3.7	+
potassium gluconate	GNT	2	2	2	2.0	V
methyl-aD-glucopyranoside	MDG	1	1	1	1.0	-
levulinic acid (leuvulinate)	LVT	4	3	4	3.7	+
D-mannitol	MAN	3	3	3	3.0	V
D-glucose	GLU	5	5	5	5.0	+
D-lactose	LAC	1	1	1	1.0	-
L-sorbose	SBE	5	5	5	5.0	+
inositol	INO	2	2	2	2.0	V
glucosamine	GLN	1	1	1	1.0	-
no substrate	No	1	1	1	1.0	-
esculin ferric citrate	ESC	+	+	+	+	Black +

Table 8: Carbon source utilization values of *E. viscosa* JF 03-4F

***E. viscosa* JF 03-4F**		***# 1***	***# 2***	***# 3***	***Average***	***Score***
D-galactose	GAL	4	4	4	4.0	+
D-sorbitol	SOR	5	5	5	5.0	+
actidione (cycloheximide)	ACT	4	4	4	4.0	+
D-xylose	XYL	4	4	4	4.0	+
D-saccharose (sucrose)	SAC	2	2	2	2.0	V
D-ribose	RIB	2	2	3	2.3	V
N-acetyl-glucosamine	NAG	4	4	4	4.0	+
glycerol	GLY	4	4	4	4.0	+
lactic acid	LAT	3	3	3	3.0	V
L-rhamnose	RHA	4	4	4	4.0	+
L-arabinose	ARA	4	4	4	4.0	+
palatinose	PLE	4	4	4	4.0	+
D-cellobiose	CEL	4	4	4	4.0	+
erythritol	ERY	1	2	2	1.7	V
D-raffinose	RAF	1	1	1	1.0	-
D-melibiose	MEL	1	1	1	1.0	-
D-maltose	MAL	4	4	4	4.0	+
sodium glucuronate	GRT	2	2	2	2.0	V
D-trehalose	TRE	4	3	4	3.7	+
D-melezitose	MLZ	2	2	2	2.0	V
potassium 2-ketogluconate	2KG	3	3	4	3.3	V
potassium gluconate	GNT	2	2	2	2.0	V
methyl-aD-glucopyranoside	MDG	1	1	1	1.0	-
levulinic acid (leuvulinate)	LVT	3	4	3	3.3	V
D-mannitol	MAN	3	3	4	3.3	V
D-glucose	GLU	5	5	5	5.0	+
D-lactose	LAC	1	1	1	1.0	-
L-sorbose	SBE	5	5	5	5.0	+
inositol	INO	2	2	2	2.0	V
glucosamine	GLN	2	2	1	1.7	V
no substrate	0	1	1	1	1.0	-
esulin ferric citrate	ESC	+	+	+	+	Black +

Table 9: Diameter of the zone of clearing of *E. viscosa* JF 03-3F, *E. viscosa* JF 03-4F, *E. dermatitidis*, and *S. cerevisiae* with various metals.

Species	$FeSO_4$ 1 M	$CoCl_2$ 0.5 M	$AgNO_3$ 0.47 M	$NiCl_2$ 1.5 M	$CuCl_2$ 1.5 M	$CdCl_2$ 10 mM
***E. viscosa* JF 03-3F**	1.6 cm	1.5 cm	1.4 cm	3.9 cm	1.3 cm	4.5 cm
***E. viscosa* JF 03-4F**	1.8 cm	1.8 cm	1.4 cm	4 cm	1.5 cm	3.9 cm
E. dermatitidis	1.3 cm	1 cm	1.5 cm	2 cm	2.5 cm	1.2 cm
S. cerevisiae	1 cm	1.9 cm	2 cm	2.1 cm	2 cm	2.5 cm

Table 10: Annotation of melanin biosynthetic genes for *E. viscosa* JF 03-3F and JF 03-4F

	DHN/Allomelanin pathway							
Gene in *A. niger* (or *A. fumigatus*)	***E. viscosa* JF 03-3F Homologs**				***E. viscosa* JF 03-4F Homologs**			
	Mycocosm Prot. ID #	***e-value***	***Bit score***	***% ID***	***Mycocosm Prot. ID #***	***e-value***	***Bit score***	***% ID***
Pks1 An03g05440	580617	0.0E00	4077	47.0	463165	0.0E00	4081	47.0
Ayg1 An14g05350	511449	1.21E-90	852	44.0	494160	1.21E-90	852	43.9
Arp2 An02g00220	676985	5.72E-93	779	56.5	479993, 453709	5.74E-93	779	56.5, 48.7
***Arp2** Afu2g17560	625384	3.28E-48	612	48.4	242806; 441819	3.29E-48, 6.59E-75	612, 598	48.4, 51.3
Arp1 An08g09920	477931	5.58E-38	429	51.6	210894	5.59E-38	429	51.6
***Arp1** Afu2g17580	452087	2.18E-61	496	53.2	275994	2.19E-61	496	53.2
Abr2 An01g14010	603697, 153763	9.11E-155, 8.05E-142	1398, 1235	51.0, 43.9	326274, 72468	9.13-155, 8.53E-143	1398, 1235	46.8, 43.3
Abr1 An14g05370 An01g11120 An15g05520	648725, 437535	1.2E-99, 2.14E-41	1082, 551	48.4, 38.8	258543, 441397	1.20E-99, 2.14E-41	1082, 551	48.4, 38.8
	387337, 648725	5.04E-120, 4.05E-46	1274, 591	54.5, 44.0	92776, 258543	4.81E-122, 4.06E-46	1289, 591	55.0, 44.0
	648725, 653857	0.0E00, 1.7E-44	2144, 584	67.0, 42.7	258543, 102128	0.0E00, 3.27E-44	2144, 582	67.0, 42.7
	L-DOPA/Pheomelanin pathway							
Gene in *A. niger*	***E. viscosa* JF 03-3F Homologs**				***E. viscosa* JF 03-4F Homologs**			
	Mycocosm Prot. ID #	***e-value***	***Bit score***	***% ID***	***Mycocosm Prot. ID #***	***e-value***	***Bit score***	***% ID***
MelC2 An01g09220 An03g00280	140179, 643161	1.22E-78, 1.33E-49	833, 576	49.3, 40.6	84855, 433643	1.22E-78, 1.34E-49	833, 576	49.3, 40.6
	140179	2.86E-122	1084	59.1	84855	2.87E-122	1084	59.1

MelO An12g01670	-				-			
McoJ An12g05810	571417, 437535	1.06E-94, 6.08E-78	1067, 799	60.1, 52.5	465594, 441397	1.41E-97, 6.10E-78	1088, 799	61.2, 52.5
McoM An16g02020	571417, 580955	1.12E-103, 3.78E-74	1127, 807	52.6, 45.3	465594, 189119	4.27E-109, 3.80E-74	1133, 807	53.9, 45.3
McoD An11g03580	437535, 580955	2.11E-124, 5.40E-82	1178, 938	51.2, 49.6	441397, 189119	2.12E-124, 1.59E-82	1178, 942	51.2, 49.9
McoG An08g08450	437535, 580955	1.67E-110, 4.66E-88	1069, 944	49.1, 47.6	441397, 189119	1.67E-110, 1.35E-88	1069, 948	49.1, 47.9
McoF An05g02340	437535, 382943, 580955	1.79E-121, 4.03E-101, 3.80E-96	1150, 1041, 1004	44.6, 47.4, 50.3	441397, 95636, 189119	1.80E-121, 5.88E-101, 1.10E-96	1150, 1040, 1008	44.6, 47.4, 50.6
McoN An01g00860	653857, 649741	1.72E-129, 3.37E-116	1253, 1153	57.3, 55.2	102128, 454148	3.27E-129, 7.54E-97	1251, 1009	57.1, 52.6
McoI An18g02690	653857, 649741	1.96E-154, 1.47E-134	1471, 1287	57.0, 53.3	102128, 454148	3.75E-154, 7.08E-122	1469, 1193	56.7, 52.8
	L-Tyrosine degradation/Pyomelanin pathway							
Gene in *A. niger*	***E. viscosa* JF 03-3F Homologs**				***E. viscosa* JF 03-4F Homologs**			
	Mycocosm Prot. ID #	***e-value***	***Bit score***	***% ID***	***Mycocosm Prot. ID #***	***e-value***	***Bit score***	***% ID***
Tat An02g05540	606461	1.22E-169	1477	54.4	34310	1.22E-169	1477	54.4
HppD An11g02200	623446	0.0E00	1448	69.7	39306	0.0E00	1448	69.7
HmgA An11g02180	617354, 102643, 403121	0.0E00, 1.05E-92, 1.12E-104	1789, 971, 922	73, 45.1, 43.7	430149, 483886, 431641	0.0E00, 1.97E-92, 1.12E-104	1789, 969, 922	73, 44.9, 43.7
FahA An11g02170	617341	4.32E-175	1477	65.5	148504	1.38E-178	1466	65
MaiA An11g02160	213100	1.15E-55	533	51.2	198633	9.47E-57	541	45.3